THE EFFECT OF TURBULENCE ON SURVIVAL, DISPERSAL, AND SWIMMING BEHAVIOR OF GRASS CARP EGGS AND LARVAE

BY

ANDRES FELIPE PRADA SEPULVEDA

DISSERTATION

Submitted in partial fulfillment of the requirements
for the degree of Doctor of Philosophy in Civil Engineering
in the Graduate College of the
University of Illinois at Urbana-Champaign, 2020

Urbana, Illinois

Doctoral Committee:

Assistant Professor Rafael O. Tinoco, Chair
Professor Marcelo H. Garcia
Professor Gary Parker
Assistant Professor Piotr Cienciala
Dr. P. Ryan Jackson, US Geological Survey

ABSTRACT

There is an urgent need to monitor and control the spread of invasive grass carp (*Ctenopharyngodon idella*) in North America. Grass carp are reproducing in tributaries to Lake Erie and control efforts targeting reproduction are greatly needed. Current strategies for their control and removal are costly and report mixed degrees of efficacy. However, an alternative way to monitor and control their spread consists of increasing capture and mortality rates during early life stages (i.e. eggs and larvae stages) when they are more susceptible to damage via enhanced flow turbulence levels and altered flow conditions. In order for these alternative strategies to be effective, is necessary to study the physics underlying the movement of eggs and larvae in streamflow, and to quantify the turbulence thresholds that trigger those behavioral and physiological effects.

This study examines how early-life-stage grass carp interact with turbulent flows, how turbulence affects their survival, and whether turbulence-based control methods could work. An extensive series of laboratory experiments were conducted with live grass carp eggs and larvae in a grid-stirred turbulence tank and in a race-track flume to: a) explore the effect of turbulence intensity on egg mortality, and b) to document the behavioral response of grass carp larvae to spatially-variable, turbulent flows.

A turbulence intensity threshold was identified, above which egg mortality substantially increased due to short- (10 seconds) and long-term (5 minutes) exposure at different turbulence levels. Larvae actively responded to changes in turbulence intensity and shear stresses produced by obstructions in the flow (e.g. rocks, piers, and submerged vegetation), avoiding areas of high shear and seeking low-turbulence, low-vorticity regions. These swimming capabilities were quantified by estimating burst swimming speeds and were correlated with the spatial distributions of turbulent kinetic energy, vorticity, and Reynolds stresses for future predictions of larvae dispersion on natural streams.

This study produced a unique and extensive data set that may allow for the development of turbulence-based control methods for grass carp. Such control methods could include increasing egg mortality by increasing turbulence intensity through temporary and permanent in-stream structures or using natural or modified hydrodynamics to attract, guide, and aggregate larvae at predefined control points for collection or extermination.

ACKNOWLEDGMENTS

I would like to express gratitude to my advisor Dr. Rafael Tinoco for all the guidance and support he has given me along this journey. I extend this gratitude also to the rest of the doctoral committee members for their insightful feedback and comments during the qualifying and preliminary exams, as well as the final defense. They greatly helped me to clarify many aspects of the fundamental principles behind this research project, and to improve the results reported in this document.

Special thanks to the US Geological Survey (USGS) for providing the funding for my stipend, tuition, and laboratory experiments through the Cooperative Agreements G17AC00060 and G18AS00001 for CESU-affiliated Partner with USGS - Great Rivers Cooperative Ecosystem Studies Unit. I am also very grateful with the staff at the USGS Columbia Environmental Research Center (CERC) in Columbia MO, especially with Duane Chapman, Amy George, and Ben Stahlschmidt for their support conducting the experiments at both the Ven Te Chow Hydrosystems Laboratory and CERC. They all worked very hard with me to obtain the best possible outcome from this study.

To all my officemates who helped me many times with different issues analyzing the data from the experiments, thank you all very much. And the awesome EELs for the valuable comments they gave me during our group meetings.

Any opinions, findings, and conclusions or recommendations expressed in this material are those of the authors and do not necessarily reflect the views of the USGS. Any use of trade, firm, or product names is for descriptive purposes only and does not imply endorsement by the U.S. Government.

To my parents, my sisters, and the rest of my family

TABLE OF CONTENTS

CHAPTER 1: INTRODUCTION

1.1. Research objectives

Management measures to reduce population growth at spawning times have been proposed for the control of invasive fish populations at the early stages of life (i.e. egg and larval stages), by identifying survival and dispersal bottlenecks due to physical interactions as they are transported by the flow. In the case of North America, populations of invasive grass carp have been growing exponentially since their introduction since the 1970s, but only in the recent years, numerical tools (e.g. FluEgg (Garcia et al. 2013)) have been developed to support these management measures.

FluEgg is capable of simulating the transport of fish eggs in fluvial environments from spawning locations in a Lagrangian framework, but simulations end when eggs hatch, and it does not account for egg survival rates or larval behavior. Hatching time is estimated based on the water temperature, and model does not inform mortality rates due to boundary interactions or increased levels of turbulence. Extensive analysis of experimental live-fish laboratory data is then needed to predict more precisely where grass carp eggs and larvae are more likely to be found in natural waterways. Some recent experiments used surrogate eggs (e.g. Garcia et al. 2015b), lacking in documenting the hatching transition and the early behavior of larvae.

The main objective of this research project is to study the transport of live grass carp eggs and larvae in turbulent flows on a controlled laboratory setup, asserting possible causes of egg mortality, and documenting the swimming behavior of larvae in the vertical and streamwise directions.

Specific objectives include:

- Examine enhanced flow turbulence as an alternative control strategy through turbulence-induced mortality before the hatching transition.

- Investigate preferential locations of larvae under altered flows to determine thresholds of turbulence that triggers larval response.

- Understand larvae swimming capabilities as a response to flow conditions to expand prediction capabilities of numerical tools.

The specific research questions addressed in this project are:

- Is turbulence an external factor affecting grass carp egg survival? If so, what is the threshold turbulence and exposure time to damage egg's membrane preventing a successful hatching?

- Are grass carp larvae able to response to turbulent flows? Do they prefer or avoid turbulence? What are the desirable or undesirable levels of turbulence?

- How does the presence of common in-stream obstructions (e.g. a bump, a bridge pier, or submerged vegetation) influence the dispersion and survival of eggs and larvae? Do the flow conditions generated by these obstructions affect the behavior of larvae?

- What is the range of swimming speeds of larvae in altered turbulent flows, and what are the turbulence time and length scales that determine their swimming response?

1.2. Literature review

After being introduced in the United States in the 1970s for private aquaculture, grass carp and their relatives, the bigheaded carps (silver carp *Hypophthalmichthys molitrix* and big head carp *H. nobilis*) moved into the Mississippi River basin where they became well established and are now considered highly undesirable invaders (Fig 1.1) (Chick and Pegg 2001; Parker et al. 2016; Kočovský et al. 2018). Conversely, grass carp is a highly desirable species in their native rivers in China, where their populations have declined due in part to anthropogenic river modifications, such as large dam constructions (Chapman et al. 2016). In their native range, they are important culturally and economically as a food fish (Kočovský et al. 2018).

Fig 1.1. Spread of bigheaded and grass carp in the US in 1970 (a), 1980 (b), 2017 (c). Source: https://nas.er.usgs.gov

Grass carp is of particular ecological concern in North America for their rapid population growth and their high consumption capacity of aquatic vegetation (i.e. macrophytes) (Conover et al. 2007). They can consume up to 40% of their body weight per day (Laird and Page 1996). Grass carp have now reached the Laurentian Great Lakes (Chapman et al. 2013; Embke et al. 2016) where desirable macrophytes are already in decline (Cudmore et al. 2017). Reduction of macrophytes may result in increase of turbidity and alkalinity, and depletion of dissolved oxygen (Lembi et al. 1978; Mitzner 1978; Leslie et al. 1983); as well as in direct degradation of the habitat of native fish species which depend upon macrophytes for all or part of their life cycle (Chilton and Muoneke 1992; Cudmore et al. 2017).

Preventing the spread and negative effects of the presence of grass carp in North America has become an area of intense concern and a research subject among different disciplines (Cudmore et al. 2017; Wittmann et al. 2017; Wieringa et al. 2017; Jones et al. 2017; Gertzen et al. 2017). Several approaches to deter fish movements have been developed and tested such as: electric barriers, strobe lights, acoustic fish deterrents, bubble curtains, velocity barriers, oxygen

availability, pheromones, magnetic fields, and the use of chemicals (Noatch & Suski 2012, and references therein). However, none of them has effectively controlled the exponential growth and dispersal of grass carp.

An alternative strategy to control the spread of grass carp, and reduce their population growth, is to identify survival and dispersal bottlenecks due to physical interactions between the early-life fish (i.e. eggs and larvae) and the riverine environment. George et al. (2015) showed a reduction in survival when eggs are buried in the riverbed, inferring that grass carp require turbulent-flowing water for reproduction with sufficient levels of turbulence to keep eggs afloat. Murphy and Jackson (2013) reported that flow velocities as low as 0.15 to 0.25 m/s in natural streams could maintain eggs in suspension.

Regions of high mixing levels (e.g. river confluences, rapids, behind sandbars, over vegetation canopies and gravel beds) are often used as spawning grounds (Jennings 1988; Chapman 2006; Stainbrook et al. 2007; Garcia et al. 2013), and spawning of grass carp is proportional to the size and weight of the female, with an average spawn of 500,000 eggs for a 5 kg female (Shireman and Smith 1983; Chilton and Muoneke 1992). Eggs develop and hatch while drifting in currents (Schrank and Guy 2002; Lamer et al. 2015; George et al. 2015), and can disperse in flow from the spawning site to as far as 180 km downstream (Fedorenko and Fraiser 1978). Dispersal distance can also be relatively short depending on temperature and flow conditions (Garcia et al. 2015a; Embke et al. 2019), so river-reaches as short as 25 km could allow enough length for hatching (Murphy and Jackson 2013).

The dispersal of grass carp eggs in rivers has been simulated applying Advection-Dispersion models (e.g. Fluvial Egg Drift Simulator "FluEgg" (Garcia et al. 2013)), given as:

$$\frac{\partial c}{\partial t} + u\frac{\partial c}{\partial x} + v\frac{\partial c}{\partial y} + w\frac{\partial c}{\partial z} + \frac{\partial (cV_s)}{\partial z} = K_H\left(\frac{\partial^2 c}{\partial x^2} + \frac{\partial^2 c}{\partial y^2}\right) + \frac{\partial}{\partial z}\left(K_V\frac{\partial c}{\partial z}\right) \quad (1.1)$$

The numerical approximation to the solution of this ADE equation is computed by applying the Random Walk method in the 3 dimensions within a fluvial environment of one-dimensional discrete cells. These cells are defined by a width, length, and water depth, including the 3 components of flow velocity (i.e. longitudinal (u), transversal (v), and vertical (w)). The random displacements of each egg at every time step (Δt) is computed in the longitudinal and transversal directions as:

$$X_e^{t+\Delta t} = X_e^t + u\Delta t + R\sqrt{2K_H\Delta t} \quad (1.2)$$

$$Y_e^{t+\Delta t} = Y_e^t + v\Delta t + R\sqrt{2K_H\Delta t} \quad (1.3)$$

where R is a random factor from a normal distribution with mean zero and standard deviation one. K_H is the longitudinal and transversal turbulent diffusion which depends on the shear velocity at every cell estimated by fitting the vertical velocity profile to the law of the wall. As we can see from the advective terms (i.e. $u\Delta t$ and $v\Delta t$), the velocity of eggs is assumed to be the same as the flow velocity in these two components.

Vertical displacements of eggs are a function of the vertical velocity component (w), the egg settling velocity (V_s), and the vertical turbulent diffusion (K_v) which is constant in x and y directions but varies with z. The vertical displacement of every egg in each time step is computed as:

$$Z_e^{t+\Delta t} = Z_e^t + w^t\Delta t + \frac{1}{2}(V_s^t + V_s^{t+\Delta t})\Delta t + K_V' Z_e^t \Delta t + R\sqrt{2K_V\left(Z_e^t + \frac{1}{2}K_V' Z_e^t \Delta t\right)\Delta t} \quad (1.4)$$

where K_V' is the first derivative of the vertical turbulent diffusion (K_v) in the z direction and is computed in FluEgg as a function of z, using either of the following three functions: a constant depth-averaged, a parabolic, or a parabolic-constant profile.

This discrete solution of the ADE equation is applied in FluEgg within a hydraulic model that in its current form is limited to flat bed scenarios, and considers reflective boundary conditions only. In the model, eggs are assumed to be in suspension as they are transported, which is true for flat bed conditions where vertical flow fluctuations overcome the egg settling speed, but may not be the best representation for a natural river system where in-stream obstructions, dead zones, or different flow velocities at the banks may be present. FluEgg simplifies the river as a rectangular channel with a specific bed resistance, and all these stream features that may affect both dispersal and mortality of eggs as observed in the flume experiments, are neglected.

FluEgg is used to determine probable spawning and hatching locations, and as the model predicts the position of every egg at each time step, it incorporates the changes in egg density and diameter based on time after spawning and water temperature. The fluvial environment considered by the model consists of one-dimensional discrete series of cells with reflective boundaries (Fig 1.2). The model has been successfully tested with field measurements over some Great Lakes tributaries: Sandusky River (Garcia et al. 2013) and Saint Joseph River (integrating HEC-RAS model data as river hydrodynamic input) (Garcia et al. 2015a).

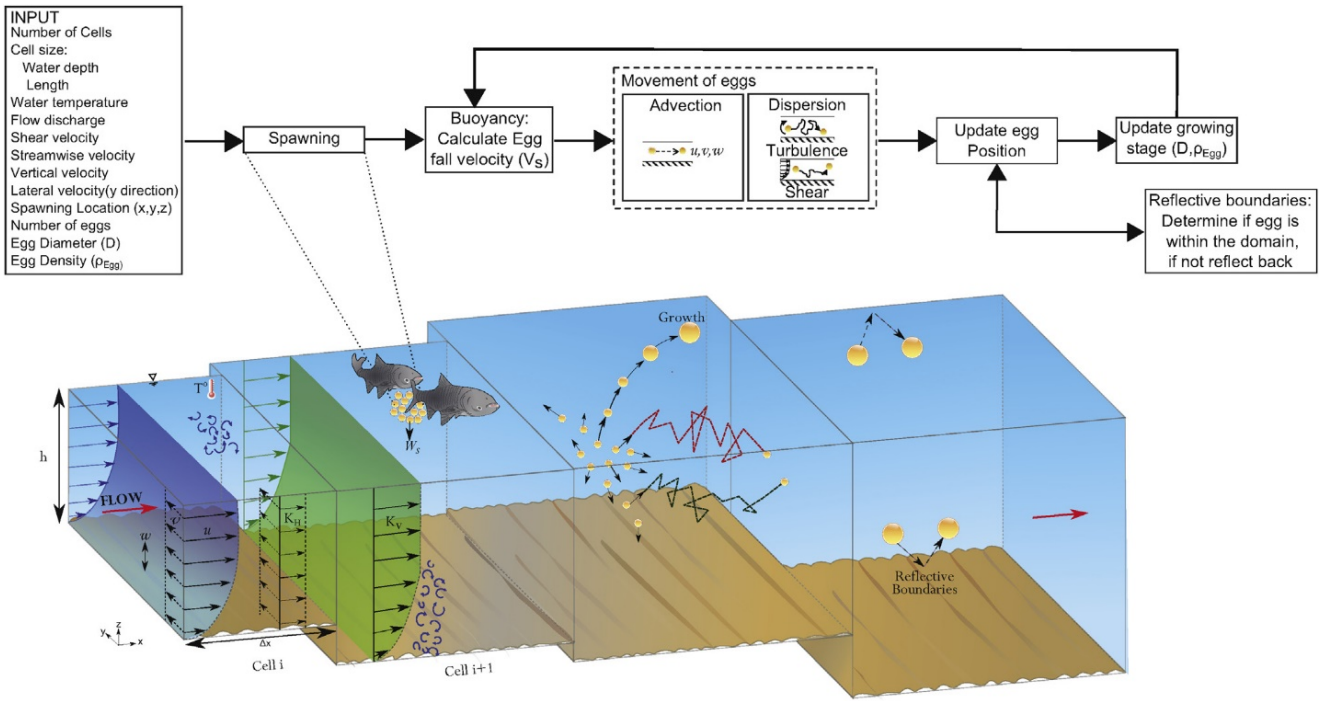

Fig 1.2. Conceptual schematic of variables and submodels included in FluEgg (figure from Garcia et al. 2013).

The implementation of numerical models for egg transport motivated the carrying out of laboratory experiments for further validation and better understanding of the physical processes. Garcia et al. (2015b) used styrene plastic beads in a laboratory flume as surrogates to evaluate suspension and settling dynamics of grass carp eggs. They estimated the egg settling velocity and documented the vertical distribution of eggs under four different mean flow velocities (0.04, 0.07, 0.2, 0.4 m/s). They reported that for the flow velocity of 0.07 m/s over a flat bed, about 65% of the eggs remained in suspension (Fig 1.3a-b), which was almost half of the minimum velocity reported by Murphy and Jackson (2013) of 0.15 m/s to maintain eggs in suspension.

Garcia et al. (2015b) also used Hearn's criteria (2008) for sediment to classify the eggs as suspended particles using the inverse of the Rouse number, $1/Z_{R,}$ and dimensionless ratios between vertical turbulent intensities, friction velocities, and egg settling velocity. They found that even for a flow velocity as low as 0.04 m/s eggs can be classified as 50% suspended load (Fig 1.3c).

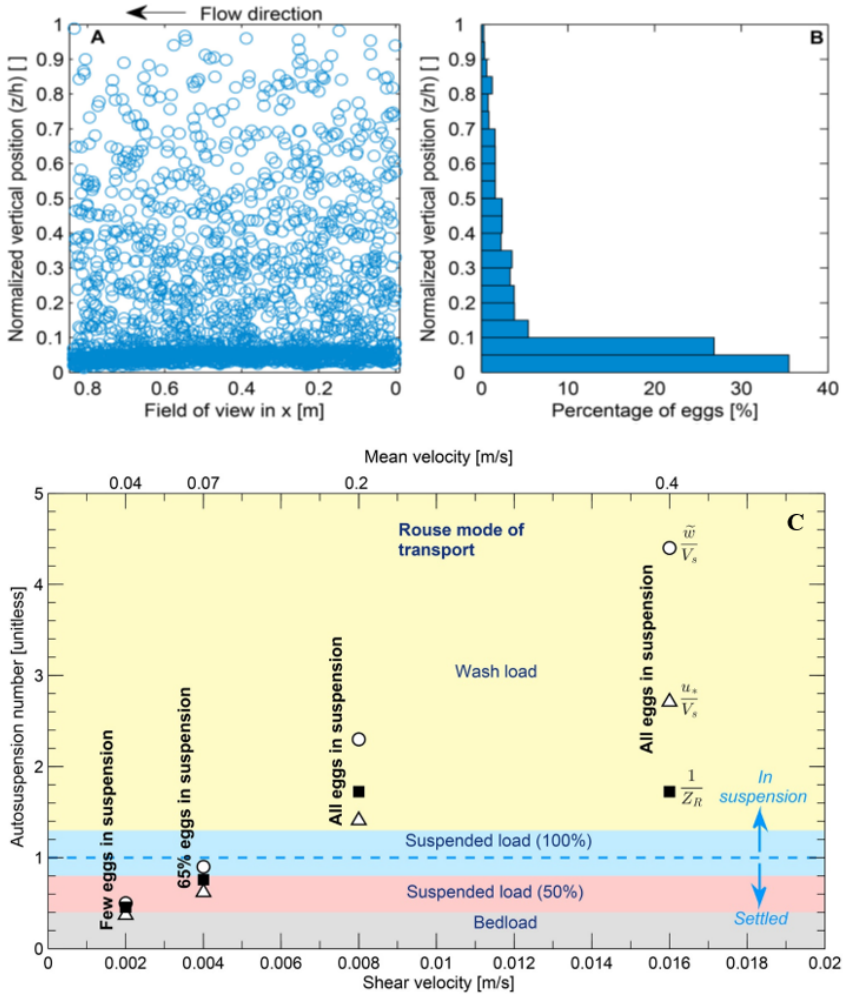

Fig 1.3. Vertical distributions of surrogate eggs at mean flow velocity of 0.07 m/s (a-b). Classification of surrogate eggs as suspended particles according to sediment transport criteria in flume experiments (c) (figure from Garcia et al. 2015b).

Field studies were also conducted for egg collection and sampling on tributaries of the Great Lakes. Embke et al. (2016) reported "the first direct confirmation of grass carp spawning in a Great Lakes tributary". In this field work, researchers struggled to collect even a few eggs using paired bongo nets of 0.5 m diameter during high-flow events on the Sandusky river. They

cast the nets just below the water surface for an interval of 5 minutes without considering sampling at lower depths where more accumulation of eggs can be expected as Garcia et al. (2015b) observed in their flume experiments.

Later, George et al. (2017) estimated physical properties of real grass carp eggs, e.g. diameters, density, and terminal fall velocity. They reported that eggs begin to absorb water after fertilization (water-hardening period), increasing their size and decreasing their density over time. But once they are water-hardened, the egg size is fairly constant until hatching (Fig 1.4a). They estimated diameters (d) of water-hardened eggs of 4.5 ± 0.6 mm, terminal fall velocities (w_s) of 0.74 ± 0.16 m/s (Fig 1.4b), and densities (ρ_s) of 999.87 ± 1.2 kg/m^3 (Fig 1.4c). The estimated density shows that grass carp eggs can be heavy enough to sink in still water but light enough to remain in suspension at low flow velocities, thus potentially avoiding burial and abrasion with bed material.

George et al. (2018) conducted more laboratory experiments, this time no longer with eggs but with live grass carp larvae, to observe swimming capabilities as a paramount factor in the dispersion of grass carp after hatching. George and Chapman (2015) described that larvae begin vertical swimming, which continues until Gas Bladder Inflation (GBI), when they swim horizontally maintaining a specific depth. George et al. (2018) estimated larvae swimming speeds at both pre-GBI and post-GBI stages. They reported speeds of "routine swimming" (or free swimming) which is defined as a spontaneous swimming in the absence of flow (Muller, 2008), and "maximum swimming" (or intense short-term swimming) which is a burst swimming that can only be maintained for periods under 20 s (Beamish, 1978). For routine swimming, George et al. (2018) estimated mean vertical speeds pre-GBI of 0.024 ± 0.012 m/s (with downward velocity up to twice as fast as upwards velocity), and mean horizontal speeds post-GBI of 6.6 $x10^{-3}$ ± 7.7 $x10^{-3}$ m/s. For maximum swimming, at 4 days post-hatch (post-GBI), the estimated speed was 0.11 ± 0.052 m/s.

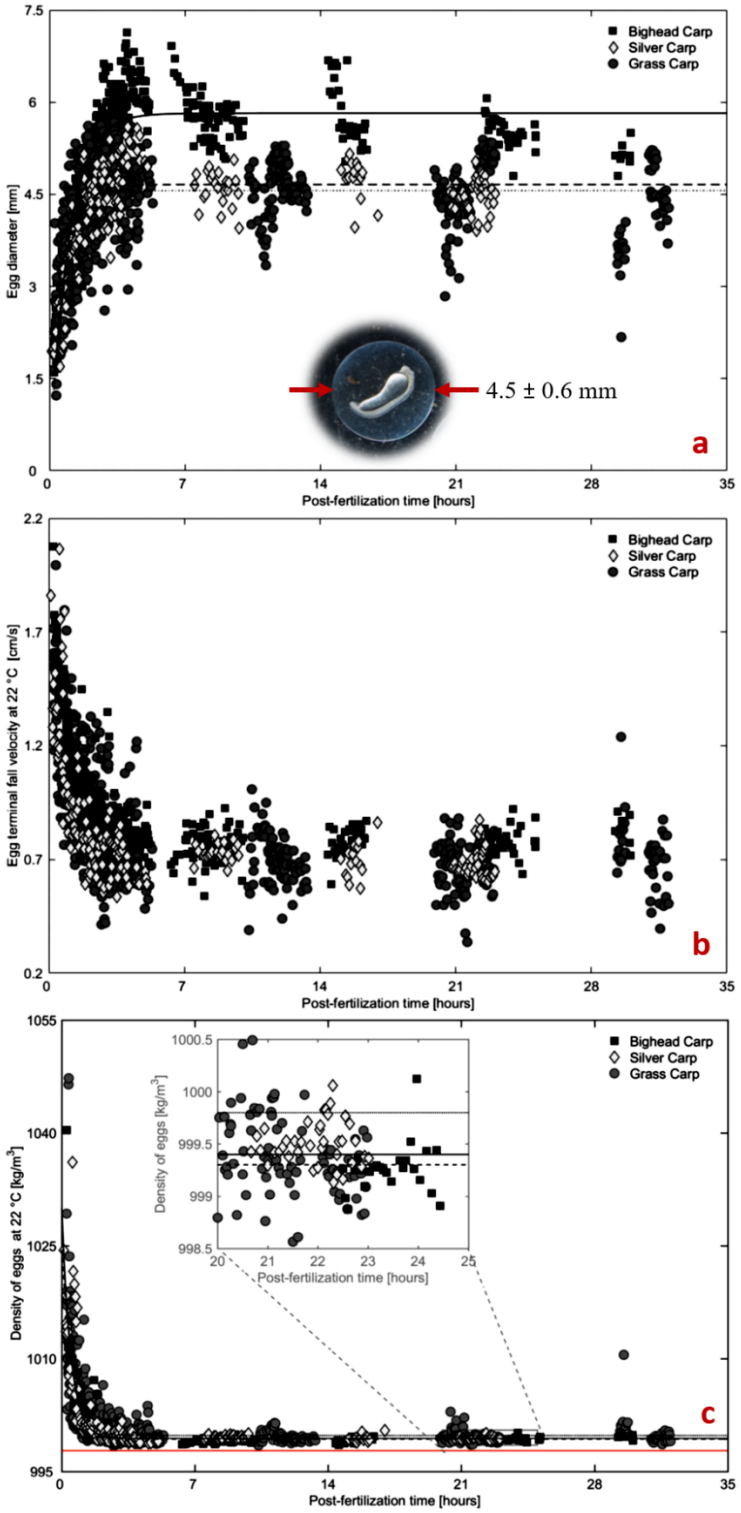

Fig 1.4. Measured diameter of Bighead Carp, Silver Carp, and Grass Carp eggs at different post-fertilization times with an inset of a grass carp egg (a). Terminal fall velocity of Bighead Carp, Silver Carp, and Grass Carp at different times post-fertilization (b). Density of Bighead Carp, Silver Carp, and Grass Carp eggs at different times post-fertilization (c) (figure from George et al. 2017).

One possible improvement to a transport model such as FluEgg would be to couple the ADE equation with a more elaborated 3D fluvial environment that considers the river morphology, as well as the obstructions that a natural channel may have. Some members of the Environmental Fluid Mechanics group of the University of Toronto have been recently working on these kind of models, and developed a 3D Environmental Fluid Dynamic Code (EFDC) model of the lower Sandusky river with the Random Walk approximation built into (Heer et al. *in review*). This 3D model will certainly lead to more accurate transport predictions, and opens the doors also to the possibility of estimating the egg mortality due to turbulence, as it allows to compute more precisely the magnitudes of turbulence along the channel.

Having an improved model with a more realistic fluvial environment, we can also think on including the simulation of the hatching transition and the transport of larvae at the early-life stages. As observed in the flume experiments, larvae showed a vertical swimming stage, and then after GBI, they showed horizontal swimming capabilities where they can maintain an elevation and also choose preferential locations depending on the flow conditions. These capabilities of larvae will definitely modify the Random Walk approximation that is being implemented for eggs. Larvae will no longer be advected at the same velocity with the flow in the longitudinal and transversal directions, as it is assumed for eggs ($u\Delta t$ and $v\Delta t$), but they will have a relative velocity that can be estimated from the PTV analysis. However, results from this study are limited to the short width of the flume, thus swimming speeds will be characterized in the longitudinal and vertical directions, not in the transversal direction. To characterize speeds in the lateral direction, more experimentation is needed in a wider flume.

For vertical displacements of larvae, the term considering the settling speed of eggs $[\frac{1}{2}(V_s^t + V_s^{t+\Delta t})]$ will no longer play a role for post-GBI larvae since they can maintain their elevation at the preferable location. The vertical movement would also be driven by their own velocity, and not by the vertical turbulent diffusion (K_v) as it is assumed for eggs.

1.3. Research plan

In collaboration with the US Geological Survey (USGS), we have studied the transport of grass carp at egg and larval stages in open channels. The motivation to perform this study was to explore alternative strategies in the control of this fish species in North America, where they are considered problematic invaders. Hydrodynamic experiments with live grass carp eggs and larvae were conducted at the Ven Te Chow Hydrosystems Laboratory (VTCHL) at the University of Illinois in Urbana-Champaign. The Illinois Department of Natural Resources granted us the authorization to possess the live fish in the laboratory facility for research purposes only (Permit No. 18-050).

Fish biologists from the USGS Columbia Environmental Research Center (CERC) in Columbia MO, were in charge of culturing the eggs at CERC and then take them to the VTCHL in Urbana IL. Initially two rounds of experiments were planned and conducted, the first one was in summer 2017, and the second one was in summer 2018. After these two rounds, we decided to do some extra tests directly at CERC in summer 2019. Measures were always taken to prevent release of the fish from the facilities, and waste water was disposed so as to prevent egg and larva escapement. MS-222 (*tricaine methanesulfonate*) was used to euthanize all surviving larvae. Remaining organic material was filtered and incinerated to prevent contamination and potential escapement of organic material.

The results from all rounds of experiments are reported in this document in 4 separate chapters:

- CHAPTER 2: *Survival and drifting patterns of grass carp eggs and larvae in response to interactions with flow and sediment in a laboratory flume*.
  Settling velocity and density of a representative sample of eggs were estimated, and three trials of flume experiments with different flow conditions were conducted with live eggs in a temperature-controlled setting with a mobile sediment bed. In these trials, egg and larval stages were continuously analyzed over periods of 80 hours; and eggs and larvae interactions with the flow and sediment bed were monitored and characterized qualitatively and quantitatively. Survival rates were quantified after each trial, highlighting physical causes for increased mortality. Detailed flow analysis was correlated to the observed drifting and swimming behavior of eggs and larvae, to estimate distributions across the water depth, as well as traveling and swimming speeds. Evidence

of the influence of mean and turbulent flow in the suspension and transport of eggs are reported, and swimming patterns of larvae at different developmental stages are described. Chapter 2 has been published as Prada AF, George AE, Stahlschmidt BH, Chapman DC, Tinoco RO (2018) Survival and drifting patterns of grass carp eggs and larvae in response to interactions with flow and sediment in a laboratory flume. PLoS ONE 13(12):e0208326. https://doi.org/10.1371/journal.pone.0208326.

- CHAPTER 3: *Influence of turbulence and in-stream structures in the transport and survival of grass carp eggs and larvae at various developmental stages*.
  A comprehensive set of hydrodynamic experiments was conducted with live grass carp eggs and larvae, to better understand their drifting and swimming patterns with 3 different in-stream obstructions: (1) a gravel bump, (2) a single cylinder, and (3) submerged vegetation. The hydrodynamic behavior of eggs and larvae with each obstruction was continuously monitored for about 85 consecutive hours. Transient spatial distributions of the locations of eggs and larvae throughout the water column were generated for each flow scenario. Results show that the active swimming capabilities of larvae allow them to seek areas of low turbulence and low shear stresses, and that eggs are susceptible to damage by high levels of turbulence. Chapter 3 has been published as Prada AF, George AE, Stahlschmidt BH, Jackson PR, Chapman DC, Tinoco RO (2020) Influence of turbulence and in-stream structures on the transport and survival of grass carp eggs and larvae at various developmental stages. Aquat Sci 13(12):e0208326. https://doi.org/10.1007/s00027-019-0689-1.

- CHAPTER 4: *Lethal and sublethal effects of turbulence on grass carp eggs prior and after hatching*.
  We examined enhanced flow turbulence levels as an alternative grass carp control strategy through turbulence-induced mortality. We used an oscillating grid-stirred turbulence tank to test several batches of pre-water-hardened and water-hardened grass carp eggs to find threshold values of turbulence and shear stresses that can cause immediate and post-hatching harm. A post-hatching inspection revealed larval abnormalities that ranged in severity from yolk sac deterioration, pericardial edema, and

underdevelopment to spinal deformities and missing heads. Many of these malformations are lethal, and the others have potential long-term sublethal effects that reduce the fitness and competitive ability of the larvae. This susceptibility to mechanical damage at embryonic stages is a key factor in the design of alternatives that promote or reduce the trapping of grass carp eggs at high turbulence, thus affecting the probability of successful hatching in natural streams. Chapter 4 is under preparation for submission as a standalone publication.

- CHAPTER 5: *Turbulence as a barrier for invasive fish in rivers: A laboratory study on grass carp larvae*.

  In addition to the long-term (4-days) tests documented in Chapter 5, shorter experimental series were conducted with the three different configurations built in the flume. We varied the flow velocities and water depths to study the swimming response of grass carp larvae in stage 38 (based on stages described by Yi et al. 1988 and George and Chapman 2015). We found threshold values of turbulent kinetic energy and Reynolds stresses that triggered the response of larvae, and estimated horizontal and vertical swimming speeds for each flow condition. Increased levels of turbulence forced them to swim away from those, moving faster and spending more energy. These findings support the development of new strategies for monitoring the spread of grass carp eggs and larvae in rivers, as well as to the development of numerical tools for larvae transport in natural streams that consider their active swimming capabilities. Chapter 5 is under preparation for submission as a standalone publication.

CHAPTER 2: SURVIVAL AND DRIFTING PATTERNS OF GRASS CARP EGGS AND LARVAE IN RESPONSE TO INTERACTIONS WITH FLOW AND SEDIMENT IN A LABORATORY FLUME

2.1. Introduction

Grass carp (*Ctenopharyngodon idella*) are native to eastern Asia, but they have been introduced and have become established in the central United States, where they are considered problematic invaders. In their native range, where wild populations are in severe decline (Chapman et al. 2016), they are important culturally and economically as a food fish (Kocovsky et al. 2018).

The primary ecological effect of the introduction of grass carp is reduction in aquatic macrophytes (Cudmore et al. 2017, Garner 2008, Kirkagac and Demi 2003), which can be problematic where macrophytes are considered beneficial and where they serve as spawning locations and nursery habitat for native fishes. Grass carp have now invaded the Laurentian Great Lakes (Chapman et al 2013, Embke et al 2016) where desirable macrophytes are already in decline and where grass carp are predicted to become a nuisance (Cudmore et al. 2017). Forecasting the spread and effects of grass carp in the Great Lakes has become an area of intense concern and of research (Cudmore et al. 2017, Wittmann et al 2017, Wieringa et al 2017, Jones et al 2017, Gertzen et al 2017). Several approaches to deter fish movements have been tested: electric barriers, strobe lights, acoustic fish deterrents, bubble curtains, velocity barriers, oxygen availability, pheromones, magnetic fields, and the use of chemicals (Noatch and Suski 2012, and references therein).

Management measures at spawning times could also be adopted to prevent recruitment and to reduce population growth, by identifying survival and dispersal bottlenecks due to physical interactions during early life stages. After ecosystem invasion, it is difficult or impossible to eradicate them, thus prevention becomes a more effective mitigation tactic.

Grass carp and their relatives, the bigheaded carps (silver carp *Hypophthalmichthys molitrix* and big head carp *H. nobilis*) which are also considered highly undesirable invaders in the United States and highly beneficial in Asia, can spawn hundreds of thousands of eggs at a time in turbulent flows of large rivers and their tributaries. Eggs subsequently develop and hatch while drifting in the currents (Schrank and Guy 2002, Lamer et al 2015, George et al 2015).

Therefore, understanding grass carp and bigheaded carp response to flow and turbulence regimes at early life stages is fundamental to monitoring and controlling their dispersal and drift.

Experiments on still water have found that egg survival is poor if they settle to the bottom and are buried in the sediment bed (e.g., George et al 2015b, Chapman and George 2011, George and Chapman 2015). Synthetic eggs have also been used in experiments to study egg transport under turbulent flow conditions, to evaluate suspension and settling dynamics of water-hardened eggs (Garcia et al 2015). Numerical tools have been developed to simulate the drifting behavior of grass carp and bigheaded carps during their early life stages (e.g. FluEgg, Garcia et al 2013) and have been tested on rivers in Michigan and Illinois (Garcia et al 2015a, Murphy et al 2016). FluEgg incorporates the influence of flow velocity, shear velocity, and turbulent diffusion on the transport and dispersal patterns of grass carp and bigheaded carp eggs. However, it does not account for egg survival rates or larval behavior after hatching. Simulations end when eggs hatch, which is estimated based on the water temperature specified, and it does not inform mortality rates due to boundary interactions or the dispersal and drift of larvae. Physical experimentation is thus required to evaluate the influence of the river bed on survival rates and study the swimming behavior of larvae.

Recent laboratory experiments with live grass carp and bigheaded carp eggs (George et al 2017) aimed to physically characterize eggs (i.e. estimate diameters, density, and terminal fall velocity) to better inform numerical models to estimate drifting. However, a comprehensive study that documents the hatching transition and the early behavior of larvae in moving water has not been conducted yet. A better understanding of the drifting of eggs and larvae under different flow and turbulence conditions, along with their interactions with a sediment bed would enhance model predictive capabilities for tracking the dispersal and drift of the early life stages of these invasive fishes.

In this study, three comprehensive trials of laboratory experiments were conducted in both still and moving water to determine the drifting and swimming behaviors of live grass carp eggs and larvae. Ranges of diameters, densities, and settling fall velocities of eggs were estimated in still water, whereas traveling speeds of eggs and larvae, as well as the swimming capabilities of larvae against the flow, were quantified in moving water. Continuous vertical distributions were also generated to observe the location and the transition from eggs to larvae across the water

depth at different flow conditions; and survival rates were monitored at the end of each trial to ascertain possible causes of mortality based on both hydrodynamics and biological interactions.

2.2. Materials and methods

Experiments were conducted at the Ven Te Chow Hydrosystems Laboratory (VTCHL) at the University of Illinois in Urbana-Champaign. Fertilized grass carp eggs were cultured and transported from the U.S. Geological Survey (USGS) Columbia Environmental Research Center (CERC) in Columbia, MO. Three trials of experiments were conducted. During trial 1, two females (5.09 and 3.21 kg) and four males (2.81, 2.23, 2.79, 1.86 kg) were used for spawning. During trial 2, one female (6.53 kg) and four males (3.60, 3.37, 3.61, 3.24 kg) were used, and during trial 3, three females (4.76, 5.36, and 5.60 kg) and four males (4.76, 4.00, 4.40, 4.40 kg) were used.

George and Chapman (2015), and George et al. (2017) showed that there can be large variations in egg size, due to maternal effects (larger females producing larger eggs), and temperature effects, with eggs from cooler water being larger than eggs from warmer conditions. For the present study, eggs were purposely obtained from individuals of similar size amongst all trials, to account for the response to flow conditions using similar eggs. However, the wide range in sizes presented in the following sections indicate that the sizes studied are representative of most of the expected range of grass carp eggs in nature. Spawning on trials 1 and 3 resulted in batches of good quality eggs (well-defined membrane and well-formed fish inside). However, the batch for trial 2 was negatively affected by high water temperatures at spawning (temperatures over 24°C), resulting in poor quality eggs.

2.2.1. Settling column test

Settling speeds (w_s) of eggs were determined at different times after fertilization during trial 1 (at 6, 10, 14, 18, and 22 hours after fertilization) by taking photos of individual falling eggs (25 eggs at each time) at 1 frame every 3 seconds with a Nikon D200 camera (10.2MP) on a backlit rectangular settling column 1.6 m tall, 0.2 m long, and 0.1 m wide, with a 1x1cm vertical grid for spatial calibration (Fig 4.1a). A Nikon SMZ-1500 stereomicroscope was used to measure egg diameter prior to release, using the mean of two perpendicular measurements, with a tolerance of 0.01 mm (inset in Fig 2.1a).

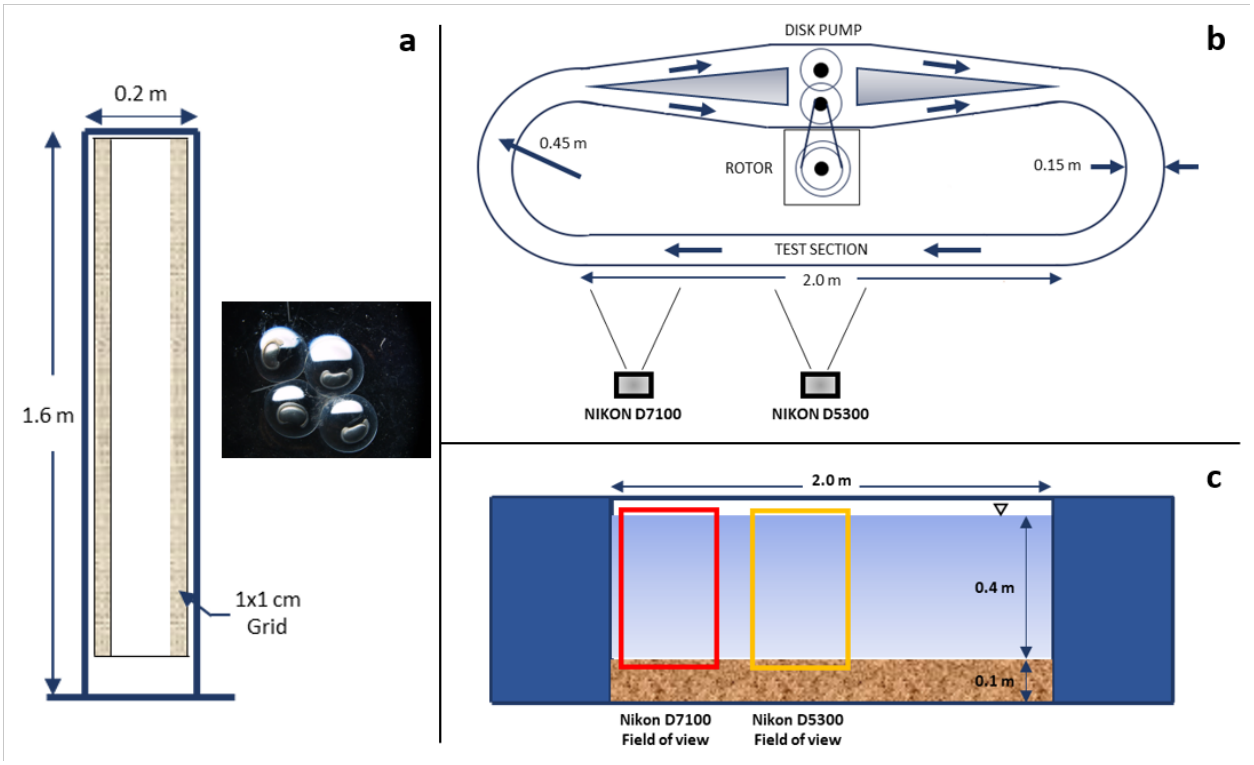

Fig 2.1. Facilities used to conduct the experiments (not to scale). (a) Settling water column with an inset of microscope image of the eggs. (b) Plan view of Race-Track Flume (RTF), Odell-Kovasznay type flume, with the setup of side-view cameras. (c) Side-view of the Race-Track Flume with the field of view of each camera.

Custom particle image processing MATLAB (MathWorks, Inc.) routines were developed to track the position of individual eggs and larvae in a series of consecutive frames. These routines produced binary images, which were processed using morphological processing tools to obtain the center of mass (x, z coordinates). Using such coordinates for each centroid and the difference in time between captures from video recordings, the traveling speeds between frames were calculated.

The slow settling speed of the eggs allowed the use of Stokes' law to estimate the density of eggs (ρ_s) over time as (Garcia 2017):

$$\rho_s = \frac{18\mu w_s}{g d_s^2} + \rho \tag{2.1}$$

Where ρ and μ are the density and dynamic viscosity of water, and d_s is the egg diameter.

A one-way Analysis of Variance (ANOVA) was performed to test whether the settling speed of the eggs and their density changed over time before hatching. A significance level of α

= 0.05 was considered statistically significant between the batches of eggs at the time intervals specified.

2.2.2. Race-Track Flume test

Drifting behavior of eggs and larvae under different flow conditions, and their interaction with the sediment bed and turbulent structures, were monitored with cameras on each trial for ~80 consecutive hours in the RTF; an Odell-Kovasznay type flume (Odell and Kovasznay 1971), shown in Figs 4.1b and 4.1c. For trial 1 and trial 3, 4000 eggs were released on the flume, but for trial 2 only 1604 due to the poor-quality spawning.

Water depth in the RTF was maintained at H = 0.4 m, above a 0.1-m thick sediment bed, composed of a mixture of walnut shells and sand (bulk sediment density $\rho_p = 1250$ kg/m^3, and size $\{D_{16}, D_{50}, D_{84}\} = \{0.41, 0.54, 0.66\}$ mm), placed only in the straight test section. All substrate material was washed and dried in an oven at 170 F (77 ºC) for 48 hours before each trial to help prevent biological contamination and control the spread of fungus. Settling velocity of the sediment was calculated as $w_p = 1.89x10^{-2}$ m/s, using the simple universal equation for grain settling velocity presented by Ferguson and Church (2004):

$$w_p = \frac{Rgd_p^2}{C_1 v + \sqrt{0.75 C_2 Rgd_p^3}} \tag{2.2}$$

where R is the submerged specific gravity $\left(R = \frac{\rho_p - \rho}{\rho}\right)$, g is the gravity, d_p is the nominal particle diameter (D_{50} was used), and v is kinematic viscosity of water, respectively. C_1 and C_2 are 20 and 1.1, respectively, based on shape factors associated with natural sediment (Ferguson and Church 2004).

The vertical distribution of eggs was captured by taking consecutive photos (1 per minute) during the first ~30 hours (Nikon D7100 camera, 24.1MP) over a straight test-section of the flume (Figs 4.1b and 4.1c). Egg trajectories and their interaction with a flat sediment bed were also recorded through 10-min videos every 4 hours at 60 fps (Nikon D5300, 24.2MP). After eggs hatched, the same analysis was conducted to evaluate swimming behavior of larvae until ~80 hours. The 0.40 m water depth in the images was divided into 9 equal intervals (0.044 m each) to count the number of eggs or larvae detected in each interval (1 minute). Nearly translucent eggs were visible in the images due to the opacity of the yolk. Once they hatched,

approximately 27 hours after fertilization, larvae were almost transparent, hard to see with the naked eye, but identifiable against the lit background. At approximately 60 hours post fertilization, pigmentation in the eyes and back of the larvae increased, allowing for easier detection.

Vertical distributions were then plotted through the duration of the experiment, showing different patterns at various fish development periods. Three developmental periods were defined:

Period 1 - embryonic stages; eggs prior to hatching (0 to 27 hours depending on the water temperature; developmental stages 8-30 (Yi et al 1988)), which drift passively and settle in the absence of turbulence.

Period 2 - after egg hatching and before gas bladder emergence (27 to 65 hours; stages 31-36 (Yi et al 1988)); in laboratory studies, this stage is characterized by vertical swimming and falling (George et al 2017).

Period 3 - after gas bladder emergence (65 to 90 hours; stages 37-39 (Yi et al 1988)). This period is characterized by horizontal swimming and the ability to maintain vertical position without swimming. Larvae of this period are often captured in off-channel low velocity habitats (George et al 2017), which are often considered nursery areas for grass carp and, where development to older juvenile stages occurs.

In period 3, when fish began swimming horizontally, the horizontal swimming speed (u_{sw}) was defined as:

$$u_{sw} = U - u_t \tag{2.3}$$

where U is the mean flow velocity and u_t is the horizontal traveling speed, obtained from the absolute displacement between consecutive frames and defined as positive in the direction of the flow. Swimming speed is thus defined as positive if the larva moves against the flow, and negative in the same direction of the flow.

2.2.3. Flow Characterization in RTF

A different flow condition was applied in each trial. Flow is driven by a vertical-axis disk pump, controlled by a frequency inverter. A linear relationship exists between the assigned inverter frequency and the rotation speed of the disk pump, given by Ω [RPM] = 6.6 f [Hz]. For trial 1, a disk rotation rate of f = 10 Hz yielded a mean velocity of 0.08 m/s. For trial 2, f = 30 Hz

yielded 0.22 m/s, and for trial 3 f = 40 Hz yielded 0.30 m/s. These mean velocities were chosen to recreate three different scenarios of turbulence and sediment transport, with means speeds fast enough to keep eggs in suspension, but not too fast as to create large bedforms or sheet flow conditions able to sweep away all sediment from the test section. The selected range of velocities is also found in natural streams where grass carp eggs and larvae have been collected (e.g. the Sandusky river (Embke et al 2016)), where mean water velocities in some portions of the river rarely exceed 0.3 m/s (USGS gage station 04198008 near Wightmans Grove OH).

Vertical profiles of longitudinal velocity u (in the x-direction), transverse velocity v (in the y-direction), and vertical velocity w (in the z-direction), were measured by recording instantaneous velocities for 3 minutes at each point, at a sampling rate of 100 Hz. Measurements were taken at every millimeter in the z-direction along the first centimeter from the sediment bed, and then at every 2 centimeters until the free surface, using an Acoustic Doppler velocimeter (ADV, Nortek-Vectrino). Given the configuration of the ADV, no measurements were taken within the top 5 cm of the water column. From these ADV measurements, two dimensionless numbers (Reynolds (Re) and Froude (Fr) numbers) were estimated to characterize the turbulence ($Re > 4\text{x}10^3$ fully turbulent flow) and to readily identify subcritical ($Fr < 1$) and supercritical flows ($Fr > 1$) for each condition. Reynolds numbers are computed as $\boldsymbol{Re = UR_h/\nu}$, where R_h is the hydraulic radius. And Froude numbers are computed as $\boldsymbol{Fr = U/\sqrt{gH}}$. Turbulence statistics were calculated using Reynolds decomposition to obtain velocity fluctuations for each velocity component $(\boldsymbol{u', v', w'})$, as:

$$u' = u - U \tag{2.4a}$$

$$v' = v - V \tag{2.4b}$$

$$w' = w - W \tag{2.4c}$$

where u, v, w are the instantaneous flow velocities and U, V, W are the time averaged velocities. To evaluate turbulent statistics, Reynolds stresses, ($\langle u'v' \rangle$, $\langle u'w' \rangle$, $\langle v'w' \rangle$, indicators of fluxes of momentum in the flow), turbulence intensities, (u_{rms}, v_{rms}, w_{rms}), and turbulent kinetic energy, k, are thus calculated as:

$$u_{rms} = \sqrt{\overline{u'^2}} \tag{2.5a}$$

$$v_{rms} = \sqrt{\overline{v'^2}} \tag{2.5b}$$

$$w_{rms} = \sqrt{\overline{w'^2}} \tag{2.5c}$$

$$k = 0.5\left(\overline{u'^2} + \overline{v'^2} + \overline{w'^2}\right) \quad (2.6)$$

Friction velocity, $u_* = \sqrt{\tau_b/\nu}$, with τ_b as the bed shear stress, was calculated using two methods:

1. Fitting the measured velocity profile to the law of the wall (Schlichting 1979):

$$u^+ = \frac{1}{\kappa}\ln(z^+) + 5.1 \quad (2.7)$$

where $u^+ = u/u_*$, $z^+ = u_* z/\nu$, z is the vertical distance from the bed, and $\kappa = 0.41$ is the von Karman constant (Long et al 1993).

2. Using a turbulent kinetic energy approach, estimating shear stress as (Soulsby and Dyer 1981, Stapleton and Huntley 1995):

$$\tau_b = C_1\rho\left[0.5\left(\overline{u'^2} + \overline{v'^2} + \overline{w'^2}\right)\right] \quad (2.8)$$

where C_1 = 0.19 (Thompson et al 2003).

Different criteria exist to analyze the expected behavior of particles (eggs and larvae in our study) in suspension (Van Rijn 1984, Hearn 2008). We compared the settling velocity of the particle with the friction velocity and the vertical turbulent intensity, assuming that vertical fluctuations generated by the bed shear stress will overcome the settling speed to maintain the particles in suspension (Van Rijn 1984). Dimensionless ratios between vertical turbulent intensities, friction velocities, and settling velocity, were calculated to better explore the variable space regarding critical resuspension parameters. A suspension parameter, evaluated as the inverse of the Rouse number, Z_R, (Van Rijn 1984) was calculated as:

$$\frac{1}{Z_R} = \frac{\beta\kappa u_*}{w_s} \quad (2.9)$$

where $\beta = 1 + 2\left(\frac{w_s}{u_*}\right)^2$ is a coefficient related to diffusion of sediment particles, with a maximum value of $\beta = 3.0$. Following Hearn's criteria (2008) for sediment particles in suspension as bedload ($1/Z_R$ <0.4), approximately 50% suspended sediment (0.4<$1/Z_R$ <0.8), approximately 100% suspended sediment (0.8<$1/Z_R$ <1.3), or wash load ($1/Z_R$ >1.3), we classified the eggs as suspended particles using the inverse of Z_R.

2.2.4. Survival rates in RTF

On day 5 of each trial, surviving larvae were counted to determine survival rates. A water bath with similar water temperature as in the RTF (23-24°C) was used as a baseline to ascertain

survival differences with the RTF. The water bath (1.8 m *x* 0.9 m) housed 4 aquaria (0.3 m *x* 0.6 m *x* 0.3 m each) with hatching jars where a subset of eggs was kept under ideal oxygenation conditions and gentle upwelling flow to prevent external damage. Each aquarium kept 500 eggs during trial 1 and trial 3; but only 100 during trial 2. Water temperature in the water bath and RTF was monitored with HOBO temperature loggers (Onset Computer Corp) recording at 15-min intervals. A 500-gallon tank, refilled in every trial with well water from the same source, supplied the water bath and the flume throughout the experiments.

2.3. Results and discussion

2.3.1. Settling column test

Error bars were used to present the results for the settling velocities (w_s) and densities (ρ_s) of eggs at 6, 10, 14, 18, and 22 hours after fertilization (Figs 2.2a and 2.2b). These plots show almost no change between mean settling velocities and mean densities (middle squares) as the fish develops inside the membrane. Mean settling velocities of $7x10^{-3} \pm 3.5x10^{-4}$ m/s with standard deviations within each batch of $\{5.5 – 9.4\}x10^{-4}$ m/s were estimated. The ANOVA test revealed a p-value of 0.0538 (>0.05), which confirms that no significant difference exists between the mean settling velocities of water-hardened grass carp eggs at post-fertilization time. This result is consistent with previous experiments reporting a constant terminal fall velocity of $7.4x10^{-3} \pm 1.6\ x10^{-3}$ m/s (George et al. 2017).

Mean densities of $998.81 \pm 7.2x10^{-2}$ kg/m^3 with standard deviations within each batch of $\{7.7 – 31.5\}x10^{-2}$ kg/m^3 were estimated. This is a very narrow range of mean densities considering the wide range of diameter sizes (3 – 6 mm) (Fig 2.2c), which also falls within the constant range estimated by George et al. (2017) (999.87 ± 1.2 kg/m^3). The ANOVA test revealed in this case a p-value of 0.1019 (>0.05), which also confirms that no significant difference exists between the mean densities. The estimated density proves that grass carp eggs can be heavy enough to sink in still water but light enough to remain in suspension at low flow velocities, thus avoiding burial and abrasion with bed material. In addition, as discussed by George et al. (2017) this strategy provides for reduced mortality resulting from both sight-feeding and filter-feeding predators, and distributes the eggs and larvae broadly within the water

column, rather than creating easily-attacked concentrations at the sediment-water or air-water boundaries.

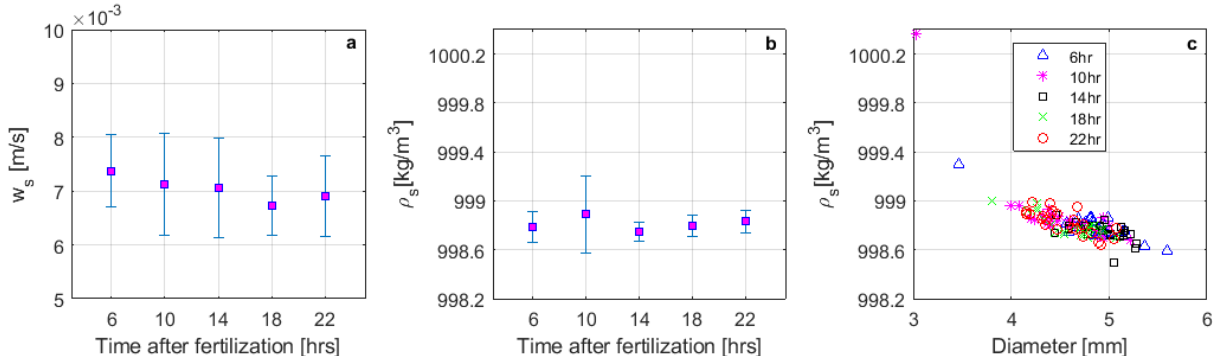

Fig 2.2. Settling column results for all 4-hour intervals after fertilization. (a) Error bars for egg settling velocity. (b) Error bars for egg density. (c) Comparison between egg diameter and egg density for all samples at each time interval.

4.3.2. Race-Track Flume test

4.3.2.1. Flow Characterization

Reynolds numbers of $Re = \{5 - 19\}\text{x}10^3$ and Froude numbers of $Fr = \{0.04 - 0.15\}$ were computed for the three mean velocities. These values indicate that all trials had fully turbulent and subcritical flow conditions. Vertical profiles of time averaged velocities are shown in Fig 2.3a,e,i. Data show low values of both V and W, below 5% of the longitudinal speed U. Fig 2.3 also shows turbulence intensity and turbulent kinetic energy, k, increasing with increasing mean velocity. Profiles of k (Fig 2.3b,f,j) show near-uniform values through the water column except for the expected peak near the bed. Reynolds stresses profiles show the expected large near-bed values of $\langle u'w' \rangle$ (Fig 2.3c,g,k).

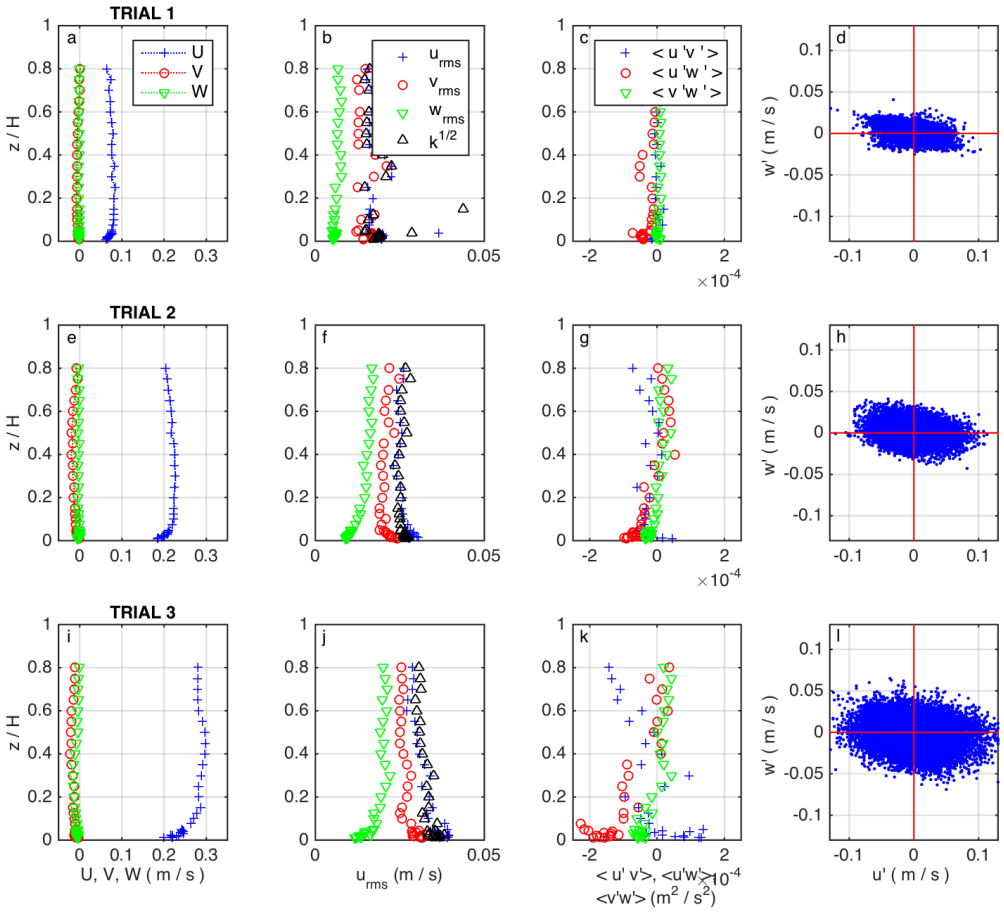

Fig 2.3. Flow and turbulence conditions over the flume's straight test section in each trial. (a,e,i) Mean velocities U, V, W. (b,f,j) turbulence intensities u_{rms}, v_{rms}, w_{rms} and turbulent kinetic energy k. (c,g,k) Reynolds stresses $\langle u'v' \rangle, \langle u'w' \rangle, \langle v'w' \rangle$. (d,h,l) Quadrant analysis from instantaneous velocity measurements 1 mm above the bed.

Friction velocity values were calculated as $u_* = \{0.47, 1.17, 1.39\} \times 10^{-2}$ m/s and $\{0.43, 1.19, 1.50\} \times 10^{-2}$ m/s, using log-law (Eq 2.7) and turbulent kinetic (Eq 2.8) approaches for the three mean flows studied, respectively, showing a good agreement between both methods (variation from 2% to 9%). Instantaneous turbulent fluctuations (*u'*,*v'*,*w'*) can be used to identify the presence of instantaneous events that may influence the resuspension of eggs and larvae and their interaction with the sediment bed. We identified a large proportion of instantaneous events where the instantaneous longitudinal velocity, *u*, fell below the mean value, whereas the instantaneous vertical velocity, *w*, was above the mean vertical component, leading to parcels of

fluid moving slower than the mean flow (i.e., $u'(= u - U) < 0$) experiencing an upwards displacement (i.e., $w'(= w - W) > 0$), an event commonly known as 'ejections'.

Another large proportion of events is represented by faster moving parcels displacing downwards ($u' > 0$, $w' < 0$), which are commonly known as 'sweeps'. Dominance of near-bed sweeps and ejections (Fig 4.3d,h,l) indicates a high frequency of events able to lift or re-suspend material from the bed into the water column. For eggs, with a density slightly above that of water, these events are sufficient to keep them in suspension even at the lowest velocities, as seen in previous studies (e.g. Garcia et al. (2015b)). For larvae, we also expect that these coherent flow structures help them stay suspended during period 2 when the larvae swim only vertically. However, once they reach period 3, they have the ability to swim and remain over less turbulent regions.

Moreover, we classified the eggs as suspended particles using the inverse of Z_R. Fig 2.4 shows calculated values of $1/Z_R$, as well as the ratios w_{rms}/W_s measured at several water depths, and the ratio friction velocity to settling speed u_*/W_s. Notice the agreement with Hearn's criteria, with an expected 100% of particles in suspension even at the lowest speed.

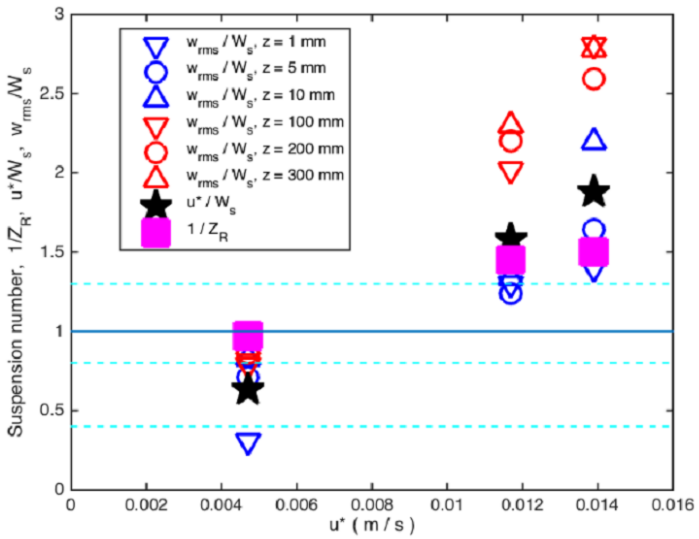

Fig 2.4. Suspension parameter $\frac{1}{Z_R}$, and ratios $\frac{w_{rms}}{W_s}$ and $\frac{u_*}{W_s}$ to classify eggs as suspended particles according to sediment transport criteria. Dashed lines mark delimiting values of the inverse of the Rouse number for bed load ($1/Z_R$ <0.4), approximately 50% of suspended sediment (0.4<$1/Z_R$ <0.8), approximately 100% of suspended sediment (0.8<$1/Z_R$ <1.3), and wash load ($1/Z_R$ >1.3).

2.3.2.2. Survival rates

Survival rates in the hatching jars for each trial were 53% in trial 1, 4.5% in trial 2, and 75% in trial 3; whereas in the RTF, where similar temperature with the hatching jars was maintained, were 51% (-3.8% with respect to the hatching jars) in trial 1 (low flow speed), 0.3% (-93.3% with respect to the hatching jars) in trial 2 (medium flow speed but low quality eggs), and 8% (-89.3% with respect to the hatching jars) in trial 3 (high flow speed), as shown in Table 2.1. Mortality for trial 1 in the RTF, with the lower flow speed (0.08 m/s), was not substantially different than the control jars, suggesting that there was very little impact of the physical processes on the eggs themselves at that speed. The eggs had optimal conditions for suspension (i.e., low turbulence levels, low shear levels, and fewer interactions and collisions with fast-moving sediment particles in suspension), avoiding abrasion or burial. Observations and recordings at the disk pump revealed that the shear generated by the rotating disks created a higher speed at the centermost region within pairs of disks. This velocity gradient pushed the eggs towards the center within parallel disks, avoiding collision with the disks themselves (S1 Videos in Supporting Information). The use of this flume, driven by a vertical axis disk pump, minimizes damage to the eggs and larvae due to the propulsion system in comparison to centrifugal pumps.

Mortality for trial 2, in both hatching jars and RTF, was mainly influenced by the poor quality of the eggs due to the high temperatures at spawning. In this trial, the physical processes of interaction with sediment particles or high turbulence levels were not the main factor driving mortality. For trial 3, at the highest speed considered (0.30 m/s), the combined effect of higher levels of turbulence and shear experienced by eggs and larvae, as well as abrasion by interaction with fast moving sediment particles in suspension, substantially increased mortality in comparison to the hatching jars (-89.3%). In this trial, the mortality rates were thus driven by a combination of these abiotic factors, but the contribution towards increased mortality from each individual process could not be quantified. This will be the focus of a future study, isolating pure turbulence and shear effects.

In this study, we registered some percentage of mortality in all trials in the hatching jars, with a minimum of 25% in trial 3. This confirms that mortality is always high in early life stages of fish (Houde 1997) and can occur due to purely biological reasons. George et al. (2015)

suggested that burial could be a major cause of mortality of grass carp at embryonic stages, and that settling can be detrimental to their hatching rates, even if they remain uncovered.

Table 2.1. Survival rates in RTF and hatching jars after experiment

Trial	Flow velocity [m/s]	Eggs stocked to flume	Survival rate in flume	Eggs stocked to jars	Survival rate in jars	Difference in survival rates between flume and jars
1	0.08	4000	51.0%	2000	53.0%	-3.8%
2	0.22	1604	0.3%	400	4.5%	-93.3%
3	0.30	4000	8.0%	2000	75.0%	-89.3%

2.3.2.3. Vertical distribution of eggs and larvae

For trial 1 (Fig 2.5a), in period 1, eggs were drifting mostly within the lower 75% of the water column, with relatively large abundance near the bed. In the vertical-swimming period 2, larvae were noticeably more uniformly spread throughout the water column. In period 3, larvae swam horizontally and remained suspended below the surface, in the top half of the water column, but slightly away from the free surface. Period 3 larvae showed preferential swimming far from the bed (avoiding higher shear and turbulence), and away from free surface (avoiding potential predators). Field collections of larvae in off-channel low velocity habitats often include period 3 larvae but rarely earlier periods (Yi et al 1988), thus selection of low velocity conditions detected in this study may be part of a volitional migration to nursery habitats.

For trial 2 (Fig 2.5b), in period 1, eggs spread almost uniformly across the water column, with a slightly larger number concentrated near the bottom. In period 2, as the survival rate was very low in the RTF (0.3%, only 5 larvae recovered out of 1,604 eggs), the experiment was stopped 2 hours after the end of period 1. In order to get data for period 3, at the end of trial 3, the surviving larvae in the flume (in stage 39) were tested with the velocity of 0.22 m/s to recreate conditions of trial 2. Under these flow conditions, larvae were able to swim and remain suspended preferentially near the surface and near the bottom, seemingly avoiding areas of higher speeds.

For trial 3 (Fig 2.5c), the vertical distribution of eggs and larvae was fairly constant throughout the experiment. Eggs and larvae were drifting more towards the bottom where they collided with the sediment particles that were also transported by the flow. Increased sediment

motion augmented the number of interactions of eggs and larvae with such rapidly-moving particles, increasing the potential for damage from abrasion, even though the eggs were in suspension. These interactions also affected the dispersal speeds of eggs and larvae across the water depth and their vertical distributions.

The vertical distributions presented in Fig 2.5 can be considered as a reference for research and management purposes in terms of eggs and larvae collection or sampling on field. Eggs and larvae show a prominent tendency to be located below the first quarter of the water depth, even with the fastest velocity presented, than near the water surface. This may support the fact that in previous field studies, e.g. Embke et al. (2016), researchers struggled to collect even a few eggs in what they called "the first direct confirmation of grass spawning in a Great Lakes tributary". They used paired bongo nets of 0.5 m diameter just below the water surface for an interval of 5 minutes during high-flow events on the Sandusky river. We recommend for future field campaigns the use of nets that allow sampling at lower depths to increase the probabilities of successful collection.

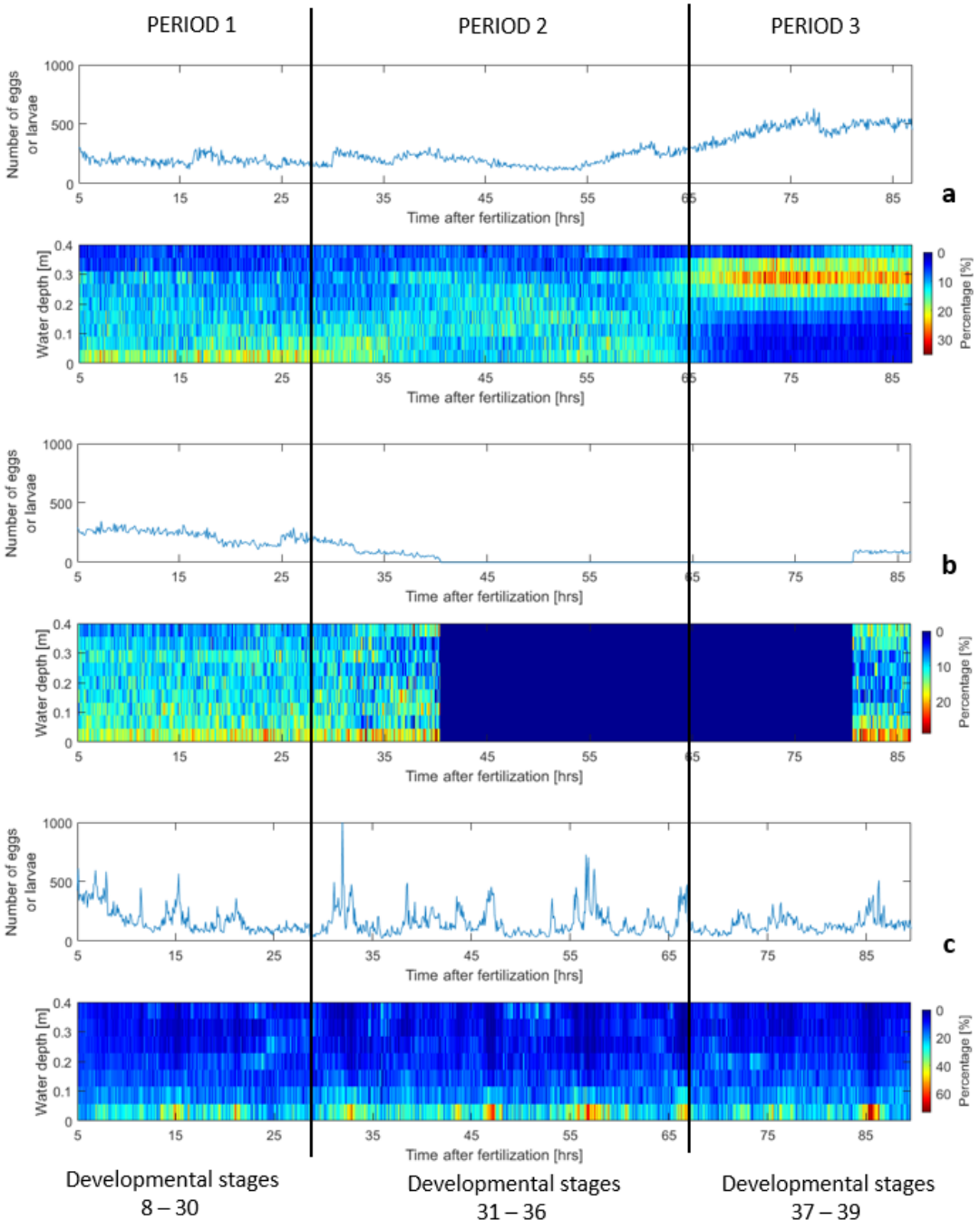

Fig 2.5. Vertical distribution of egg/larvae across the water depth and number of particles identified along the length of the experiments. (a) trial 1 (0.08 m/s), (b) trial 2 (0.22 m/s), (c) trial 3 (0.30 m/s).

2.3.2.4. Traveling and swimming speeds

Vertical traveling speeds of eggs and larvae were estimated over three regions of the water column: bottom (0 to 0.15 m from the bed), middle (0.15 to 0.30 m), and top (0.30 to 0.40 m) to quantify the effect of turbulence and coherent flow structures on drifting patterns (Table 2.2). In accordance with previous experiments (e.g. Garcia et al. 2015), we observed trajectories of eggs and larvae with both negative and positive slopes (Fig 2.6). Eggs moved downwards at speeds of up to $4.2x10^{-2}$ m/s in the middle of the water profile for the mean flow velocity of U = 0.22 m/s. This indicates that some of the eggs were not falling downward at their settling speed in the absence of flow ($\sim 7x10^{-3}$ m/s) but were being pushed downward by the flow fluctuations instead. Likewise, turbulent forces were also able to cause some proportion of eggs to rise at rates up to 0.048 m/s near the bed for the mean flow velocity of U = 0.30 m/s.

Larvae showed the active-passive drift mode described by Zens et al. (2018) (also called behavioral drift (Hogan 2005)), in which the larvae did not always actively swim, instead occasionally drifting with the current. The shape of the swimming path for larvae in period 2 for all flow speeds was a negative parabola (which opens downwards), where the focal length and general shape differ according to the speed of the water. Slower water produced a narrower, steep-sided parabola; and faster water produced a wider, more softly curving arc, showing a more active response from the larvae at higher flow speeds, compared to the behavior observed in the absence of flow (Chapman and George 2011). Vertical traveling speeds for larvae in period 2 were greater than those of the embryonic period, due to their vertical swimming capabilities; i.e. absolute vertical displacements were faster due to the parabolic self-movement. Conversely, for larvae in period 3, vertical traveling speeds are reduced compared to the period 2 since horizontal swimming is predominant at this stage.

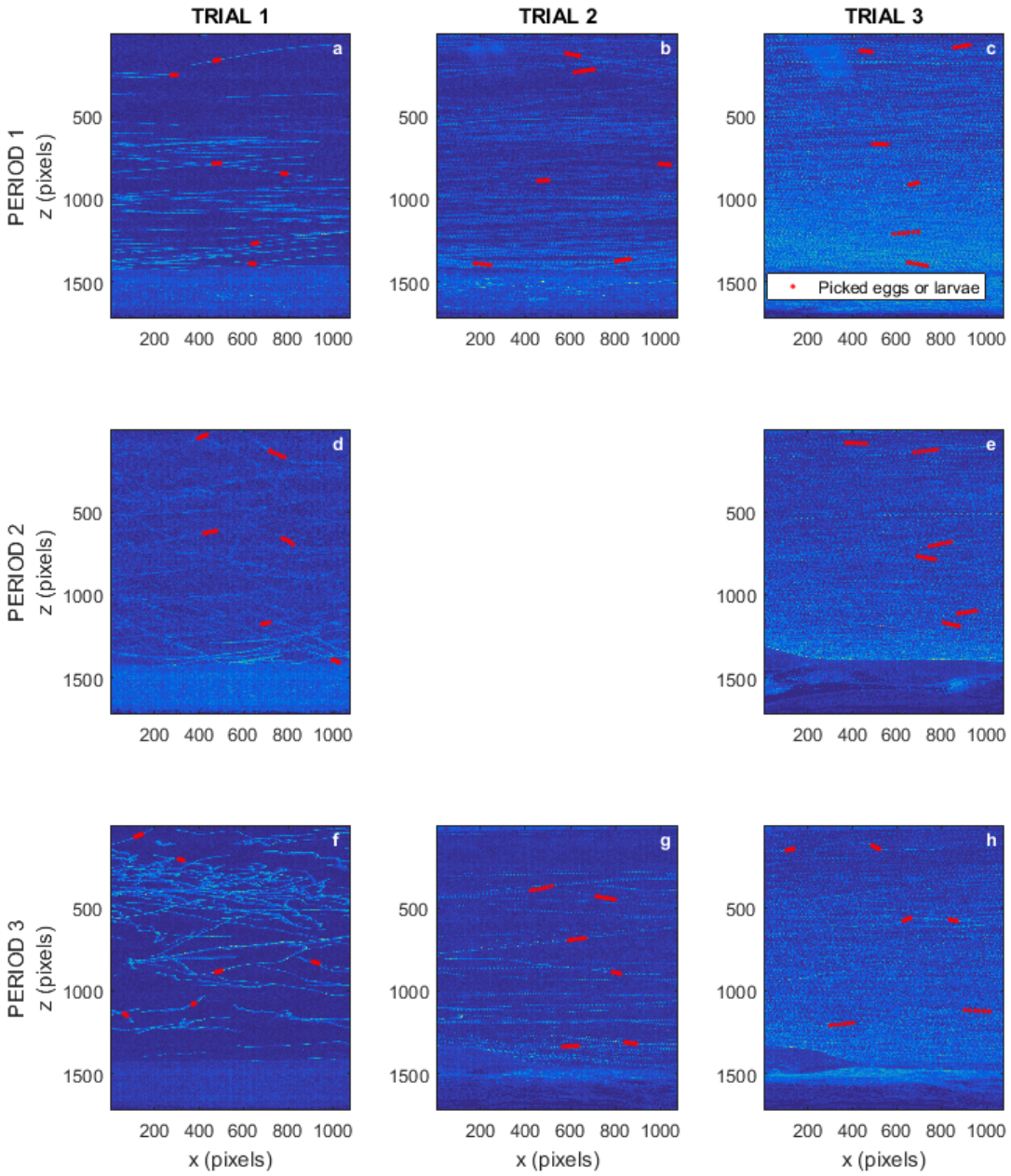

Fig 2.6. Composite images showing eggs and larvae trajectories at every developmental period and flow speed. (a,d,f) Trial 1. (b,g) Trial 2. (c,e,h) Trial 3. For developmental periods: Period 1 (a-c), Period 2 (d-e), and Period 3 (f-h). Red trajectories shown as examples of those used to estimate traveling and swimming speeds.

Table 2.2. Estimated minimum and maximum vertical traveling speeds, w_t, at each of the water profile regions defined. Bottom (0 to 0.15 m above the bed), middle (0.15 to 0.30 m), and top (0.30 to 0.40 m).

			w_t [$x10^{-2}$ m/s]		
Period	Developmental stages [27]	U [m/s]	BOTTOM	MIDDLE	TOP
1	8-30	0.08	-1.16 – 1.03	-1.25 – 0.64	-1.64 – 0.14
		0.22	-2.98 – 2.35	-1.04 – 1.18	-4.15 – 3.45
		0.30	-3.01 – 4.88	-2.42 – 0.52	-3.43 – 1.94
2	31-36	0.08	-2.62 – 4.36	-3.80 – 10.24	-5.60 – 10.40
		0.22	–	–	–
		0.30	-3.95 – 4.03	-5.54 – 4.25	-3.95 – 1.46
3	37-39	0.08	-2.33 – 3.76	-2.28 – 3.12	-4.13 – 1.84
		0.22	-0.97 – 2.08	-3.05 – 1.94	-6.02 – 4.60
		0.30	-3.64 – 1.87	-3.92 – 2.14	-2.42 – 4.92

Horizontal traveling and swimming speeds for eggs and larvae are presented in Fig 2.7. Eggs were traveling at close to the horizontal mean speed of the flow at any depth, which sounds intuitive, but provides the physical evidence to validate the streamwise drifting of grass carp eggs in numerical models such as FluEgg in its current form.

Larvae were traveling at different speeds than the horizontal mean flow speed, especially in the middle and top regions of the water depth. In period 2, the parabolic swimming trajectory of larvae in the direction of the flow increased also the horizontal traveling speeds. In period 3, larvae swim horizontally facing upstream and offering resistance to the flow. We observed that that resistance was higher as the flow velocity increased since the traveling speeds were very similar for both U = 0.22 m/s and U = 0.30 m/s, thus there were higher swimming speeds for U = 0.30 m/s. The results show that swimming capabilities of the larvae are not negligible and do have a large potential effect on dispersal. Period 2 larvae subsist entirely from endogenous nutrition and do not feed, but period 3 larvae must begin to feed. Rivers where grass carp have been found are typically turbid and carry large quantities of suspended alluvium. Such rivers have little primary productivity and low plankton availability, thus are poor habitats for a larval fish which must feed. In flowing rivers, period 3 larvae likely attempt to move from the river current into low velocity nursery areas (Yi et al 1988), and this swimming ability is fundamental in achieving that pivotal change in habitat from flowing river to low velocity feeding and growing areas.

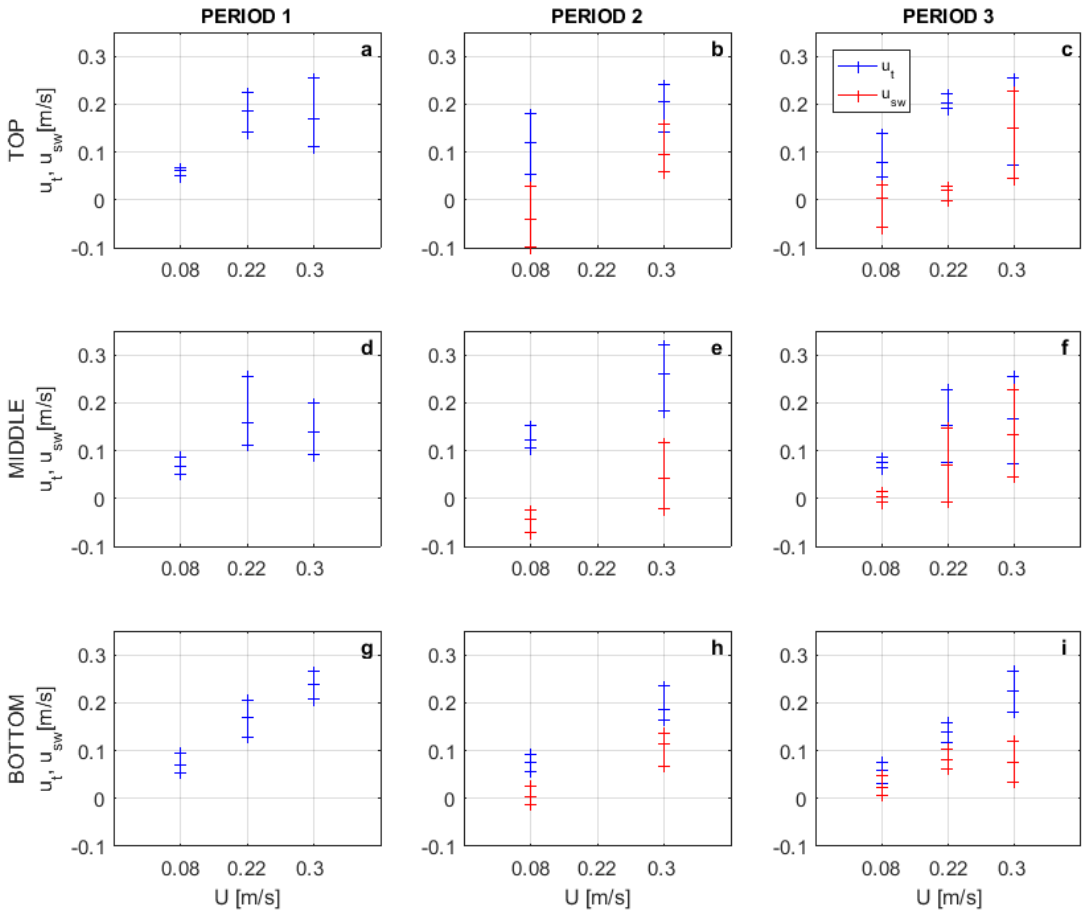

Fig 2.7. Ranges of horizontal traveling (u_t) and swimming speeds (u_{sw}). (a,d,g) Developmental period 1. (b,e,h) Developmental period 2. (c,f,i) Developmental period 3. For three regions considered across the water profile: top (a-c), middle (d-f), and bottom (g-i). Positive traveling speeds in the same direction of the flow. Positive swimming speeds against the direction of the flow.

Fig 2.8 shows the orientation of the larvae for all flow speeds at developmental periods 2 and 3, classified by their location in the water column. The inset in Fig 2.8c shows the orientation reference frame, with θ=0 degrees horizontally facing (opposing) the mean flow, and data divided in 45 degrees' ranges, positive in counter-clockwise direction. For the lowest mean flow (Fig 2.8a,d,g), we notice clear differences between developmental periods, with most larvae able to face the flow in period 2, tending to orient downwards in the bottom and middle sections of the water column, potentially in response to coherent flow structures generated at the bed pushing them towards the surface, and a clear shift once they reach period 3, with improved horizontal swimming abilities to face the oncoming flow within $\pm$45 degrees. For the fastest

flow (Fig 2.8c,f,i), there is a more uniform distribution during period 2, indicating a reduced ability of larvae to align themselves with the elevated flow speeds, and a clear shift as they reach period 3, now being able to withstand the current and align opposing the mean flow.

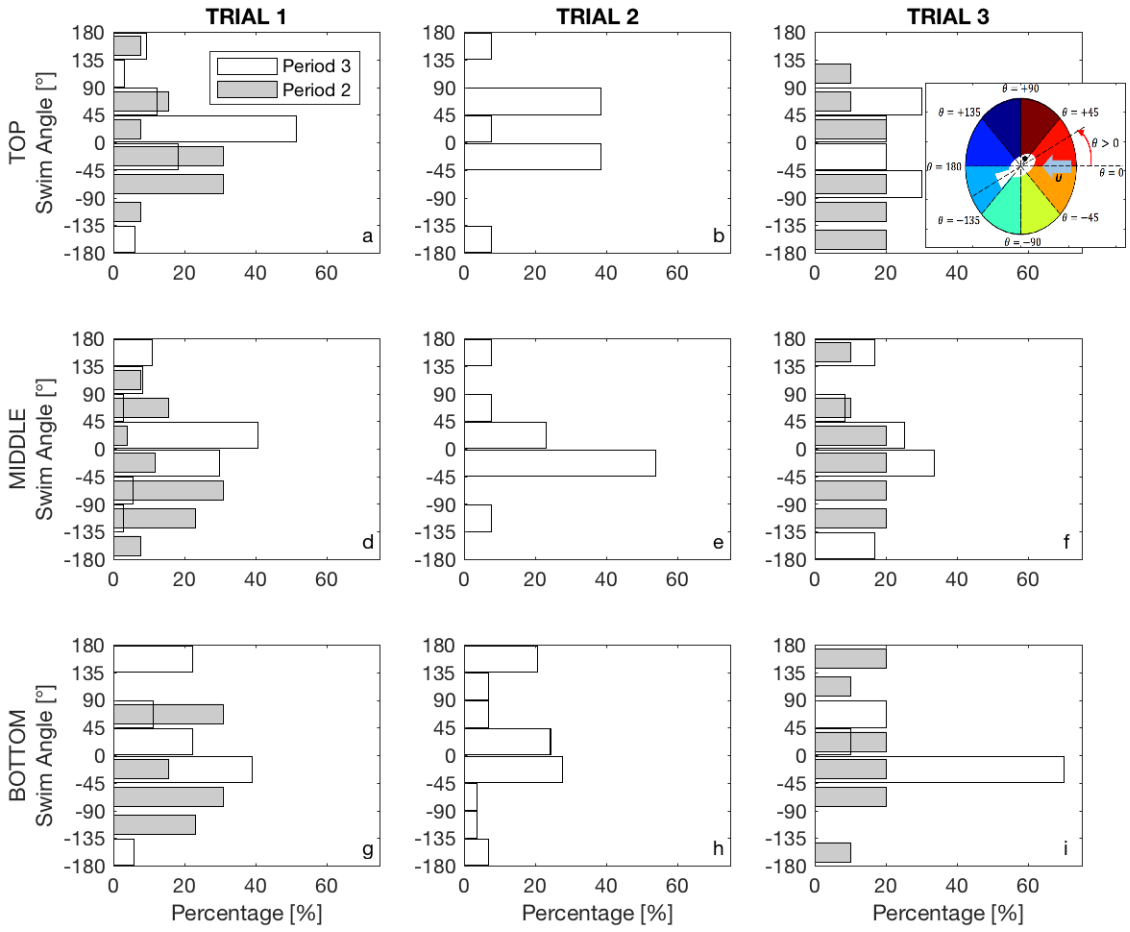

Fig 2.8. Swimming angle distribution of larvae at periods 2 (grey) and 3 (white). At least 20 larvae per water depth: top (a-c), middle (d-f), and bottom (g-i) were analyzed for each period on trials 1 (a,d,g), 2 (b,e,h), and 3 (c,f,i). Reference frame for swimming angle is indicated in the inset on *c*.

Mean values from Fig 2.7 for periods 2 and 3, from trials 1 and 3, were used to generate plots that allowed us to observe the influence of the gas bladder inflation in the horizontal swimming speeds of larvae (Fig 2.9). In Fig 2.9, we can see that the traveling speeds are reduced after the gas bladder emergence, and swimming speeds are increased; except near the bed for the case of the higher flow (Fig 2.9f). In this region, higher turbulent intensities and Reynolds

stresses are present as shown in Fig 2.3h and 2.3i and larvae showed preferences of swimming with the flow, increasing the traveling speed, instead of resisting it as in the middle or top of the water profile.

The swimming speeds opposing the flow direction in period 3 were never higher than the flow velocity, thus larvae always traveled in the same direction of the flow. This pattern was observed in all trials, even for the slowest flow velocity. Larvae adjusted their resistance to the flow proportionally to the drag forces exerted, but did not overcome the flow velocity to swim upstream. These findings provide physical evidence that will allow expansion of the capabilities of numerical tools (e.g. FluEgg (Garcia et al 2013)) towards predicting the transport of grass carp larvae, with larvae seemingly unable to swim upstream at the earliest life stages.

The observed swimming speeds can be used to estimate larval response once they are able to swim laterally towards the river banks or tributaries looking for nursery habitats, escaping from recirculation zones or areas of high turbulence levels. Because the early life stages of this species represent an important population bottleneck for survival and dispersal, the observed response to various flow conditions is paramount if sampling or collection campaigns are planned, or if management strategies are designed to either reduce the propagation of grass carp North America, or enhance the grass carp recruitment as is normally desired in Asia.

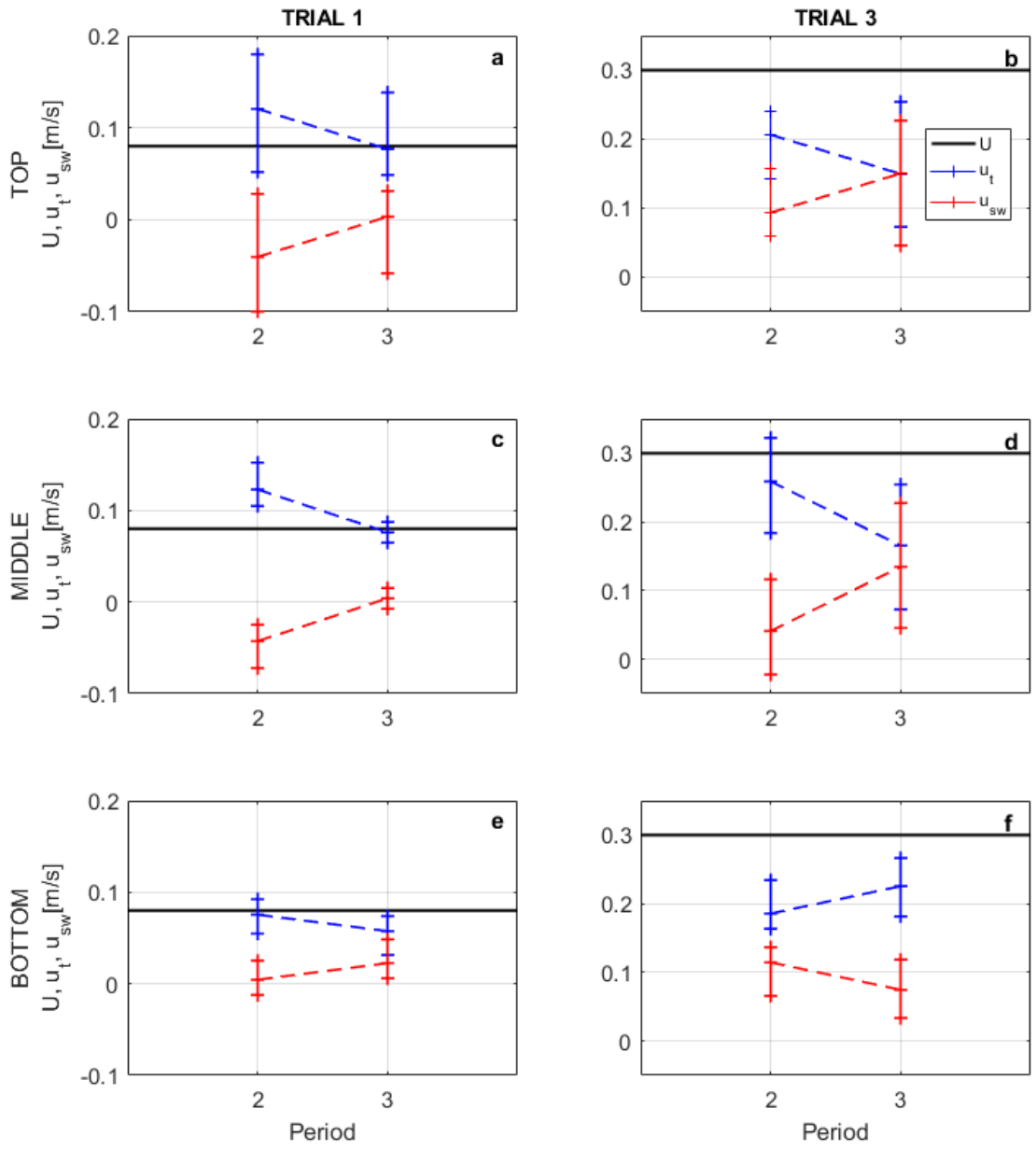

Fig 2.9. Variation of larvae traveling and swimming speeds between periods 2 and 3 analyzed at each of the three water profile regions. (a,c,e) Trial 1. (b,d,f) Trial 3. For each region in water profile: top (a,b), middle (c,d), and bottom (e,f).

4.4. Conclusions

Grass carp eggs and larvae were used to characterize the buoyancy of eggs, evaluate their drifting and swimming behavior in moving water, and estimate survival rates after their interaction with flow and sediment. Constant ranges of settling velocity and density of post-water-hardened eggs were found throughout the embryonic development (period 1) and were estimated as $7x10^{-3} \pm 3.5x10^{-4}$ m/s and $998.81 \pm 7.2x10^{-2}$ kg/m^3 respectively. This range of density makes the grass carp eggs heavy enough to settle in stagnant waters but light enough to drift even in gentle current. This property minimizes predation and damage that might result from contact with bed material.

Eggs (Period 1) were mainly distributed within the lower 75% of the water column for the three flow velocities analyzed, with a slight tendency to be more concentrated near the bottom. Larvae in period 2, against the slowest flow condition, were more evenly distributed throughout the water column, drifting with the flow on inclined trajectories of slopes of up to 78%. Larvae in period 3 had the ability to remain suspended (swimming) at preferential depths and offer resistance to the flow, with swimming speeds proportional to the flow velocity. This ability allows them to select nursery habitats on river banks or floodplain tributaries, escaping from recirculation zones or areas of higher turbulence levels. Similar depth distribution patterns were not found for the highest flow speed, in which the larvae have a decreased ability to withstand the flow and could not concentrate in preferential depths due to the increased drag exerted on them by the flow, and the increased frequency and intensity of turbulent events and coherent flow structures resulting from the enhanced turbulence field.

The highest velocity case also resulted in high suspended sediment concentrations in the water column, complicating visual identification of eggs and larvae traveling with large sediment particles, and affecting the dispersal speeds and the vertical distributions over time. A clear difference in vertical distribution of the eggs and larvae is found between trials 2 and 3, as mean velocity increases from $U = 0.22$ to 0.30 m/s and u_* goes from $u_* = 1.17 \times 10^{-2}$ to 1.39×10^{-2} m/s. This represents a change in the capability of the flow to keep particles in suspension, with both sediment and eggs and larvae facing stronger vertical velocity fluctuations for the 0.30 m/s case.

Temperatures at spawning directly influenced the quality of eggs and consequently the survival rates in hatching jars and in the RTF. Using control batches of eggs maintained under

ideal oxygen and temperature conditions in hatching jars as baseline (no damage due to interaction with sediment) we compared survival rates with those found under different flow conditions. The slowest flow studied, still energetic enough to keep eggs in suspension, yielded a survival rate similar to the hatching jars (only -3.8% in percentage difference with respect to the jars), showing optimal conditions avoiding burial and abrasion of eggs rolling in the bed, with minimal interactions with suspended sediment particles and low turbulence levels. The fastest flow, however, showed a significant increase in mortality, -89.3%. We attribute increased mortality to a combination of higher shear and turbulence experienced by the eggs and larvae, and abrasion by fast moving suspended sediment particles, although relative contributions of each process are still unknown.

These findings, along with the drifting and swimming speeds estimated, can be used to identify favorable hydraulic conditions for grass carp spawning and hatching, as well as to estimate more realistic dispersion coefficients to be applied in numerical models that simulate the fate and transport of grass carp eggs. The findings are applicable in North America, where successful reproduction by wild grass carp is generally considered problematic, and in Asia and other locations where enhancement of grass carp recruitment is considered beneficial. The decrease in survival resulting from higher turbulence is especially interesting because it might be useful in devising invasive fish control mechanisms that are based on increased turbulence which might be created by weirs or similar devices that are deployed during the carp spawning season. Changes in river morphology that remove such excess turbulence might be considered in areas where grass carp enhancement is desirable.

While further work is needed to investigate the influence of more realistic scenarios regarding bed morphology and the impact of turbulence levels in mortality, the interactions described by this study between the turbulent structures, eggs or larvae, and sediment, will allow us to reformulate prediction models (e.g. FluEgg, (Garcia et al 2013)), complement them with estimates of survival rates to expand simulation beyond the hatching stage, improve dispersal estimates, and introduce more realistic boundary conditions. While all of these measurements were performed on grass carp, grass carp have early life stages and behavior that are broadly similar to some other carps native to Asia, notably the bigheaded carps, which have achieved extremely high and problematic populations in the large rivers of the central United States. Thus, these results may be transferrable to those other species.

CHAPTER 3: INFLUENCE OF TURBULENCE AND IN-STREAM STRUCTURES IN THE TRANSPORT AND SURVIVAL OF GRASS CARP EGGS AND LARVAE AT VARIOUS DEVELOPMENTAL STAGES

3.1. Introduction

After being introduced in the United States in the 1970s for private aquaculture, grass carp (*Ctenopharyngodon idella*) and their relatives, the bigheaded carps (silver carp *Hypophthalmichthys molitrix* and bighead carp *H. nobilis*) moved into the Mississippi River basin where they became well established and are now considered highly undesirable invaders (Chick and Pegg 2001; Parker et al. 2016; Kočovský et al. 2018). These species are of particular ecological concern for their rapid population growth and their high consumption capacity (Conover et al. 2007). Specifically, grass carp can consume up to 40% of their body weight per day in aquatic vegetation (Laird and Page 1996). Reduction in aquatic vegetation may result in increases in turbidity and alkalinity, and depletion of dissolved oxygen (Lembi et al. 1978; Mitzner 1978; Leslie et al. 1983), as well as direct degradation of habitat of native fish species which depend upon macrophytes for all or part of their life cycle (Chilton and Muoneke 1992; Cudmore et al. 2012). Conversely, grass carp are a highly desirable species in their native rivers, where their populations have declined due in part to anthropogenic river modifications (Chapman et al. 2016).

Grass carp eggs need to be in suspension in the water column in order to achieve high hatch rates (Conover et al. 2007; George et al. 2015), which requires continuously flowing, turbulent flows to avoid settling. Increases in discharge are often correlated with spawning events, and studies in the Yangtze River also indicated a positive correlation between spawning activity and vorticity (for vorticity values in the order of 0.5 s^{-1}, Liu et al. 2018). However, temperature (between 15-30 °C) seems to be a primary driver of spawning behavior for grass carp and bigheaded carps (Schrank and Guy 2002; Coulter et al. 2016). Spawning of grass carp is proportional to the size and weight of the female, with an average spawn of 500,000 eggs for a 5 kg female (Shireman and Smith 1983; Chilton and Muoneke 1992). Eggs disperse in flow, from the spawning site to as far as 180 km downstream (Fedorenko and Fraiser 1978), although dispersal distance of eggs can also be relatively short depending on temperature and flow

conditions (Garcia et al. 2015; Embke et al. 2019). After hatching, larvae begin vertical swimming, which continues until gas bladder inflation (GBI), and the onset of horizontal swimming, when larvae can maintain depth and position within still water (George and Chapman 2015). In natural fluvial systems, larvae then begin to move from mainstem rivers into tributaries, backwaters, and other low velocity nursery habitats. At this point, larval grass carp must have enough swimming capacity to navigate through or avoid regions of higher turbulence, shear, and vorticity, where their natural undulating swimming style may be disturbed, and where larvae must spend more energy to maintain their position.

A strategy to prevent the spread of invasive carps, and reduce their population growth, is to identify survival and dispersal bottlenecks due to physical interactions between the early life stages and the riverine environment. George et al. (2015) showed a reduction in survival when eggs are buried by sediment, thus a balance between levels of turbulence sufficient to keep the egg suspended, but low enough to not damage eggs is necessary for survival. Understanding the response of grass carp to flow and turbulence during early life stages is fundamental to monitoring and controlling their spread. In natural fluvial systems, regions of high mixing levels (e.g. river confluences, rapids, behind sandbars, over vegetation canopies and gravel beds) are often used as spawning grounds (Jennings 1988; Chapman 2006; Stainbrook et al. 2007; Garcia et al. 2013), thus it is important to understand how mean and turbulent flow properties due to complex bed morphologies affect larval survival, dispersal, and behavior.

Prada et al. (2018) conducted laboratory experiments in moving water with live grass carp eggs and larvae in developmental stages 8-38 (blastula to GBI; based on stages described by Yi et al. 1988 and George and Chapman 2015), to quantify survival rates and observe drifting and swimming behavior under different flow conditions over a flat sediment bed. They showed vertical distributions of eggs and larvae within the water column over time. Eggs drifted mostly below the top quarter of the water column, with a slight tendency to be found more concentrated towards the bottom. Larvae were able to choose the regions with lower turbulence levels, e.g. far from the bed, as swimming capabilities developed. This initial investigation provides support for field campaigns, e.g. Embke et al. (2016) where researchers had difficulty collecting even a few grass carp eggs using ichthyoplankton nets deployed, near the water surface during high-flow events on the Sandusky River in Ohio. Prada et al. (2018) recommended sampling deeper in the

water column, to increase the probability of successful capture for future field collections, especially at lower water velocity and turbulence. However, this recommendation was made based on results over a flat bed, without the presence of in-stream obstructions typical of natural streams. More extensive analysis of experimental live-fish laboratory data is needed to identify more precisely where grass carp eggs and larvae are more likely to be found in rivers with complex river bed morphologies.

In this study, laboratory flume experiments were conducted to determine the drifting and swimming behaviors of live grass carp eggs and larvae with a constant flow velocity and three different in-stream obstructions: a gravel bump, a single cylinder, and submerged vegetation. Eggs and larvae were monitored continuously over ~85 hours as they drifted and swam and mortality rates were estimated in each scenario. Our objective was to compare the flow conditions generated by each bed morphology (streamwise flow velocity, turbulence, and vorticity) with commonly used locations of eggs and larvae across water depth, to improve the likelihood of detection during field collection.

3.2. Materials and methods

Three trials of experiments were conducted in a Race-Track Flume (RTF, Fig. 3.1), an Odell-Kovasznay type flume (Odell & Kovasznay, 1971), located at the Ven Te Chow Hydrosystems Laboratory (VTCHL) at the University of Illinois at Urbana-Champaign. The 6.0-m RTF has a 2.0-m long and 0.15-m wide test section where all measurements were taken (Fig. 5.1a). Temperatures in the flume were maintained at 23–24 ˚C using a submerged aquarium heater.

Grass carp were spawned by hormone induction and eggs were fertilized at the U.S. Geological Survey Columbia Environmental Research Center (CERC) in Columbia, MO. Fish were obtained from earthen ponds located at CERC. For trial 1, eggs were collected for fertilization from two female grass carp, both weighing 7.2 kg, and high-quality milt was collected from three male grass carp weighing 3.2, 3.2, and 2.0 kg. For trial 2, eggs were collected from one female grass carp, weighing 6.9 kg, and high-quality milt was collected from three male grass carp, weighing 2.5, 3.3 and 4.7 kg. For trial 3, eggs were collected from one female grass carp, weighing 2.6 kg, and milt was collected from two male grass carp, weighing

3.1 and 4.1 kg. Milt quality for the third spawning event was graded highly, but egg quality for this female was poor, as atresia had started. High fertilization rates were not expected.

In each trial, eggs were stripped into a bowl and fertilized with the combined milt from all males by the dry method (Piper et al. 1982), for 1 minute. Once fertilized, eggs were then rinsed and placed into a water bath for 30 minutes to allow water-hardening. Diameter from a subsample of 100 eggs was measured, using a Nikon SMZ-1500 stereomicroscope and NIS Elements software, as the mean of two perpendicular measurements, with a tolerance of 0.01 mm. Eggs were then stocked into polyethylene transport bags containing well water. Pure oxygen was used to fill the space above the water inside of the bags in order to keep the dissolved oxygen levels of the water from dropping during transport. The plastic bags were sealed and place into coolers for 4.5-hours transport to the VTCHL.

For all trials, 4000 eggs were released in the RTF, where water depth was maintained at H = 0.4 m above a 0.1-m thick sediment bed composed of a mixture of walnut shells and sand (bulk sediment density ρ_p = 1250 kg·m^{-3}, settling velocity w_p = 1.89x10-2 m·s^{-1}, and size {D_{16}, D_{50}, D_{84}} = {0.41, 0.54, 0.66} mm) (Prada et al., 2018). All substrate material was washed and dried in an oven at 170 F (77˚C) for 48 hours before each trial to help prevent biological contamination and control the spread of fungus. Flow in the RTF is driven by a vertical-axis disk pump, controlled by a frequency inverter. Frequency was set at f = 20 Hz for all trials.

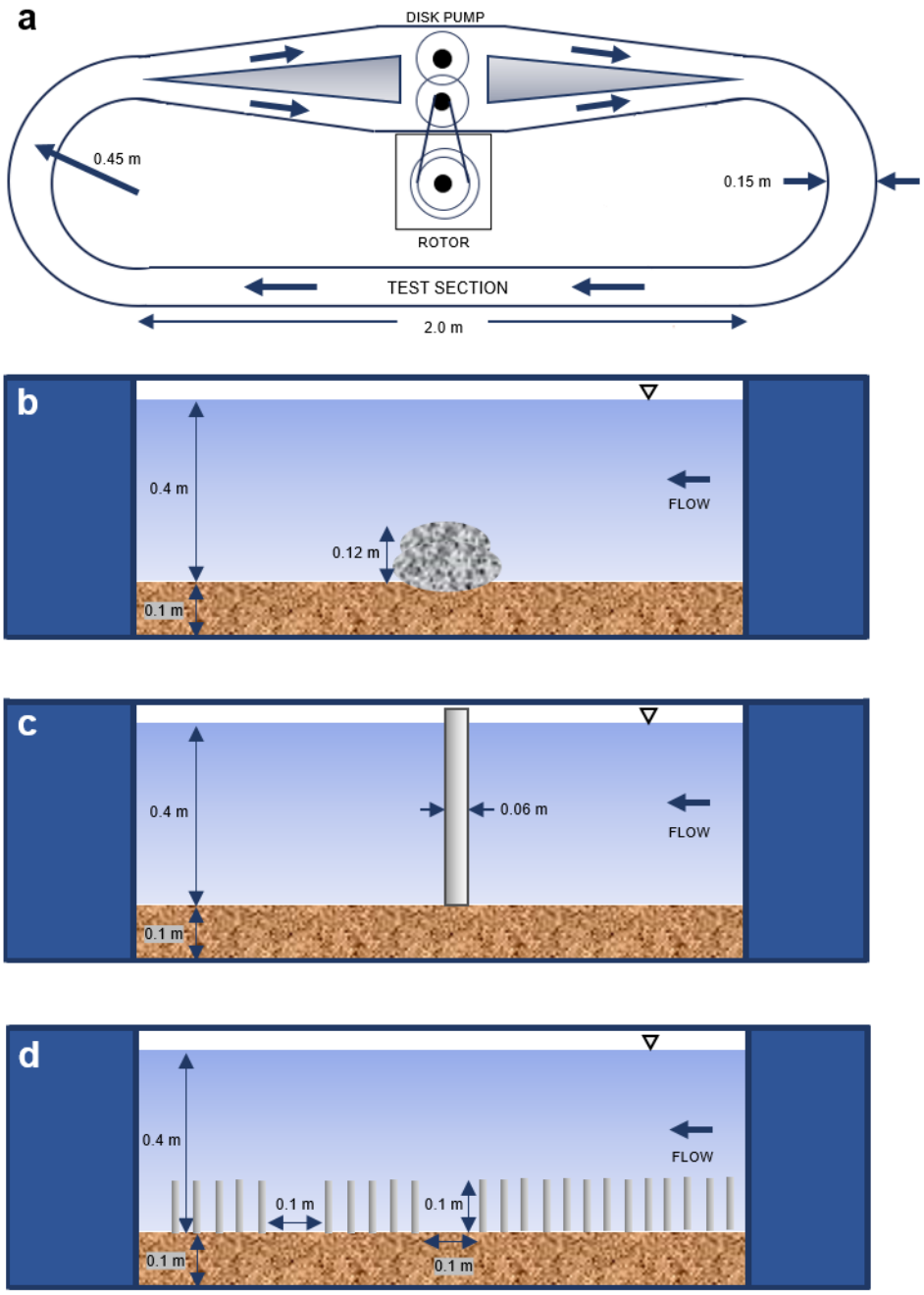

Fig. 3.1. Schematic view of the Race-Track Flume (RTF) (a), and side view of the studied in-stream obstructions (not to scale): gravel bump in trial 1 (b), single cylinder in trial 2 (c), and submerged vegetation in trial 3 (d)

The relationship between the inverter frequency and the rotation speed of the disk pump is given by Ω [RPM] = 6.6 f [Hz], so a frequency of 20 Hz corresponds to a disk rotation rate of 132 RPM, and an approximate mean velocity of 0.15 $m \cdot s^{-1}$ over the flat bed in the straight section of width-to-depth ratio of 3/8. The side walls may add no-slip boundaries that create viscous sublayers where flow velocity is reduced to zero and shear stresses increase. However, as reported by Prada et al. (2018), these boundary layers can be very thin, and may not affect the mean flow or the egg and larva distribution across the water depth.

Altered flows were created over the straight test section by 3 different in-stream obstructions, maintaining the same water depth (0.4 m) and forcing (f = 20 Hz – rotational frequency of the disk pump), to keep a constant bulk (cross sectional averaged) discharge. In trial 1, a 0.12-m high gravel bump, composed of gravel (mean size of 350 mm) contained in a mesh bag, was placed in the middle of the test section (Fig. 3.1b). For trial 2, an emergent 2" (51 mm) diameter-PVC cylinder was embedded in the middle of the test section (Fig. 3.1c), allowing for 49 mm of space between the cylinder and the walls of the flume. For trial 3, patches of submerged rigid acrylic rods (6.4 mm diameter and 100 mm in height), mimicking submerged vegetation, were placed in the sediment throughout the test section (Fig. 3.1d). The rigid vegetation followed a staggered configuration with average spacing between rods of 0.034 m, porosity of 6.3×10^{-3}, and volumetric frontal area 1.27 [m^{-1}].

3.2.1. Flow characterization

Flow fields were characterized, in both the RTF and the turbulence tank, using a 2D Particle Image Velocimetry (PIV) system, with a 60fps 5MP monochromatic camera and a 5W Continuous-Wave 532nm Laser. A vertical laser sheet was generated to illuminate neutrally buoyant silver-coated hollow glass spheres with a mean diameter of 10 μm.

In all trials, the camera was placed laterally at 0.8 m from the flume's test section and the laser sheet was generated from top, parallel to the mean flow at the in-stream obstruction. However, for trial 3 (simulated vegetation), a small gap of 0.1 m was set in the middle of the section to take the PIV measurements (Fig. 3.1d).

Images were processed using the GUI-based open-source tool PIVlab in MATLAB® (Thielicke & Stamhuis, 2014). Pairs of consecutive frames were cross-correlated to estimate the most probable particle displacement in small interrogation windows. The correlation matrix was

computed by applying a discrete Fourier transform (Soria, 1996), and a spline window deformation was used as interpolator. This cross correlation provided us with instantaneous velocity fields $\vec{u}(x,z)_i = \left(u_x(x,z), u_z(x,z)\right)_i$ across the illuminated area, where x is the horizontal coordinate increasing downstream from each obstruction and z is the vertical coordinate increasing upwards from the sediment bed.

Instantaneous velocity fields were time averaged to obtain the mean streamwise velocity $\vec{U}(x,z) = \overline{\vec{u}(x,z)_i}$. Reynolds decomposition was applied to estimate turbulent fluctuations as $\vec{u}'(x,z)_i = \vec{u}(x,z)_i - \vec{U}(x,z)$, and then compute turbulent kinetic energy (k) and Reynolds stresses (τ_{xz}) as

$$k(x,z) = 0.5\left(2\overline{u_x'^2(x,z)_i} + \overline{u_z'^2(x,z)_i}\right) \tag{3.1}$$

assuming $u_x' = u_y'$. And

$$\tau_{xz}(x,z) = \rho\left(\overline{u_x'(x,z)_i \cdot u_z'(x,z)_i}\right) \tag{3.2}$$

where ρ is the water density. Vorticity was also computed as (with negative vorticity as clockwise rotations):

$$\vec{\omega}(x,z) = \vec{\nabla} \times \vec{U} \tag{3.3}$$

3.2.2. Survival rates

A subset of eggs in each trial was kept in hatching jars with a gentle upwelling current to provide oxygenation and a similar water temperature to the RTF, at 23–24 ˚C, maintained with a submersible heater and monitored with HOBO® temperature loggers (Onset Computer Corporation, Cape Cod, Massachusetts) as a baseline to ascertain survival differences (% diff = (% flume - % jars)*100 / % jars). Each hatching jar housed 500 eggs during trials 1 and 2; but only 100 during trial 3 due to the poor-quality eggs. A 500-gallon tank, refilled as needed with well water from the same source, supplied the water bath and the flume throughout the experiments. On day 5 of each trial, the percentage of surviving larvae in the RTF was computed and compared against the percentage of surviving larvae in the water bath.

3.2.3. Eggs and larvae spatial distributions

Drifting and swimming behavior of eggs and larvae was recorded for ~85 consecutive hours in each trial with two side-looking cameras, both placed at 0.5 m from the RTF's test section, one next to each other. LED Edge Lit panels (Knema, LLC) were used to illuminate the test section from behind, creating a uniform illumination field. A Nikon D7100 camera (24.1MP) was used to take time-lapse photos (1 per minute) to generate 1D and 2D plots of transient distributions of eggs and larvae across the water column. For 1D plots, custom MATLAB® scripts were developed to detect the centroids in each photo, store, and count the number of particles within 9 equal intervals (0.044 m each) in the 0.40 m of water depth. These scripts were also used to determine the swimming angle with respect to flow with the coordinates (x and y) of the head and tail of each larvae used as reference points. The reference frame for orientation set $\theta = 0°$ horizontally facing (opposing) the mean flow with 45 degrees increments (positive in counter-clockwise direction). Fifty larvae were selected from each test, from throughout the water column, from non-consecutive frames (we selected 5-10 larvae from each frame, and selected frames that were at least 1000 frames apart to avoid counting the same larvae multiple times).

For 2D plots, a custom MATLAB® script was developed to estimate percentage distributions of eggs and larvae found on 500 images at every developmental period, thus identify in more detail the spots of higher probability for successful sampling downstream of each obstruction.

A Nikon D5300 camera (1920 x 1080 video resolution) was used to record 10-min videos (30 fps) every 4 hours, to observe drifting and swimming pathways of eggs and larvae based on each flow condition and the dependence on developmental stage. Plots of egg and larval trajectories were generated from consecutive frames extracted from the videos, which were processed to take the maximum of pixel intensities from groups of 300 frames. An extra test was conducted with the euthanized larvae on day 5 of each trial. Dead larvae were released back to the flume to record an extra 10-min video in each trial to compare their trajectories with live larvae. This test allowed us to determine whether live larvae can actively identify and swim towards specific desired locations within the flow, or if they are just drifting and being captured in recirculation zones as inert particles.

3.3. Results

3.3.1. Flow characterization

The in-stream obstructions created regions with a large contrast in mean velocity, turbulent kinetic energy, and vorticity. In the case of the gravel bump (trial 1), the resulting map of the streamwise flow velocity (Fig. 3.2a) shows values ranging from 0 to 0.2 $m{\cdot}s^{-1}$. Flow moved faster, at a magnitude of 0.2 $m{\cdot}s^{-1}$, on top of the gravel bump, and sharply transitioned towards a mean 0 $m{\cdot}s^{-1}$ immediately downstream of the bump. In this sharp transition in the velocity profile there is a region of high k and ω (Fig. 3.2b-c). Values of k_{max} = 1.5 $m^2{\cdot}s^{-2}$ and $\omega_{max} = -8\,x10^{-3}$ s^{-1} were estimated in this region. Trajectories of "inert particles", eggs (Fig. 3.2d) and dead larvae (Fig. 3.2f), were almost uniformly distributed throughout the flow. However, live larvae in stage 38 (Fig. 3.2e), capable of horizontal swimming after GBI, avoided the region of high k and ω, and actively sought low-energy flow regions.

For the single cylinder (trial 2), the flow field maps (Fig. 3.3a-c) show a reduced streamwise velocity in the wake behind the cylinder, as well as increased k and ω across the water depth. Figure 3.3a shows the velocity recovery as water moves past the cylinder, going from near 0 $m{\cdot}s^{-1}$ mean speed to around 0.1 $m{\cdot}s^{-1}$. Figure 3.3b shows the spatial evolution of turbulence along the wake, with k_{max} = 2.0 $m^2{\cdot}s^{-2}$. Figure 3.3c shows a range of vorticity between $-1x10^{-3} < \omega < 1x10^{-3}$ s^{-1}, as opposing eddies were distributed throughout the test region.

Trajectories of eggs and larvae (live and dead) at the same location (Fig. 3.3d-f) show that although high levels of k and ω are almost evenly distributed across the water depth, there are fewer larvae (both dead and alive) near the free surface within the wake of the cylinder. There is also a larger accumulation of larvae than eggs near the bed, with a tendency of live larvae to be found in that area; in contrast to dead larvae that (while still passing in greater numbers near the bed) follow a more linear trajectory past the cylinder.

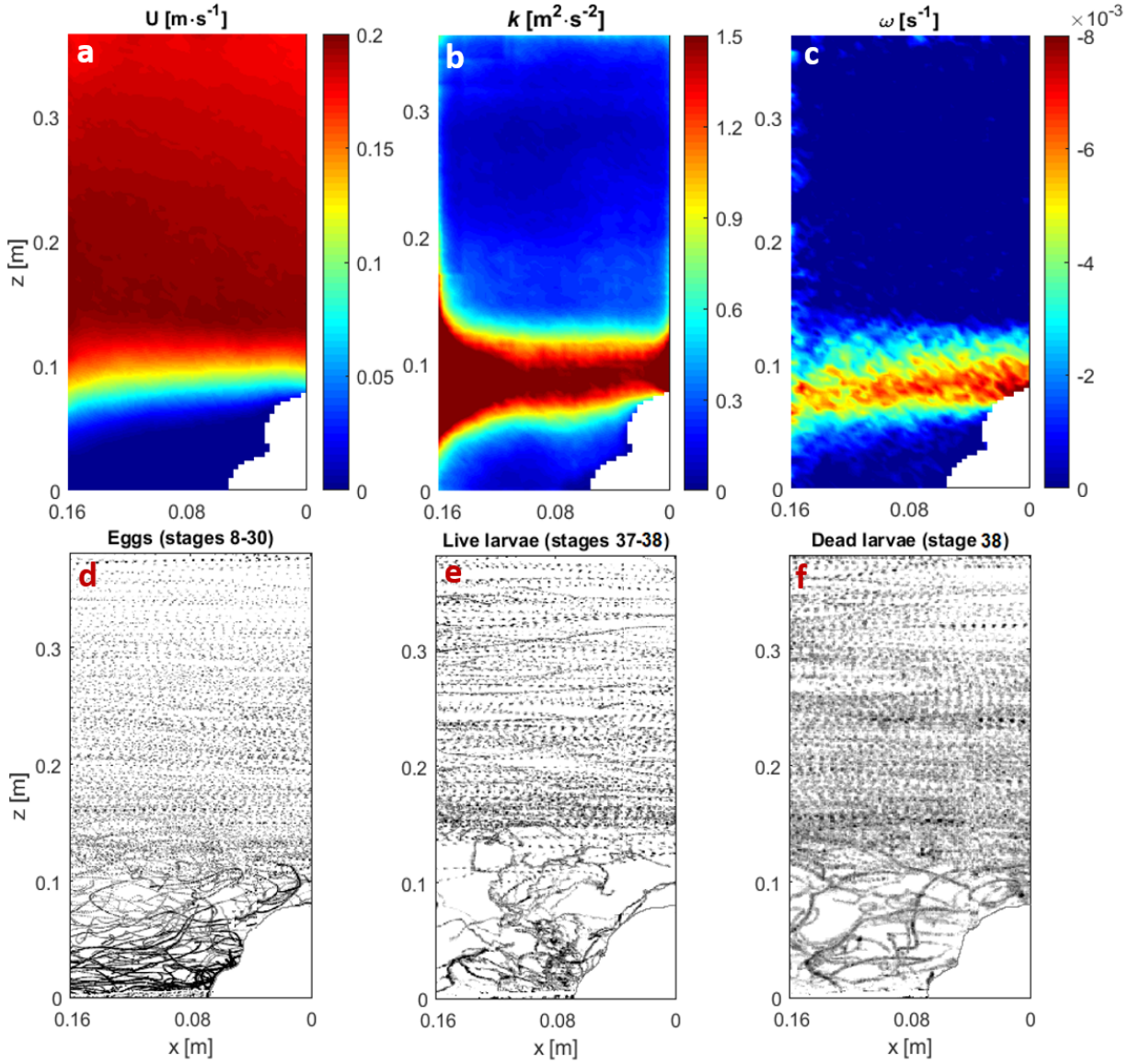

Fig. 3.2. Maps of flow conditions and trajectories of eggs and larvae under the presence of the gravel bump in the middle of the straight section. (a) Map of streamwise flow velocity. (b) Map of turbulent kinetic energy. (c) Map of vorticity. (d) Trajectories of eggs. (e) Trajectories of live larvae in stage 38. (f) Trajectories of dead larvae in stage 38.

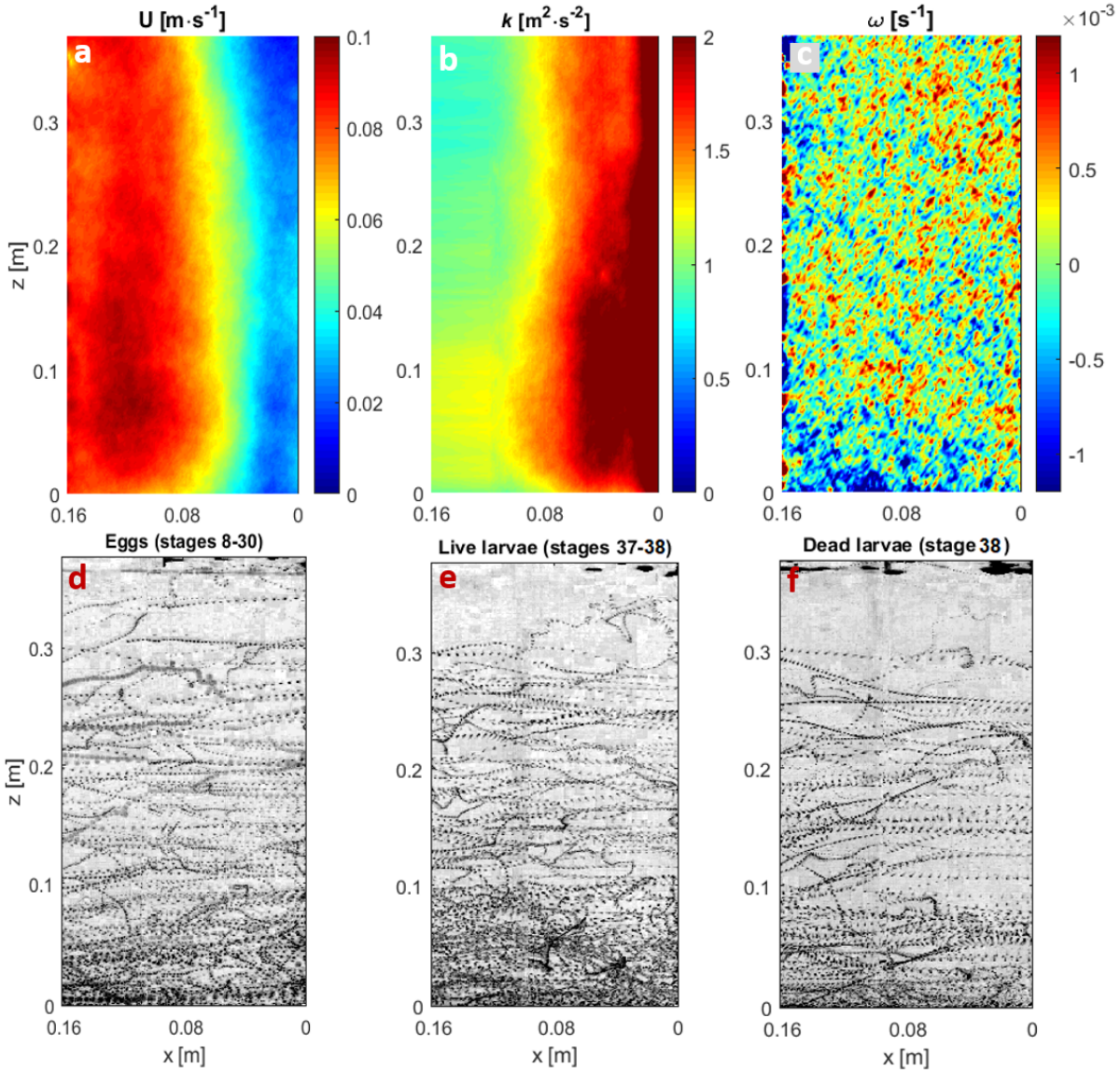

Fig. 3.3. Maps of flow conditions and trajectories of eggs and larvae under the presence of the single cylinder in the middle of the straight section. (a) Map of streamwise flow velocity. (b) Map of turbulent kinetic energy. (c) Map of vorticity. (d) Trajectories of eggs. (e) Trajectories of live larvae in stage 38. (f) Trajectories of dead larvae in stage 38.

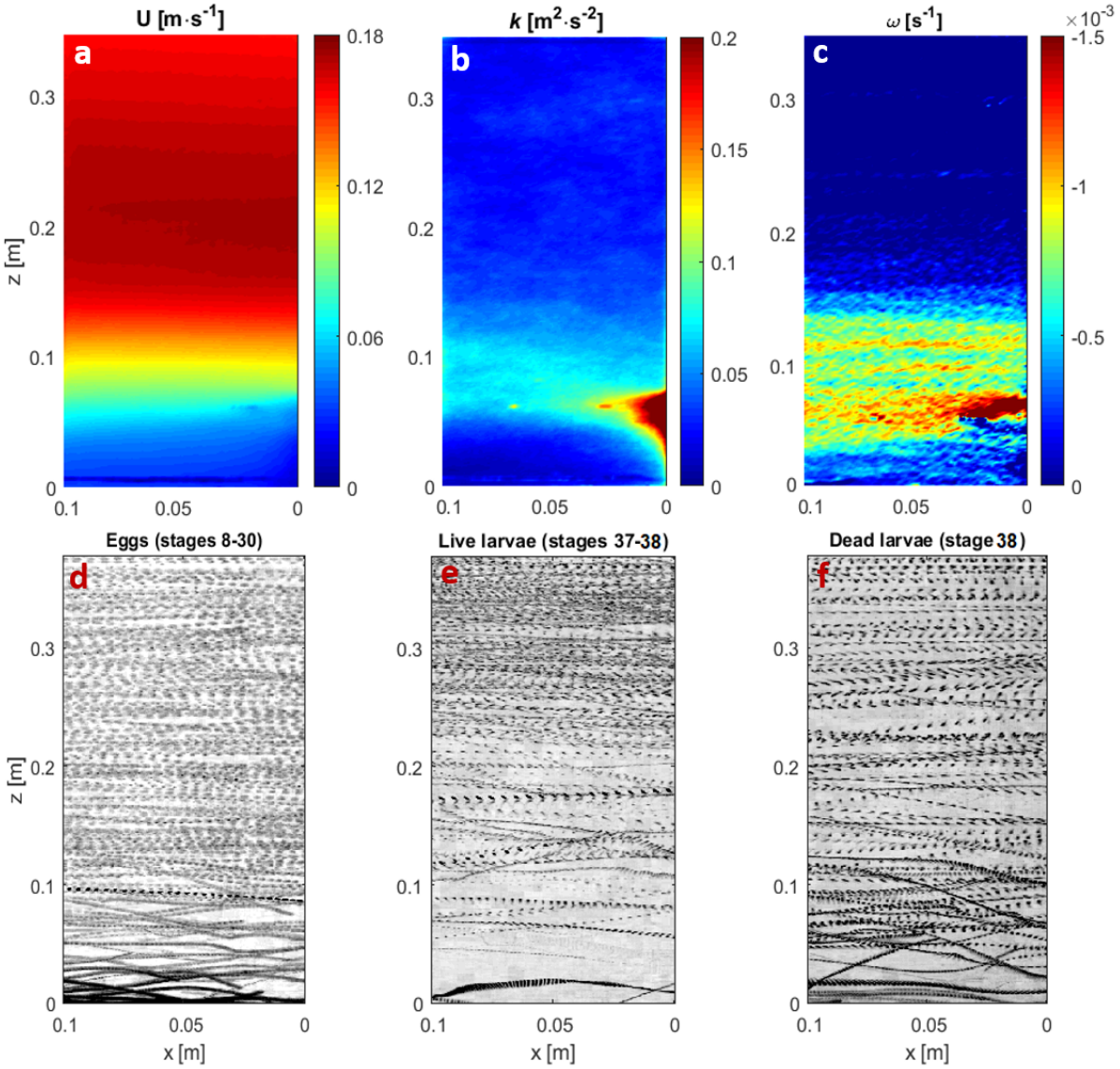

Fig. 3.4. Maps of flow conditions and trajectories of eggs and larvae under the presence of the submerged vegetation along the straight section. (a) Map of streamwise flow velocity. (b) Map of turbulent kinetic energy. (c) Map of vorticity. (d) Trajectories of eggs. (e) Trajectories of live larvae in stage 38. (f) Trajectories of dead larvae in stage 38.

For submerged vegetation (trial 3), velocity was damped within the array (Fig. 3.4a) due to the drag force exerted by the vegetation. Velocity decays from 0.18 $m \cdot s^{-1}$ at the free surface to less than 0.05 $m \cdot s^{-1}$ deep within the array. This transition, while not as sharp as the transition observed in trial 1 (gravel bump), generates a shear layer which produces similar turbulent kinetic energy and vorticity patterns as trial 1, though with lower magnitudes (k_{max} = 0.2 $m^2 \cdot s^{-2}$ and ω_{max} = -1.5$x10^{-3}$ s^{-1}) than in the gravel bump. Regions of low k (above and below the top of the array) show a clear shear layer with maximum k and ω at the top of the array (Fig. 3.4b,c). Drifting and swimming patterns for trial 3 vary amongst "inert particles" and live larvae. Eggs (Fig. 3.4d) are found almost uniformly within the water column, with slightly less accumulation deep within the array. Live larvae (Fig. 3.4e) accumulated near the free surface, as far as possible away from the array-generated shear, clearly avoiding regions of high shear and high k, while dead larvae (Fig. 3.4f) are similar in distribution to eggs, evenly distributed across the water column.

Live larvae most often oriented into the current, with at least 60% of larvae oriented between 45 and -45 degrees (Figure 3.5), regardless of the flow scenario. The orientation of dead larvae was essentially random, with approximately 50% oriented into the flow and 50% oriented away from the flow.

3.3.2. Survival rates

We compared survival rates for all trials against control test on hatching jars (as explained in Prada et al. 2018). There was a mortality of at least 55% in hatching jars, which can be attributed to biological causes since eggs and larvae were maintained under standard aquaculture conditions of oxygenation and temperature. Results of survival rates in both RTF and hatching jars can be found in Table 3.1.

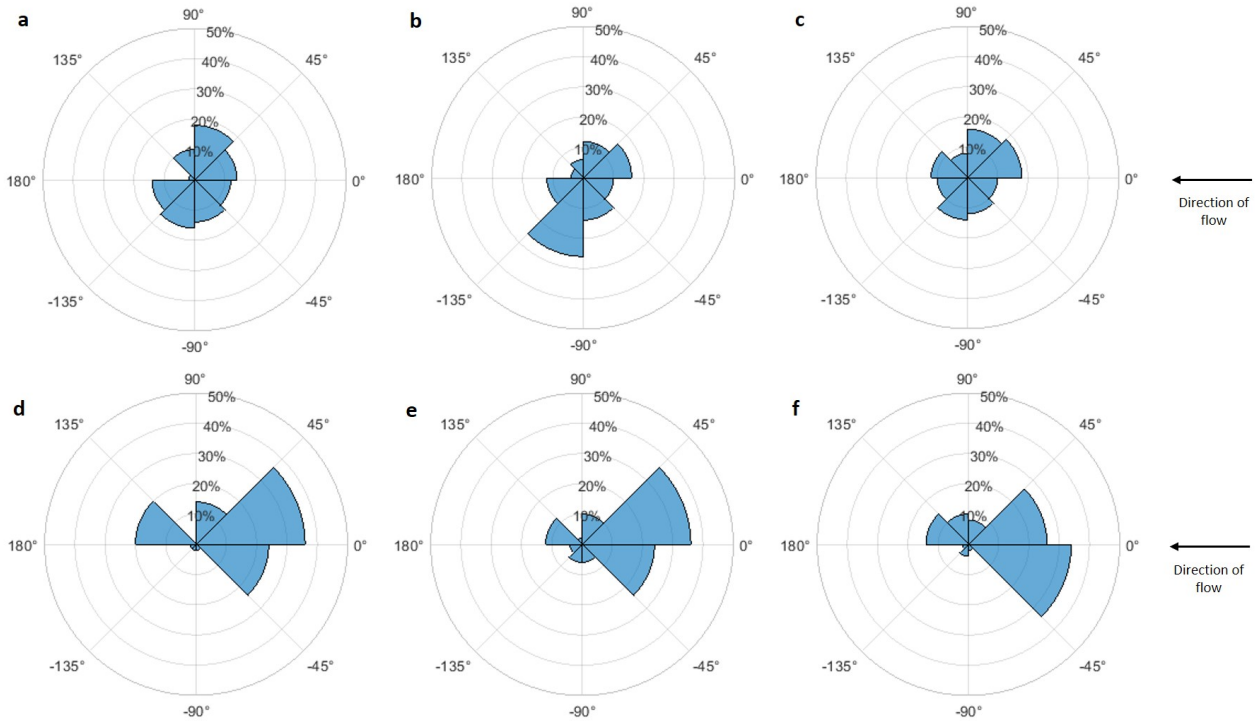

Figure 3.5. Swimming orientation distributions of dead and live larvae in relation to the mean flow with three different in-stream obstructions: a gravel bump, a single cylinder, and a submerged vegetation array. (a) dead larvae with a gravel bump. (b) dead larvae with a single cylinder. (c) dead larvae with a submerged vegetation array. (d) live larvae with a gravel bump. (e) live larvae with a single cylinder. (f) live larvae with a submerged vegetation array.

Table 3.1 Survival rates in RTF and hatching jars after experiment

Case	Eggs stocked to jars	Survival rate in jars	Eggs stocked to flume	Survival rate in flume	Difference in survival rates between flume and jars
Trial 1 - Gravel bump	2000	35.9%	4000	33.5%	-6.7%
Trial 2 - Single cylinder	2000	44.9%	4000	39.6%	-11.8%
Trial 3 - Submerged vegetation	400	5.5%	4000	3.4%	-38.2%

The poor quality of eggs in trial 3 due to atresia in the female injected for spawning highly affected the survival rates in this trial in both jars and RTF. Survival rates of only 5.5% and 3.4% respectively (–38.2% difference) were obtained in this trial, which subsequently affected the analysis of transient distributions of eggs and larvae across the water column. For the other two trials, survival rates were much higher than in trial 3, and also showed us that mortality was higher in the RTF, due to the eggs and larvae traveling through moving water, interacting with sediment and obstructions, and experiencing higher levels of turbulence both at the obstructions and at the disk pump (–6.7% and –11.8% difference in survival rates for trials 1 and 2 respectively).

In trial 1, some of the eggs in suspension were in contact with the gravel bump or settled for some time at the zone of low velocity and low turbulence downstream of this obstruction. However, they were not buried in the sediment; eggs were continuously picked up by passing eddies, thus the overall survival was not directly affected by the recirculation zone.

3.3.3. Eggs and larvae spatial distributions

A wide range in egg size was obtained amongst all trials (3–5 mm), which is a representative sample of the common range of grass carp eggs in natural settings (Korwin-Kossakowski, 2008). Nearly translucent eggs were visible in the images due to the opacity of the yolk. Once they hatched, approximately 30 hours after fertilization, larvae were almost transparent. Although difficult to see without proper illumination, larvae were identifiable against the lit background. At approximately 65 hours post fertilization, pigmentation in the eyes and back of the larvae increased, allowing for easier detection. A total of 4985 time-lapse photos was taken on trial 1, 5063 on trial 2, and 1920 on trial 3, all at 1-minute intervals. These pictures allow us to extract vertical distributions of particles detected through the ~85 consecutive hours of analysis (represented as colormaps in Fig. 3.6), along with the total number of particles detected at each time step (time series on top of each colormap on Fig. 3.6).

For trial 1 (Fig. 3.6a), in period 1 (developmental stages 8-30), eggs were detected mostly in the lower 50% of the water column, with about 40% of them just downstream of the gravel bump. In the vertical-swimming period 2 (pre-GBI, developmental stages 31-36), larvae were more evenly spread throughout the water column. In period 3 (post-GBI, developmental stages 37-38), larvae swam horizontally and remained suspended near the bottom, also downstream of

the gravel bump, but more concentrated with about 60% of them in this low-velocity area. Larvae in period 3 showed a clear tendency to swim towards zones of low turbulence and vorticity levels (Fig. 3.2b-c), and used the gravel bump as a shelter, with active swimming within that low turbulence and shear zone.

For trial 2 (Fig. 3.6b), the vertical distribution of eggs and larvae was fairly consistent throughout the experiment. Eggs and larvae were spread across the water depth although more concentrated towards the bottom, especially for larvae in period 3 (~30%). For trial 3 (Fig. 3.6c), in period 1, eggs spread almost uniformly across the water column, with a slightly larger number concentrated near the bottom. In period 2 of trial 3, because the survival rate was very low in the RTF (3.4%, only 136 larvae recovered out of 4,000 eggs), the experiment was stopped 2 hours after the end of period 1. At the end of trial 2, we predicted possible spawning issues could occur for our last trial (trial 3, submerged vegetation) due to atresia in the available females, which would result in low quality eggs and low survival rate. To ensure enough larvae to test our submerged vegetation scenario (trial 3), the surviving larvae from trial 2 (in stage 38) were used for testing the conditions of trial 3. As expected, the batch of eggs used for trial 3 allowed us to test the egg stage, but lack of successful hatching prevented us from using that batch for the larvae trials.

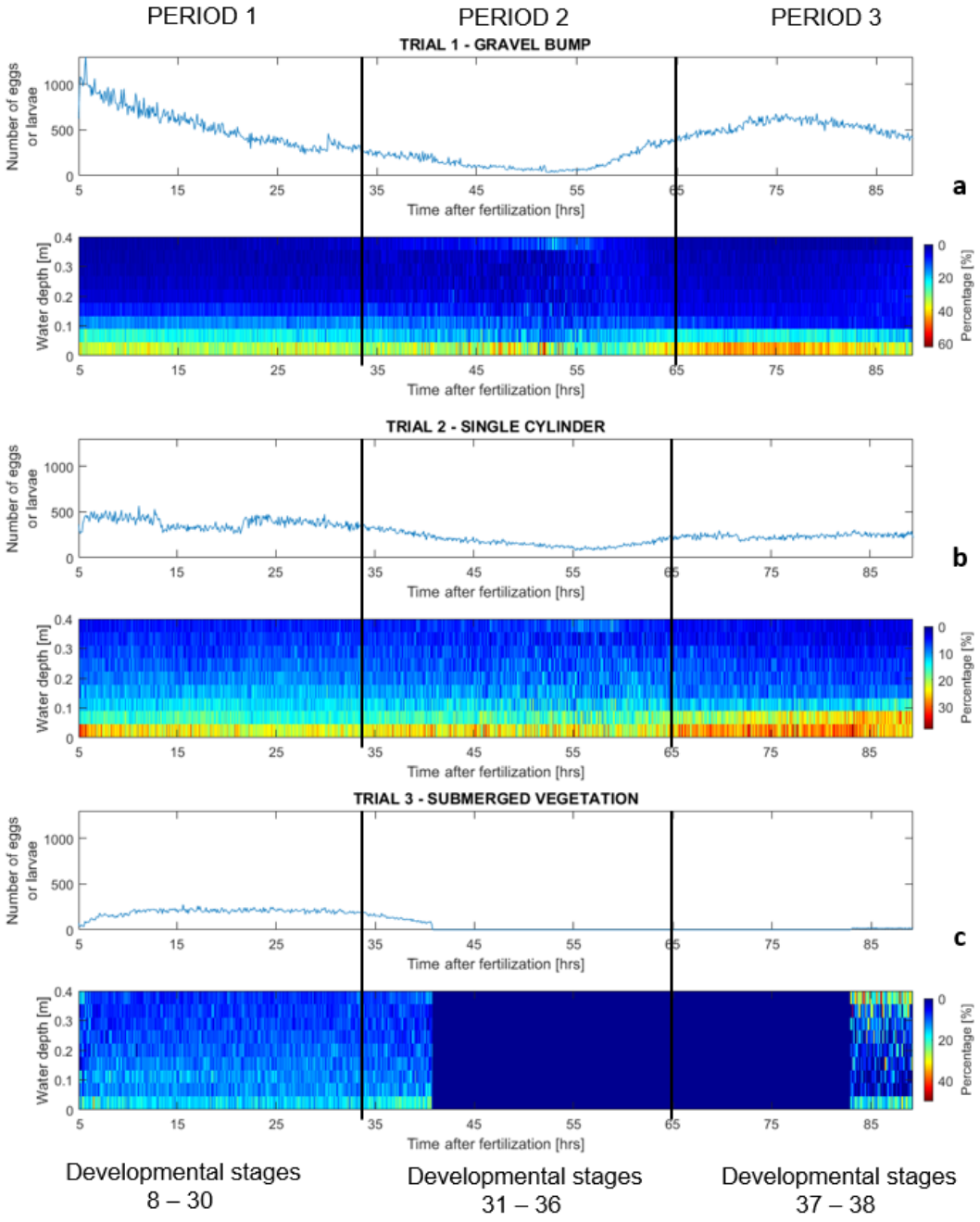

Fig. 3.6. Number of particles identified along the length of the experiments and vertical distribution of egg and larvae across the water depth. (a) trial 1 (Gravel bump), (b) trial 2 (Single cylinder), (c) trial 3 (Submerged vegetation).

Figure 3.7 shows the 2D plots of percentage distributions. Distances (x and y) in Fig. 3.7 were scaled using the water depth (h), and the obstructions, gravel bump and single cylinder, are just beyond the window of analysis, with the right border of the window corresponding to the downstream edge of the bump and the cylinder. In trial 1 (gravel bump), the majority of eggs and pre-GBI larvae were found within a distance no longer than about 0.20h from the downstream edge of the bump down in the region of low k. However, larvae in stages 37-38 were more likely to be found towards 0.3-0.6h downstream of the bump. In the other two cases, the single cylinder and submerged vegetation, eggs and larvae in both stages were more uniformly distributed within the window of analysis at the water depths observed in Fig. 3.6.

3.4. Discussion

In our characterization of the interaction between grass carp eggs and larvae with in-stream obstructions, we identified typical distributions of eggs and larvae throughout the water column in relation to turbulence and vorticity levels, and related turbulence to the rates of mortality of eggs in moving water. Survival of early life stages of fish is highly variable and mortality can result from any number of causes (Houde 2002), but the physical factors in this experiment can be important when considering natural mortality rates. In a previous experiment, Prada et al. (2018) reported an increase in mortality due to a combination of higher levels of velocity, turbulence, and abrasion by interaction with sediment particles on a flat bed. In this study, we also observed higher mortality rates due to interaction of eggs and larvae with sediment bed, in-stream obstructions, and high turbulence levels compared to the control jars. However, the in-stream obstructions did not substantially increase the egg mortality compared to Prada et al. (2018) where higher flow speeds caused: a) higher resuspension rates resulting in more egg-sediment interaction and abrasion, b) higher shear experienced by eggs and larvae as they passed through the disk pump, and c) direct impact with the disks at the highest speed. This is part of the motivation behind the turbulence tank study, to isolate the effect of pure shear and turbulence from sediment- and disk-interactions.

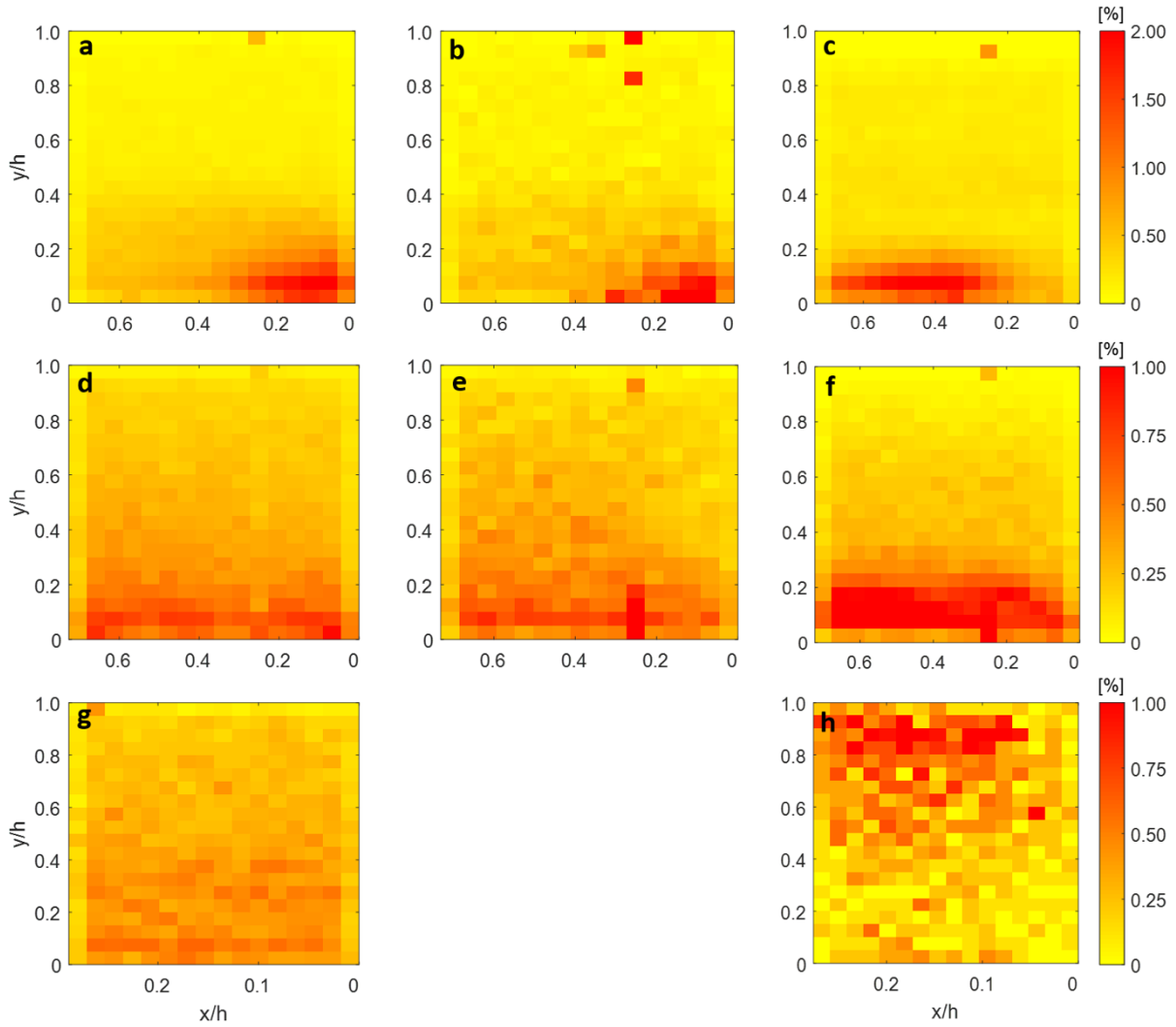

Fig. 3.7. Distributions of eggs and larvae downstream of each obstruction presented as a percentage. x-y axes were non-dimensionalized with the water depth (h). (a-c) Trial 1: eggs, pre-GBI larvae, and post-GBI larvae respectively. (d-f) Trial 2: eggs, pre-GBI larvae, and post-GBI larvae respectively. (g-h) Trial 3: eggs, and post-GBI larvae respectively. Note that the colorbar for (a-c) has a different scale.

Our vertical distributions in 1D and 2D (Fig. 3.6 and 3.7) provide insight into changes in behavior as the larvae hatch and develop their swimming capabilities. Consistent with George et al. (2018), larvae at GBI stages (37-38) showed strong active swimming capabilities including high maximum speeds that allowed them to search for and remain in areas of low shear and turbulence. As observed in Prada et al. (2018), larvae seldom exceeded the velocity of the water to travel upstream when in the main flow field, but did use short burst movements to escape zones of higher turbulence and shear. In areas with low turbulence and shear (e.g. behind the

gravel bump), movement occurred in all directions and at a range of velocities. Swimming abilities and speeds further increase with ontogeny, and more advanced larvae would be expected to be able to effectively use different areas of flow refuge when moving laterally from the mainstream river into nursery habitats. These capabilities were corroborated by contrasting the flow fields with trajectories and spatial distributions of both live and dead larvae. The trajectories followed by dead larvae were merely driven by the flow, instantaneous turbulent fluctuations, and coherent flow structures capturing larvae as inert particles suspended in flow, showing a behavior similar to eggs.

Comparing the flow fields in trials 1 and 3, we found some similarities in velocity profiles. Both are reduced towards 0 $m \cdot s^{-1}$ as flow interacts with the obstruction. However, there are two fundamental differences between these cases: 1) There is a clear recirculation zone behind the gravel bump, driven by large eddies on a vertical *x*-*z* plane, which propagates far downstream from the obstacle in trial 1; but no recirculation area within the gap in the array of rigid cylinders. 2) The gravel in trial 1 generated coherent flow structures mostly on the *x*-*z* plane, whereas the rigid cylinder array generated smaller stem-scale eddies on *x*-*y* planes. Thus, even if the flow speed was reduced within the array, larvae did not actively seek this region for shelter; they instead avoided this region.

Turbulent eddies created by the vegetation array scale with the diameter of individual cylinders (6.4 mm), which is close to the size of larvae (~10 mm). These results are specific for arrays of rigid cylinders, where a single relevant scale (i.e. stem diameter) drives the stem-scale turbulence generation. Flexible vegetation in the field could provide shelter for larvae due to the multiple length scales present in patches of flexible aquatic vegetation. A denser and more heterogeneous patch would allow for recirculation zones within the patch, more like the scenario in trial 1. However, our study with rigid cylinders allowed us to identify turbulence scales that were not attractive for grass carp larvae.

Although swimming biomechanics vary among species, fish larvae in general adopt a resistive swimming style, propelling themselves with undulations of their body, thus generating wakes and flows (Müller et al. 2000; Müller et al. 2007). The presence of coherent flow structures can further affect fish response to these flows, particularly if the size of the eddies is similar to the size of the larvae (Pavlov et al. 2000; Cada and Odeh 2001; Smith et al. 2014). As in previously reported in Prada et al. 2018, grass carp larvae were primarily oriented into the

flow (positive rheotaxis) at all water velocities and developmental stages tested. Prada et al. 2018 showed that although the percentage of fish exhibiting positive rheotaxis varied with developmental stage, flow velocity, and position within the water column, orientation into the flow was consistent (with levels exceeding 60%) at all tested stages, positions, and velocities.

Eddies of the same size as the larvae are able to destabilize their position relative to the flow, affecting their swimming capabilities (Pavlov et al. 2008). Each eddy has the energy and momentum to transfer rotation over a submerged body of similar size. As noticed in the case of submerged vegetation, where the size of stem-scale eddies was within the same order of magnitude as the size of larvae, eddies can drive larvae away from the array. Larvae prefer to swim above the array where velocity is higher but k and ω are smaller. Our data suggest the possibility to design a similar flow scenario in rivers that would allow a directed movement of larvae into particular areas to reduce or enhance recruitment, as desired, based not only on magnitude of turbulence, but also on its representative length scales. In the case of invasive species, movement could be directed to poor habitat quality that would reduce recruitment, or areas where larvae could be easily collected.

By quantifying the altered flow due to in-stream obstructions (velocity, turbulence, and vorticity fields), and relating them to changes in mortality, as well as identifying pathways and swimming capabilities of grass carp eggs and larvae, we have generated a unique dataset to better inform monitoring, sampling, and control of grass carp recruitment in streams. Our observations serve as the basis for improvements of field campaigns for sampling and collection of early life stage fish, as well as for the development of new strategies to control the spread of this species where it is invasive, or to enhance survival where it is desirable.

3.5. Conclusions

Experiments revealed that the spread across the water depth changes as fish develop, so they can be found at different locations depending on their developmental stage. We observed an active response of larvae seeking shelters and avoiding damaging areas, instead of behaving as passive particles. Larvae after gas bladder emergence showed strong active swimming capabilities including high maximum speeds that allowed them to search for and remain in areas of low shear and turbulence. Larvae at this stage seldom exceeded the velocity of the water to

travel upstream when in the main flow field, but did use short burst movements to escape zones of higher turbulence and shear. In areas with low turbulence and shear (e.g. behind the gravel bump), movement occurred in all directions and at a range of velocities.

The presence of coherent flow structures can further affect fish response to these flows, particularly if the size of the eddies is similar to the size of the larvae. Eddies of the same size as the larvae are able to destabilize their position relative to the flow, affecting their swimming capabilities. Each eddy has the energy and momentum to transfer rotation over a submerged body of similar size. Our study with rigid cylinders allowed us to identify turbulence scales, as the stem-scale, which was close to the size of larvae and was not attractive for larvae. Our data suggest the possibility to design a similar flow scenario in rivers that would allow a directed movement of larvae into particular areas to reduce or enhance recruitment, as desired, based not only on magnitude of turbulence, but also on its representative length scales. In the case of invasive species, movement could be directed to poor habitat quality that would reduce recruitment, or areas where larvae could be easily collected.

CHAPTER 4: LETHAL AND SUBLETHAL EFFECTS OF TURBULENCE ON GRASS CARP EGGS PRIOR AND AFTER HATCHING

4.1. Introduction

Natural reproduction of grass carp has been confirmed in tributaries of the Great Lakes (e.g. Chapman et al 2013, Embke et al 2016). These tributaries have enough length, and optimal hydraulic and water-quality conditions to allow successful spawning and transport of their eggs until hatching (Kocovsky et al 2012, Murphy and Jackson 2013). They all exhibit sufficient levels of turbulence to maintain eggs in suspension, as eggs transition through several stages before hatching. Egg suspension is crucial to ensure their development, as settlement represents a threat to their survival (Murphy and Jackson 2013).

After eggs are released and fertilized, water enters the egg membrane causing the egg expansion. This growing stage is known as water-hardening, and lasts for about 5 hours (George et al 2017). After those 5 hours the egg becomes water-hardened and its diameter and density remains constant until hatching, although less dense after the water absorption (George et al 2017). Despite the egg stage, the membrane is exposed to external forces that can damage it as it is transported by the flow. The mechanisms of mechanical damage of fish eggs can be detailed in terms of pressure change, acceleration, and shear stress within the fluid flow field (Ulanowicz, 1975). As early as in the 1960s, fish culturists have been aware of the sensitivity of fish eggs to mechanical damage in the control environment of the hatchery (Ulanowicz, 1975).

The susceptibility to mechanical damage at embryonic stages can be considered a key factor in the design of alternatives that promote or reduce the trapping of grass carp eggs at high turbulence, thus affecting the probability of successful hatching in natural streams. Prada et al (2018) reported some evidence of mortality of grass carp eggs due to a combined effect of turbulence, shear, egg-sediment interactions, and potential collisions with the disk-pump or flume walls in a laboratory experiment. In this study, we examine enhanced flow turbulence levels as an alternative control strategy through turbulence-induced mortality, and documented the lethal and sublethal effects prior and after hatching. We used an oscillating grid-stirred turbulence tank to test several batches of pre-water-hardened and water-hardened grass carp eggs to find threshold values of turbulence and shear stresses that can cause immediate and post-hatching harm.

4.2. Methodology

4.2.1. Experimental procedure

Batches of 100 pre-water-hardened and water-hardened eggs (Figure 4.1) were tested under increased levels of turbulence in an oscillating grid-stirred turbulence tank for time exposures of 10, 20, 80, and 320 seconds. The turbulence tank has dimensions of 0.5m *x* 0.5m *x* 0.5m, and was filled with 0.2 m of water (Figure 4.2). The grid is composed of bars with squared section of 0.012 m in width, and spacing of 0.05 m.

In each test, eggs were dropped in the tank and subjected to the turbulence generated by the oscillating grid at motor frequencies of 0, 100, 200, 240, 280, 320, 360, and 400 Hz. A linear relationship exists between the inverter frequency and the rotation speed of the motor, given by Ω [RPM] = 1.07 f [Hz]. A stable level of turbulence is reached throughout the tank after 30 seconds, based on previous ADV measurements.

A total of 32 tests were run for each kind of eggs (8 motor frequencies *x* 4 time exposures), and each test was repeated 3 times, i.e. a total of 19,200 eggs were used (9,600 pre-water-hardened and 9,600 water-hardened). After each test, eggs were removed from the tank with handheld nets and only those with intact membrane were counted as survivors in an initial screening. However, all eggs, including those with damaged membrane, were conserved to confirm survival and for later inspection of sublethal effects (i.e., mortality and abnormalities).

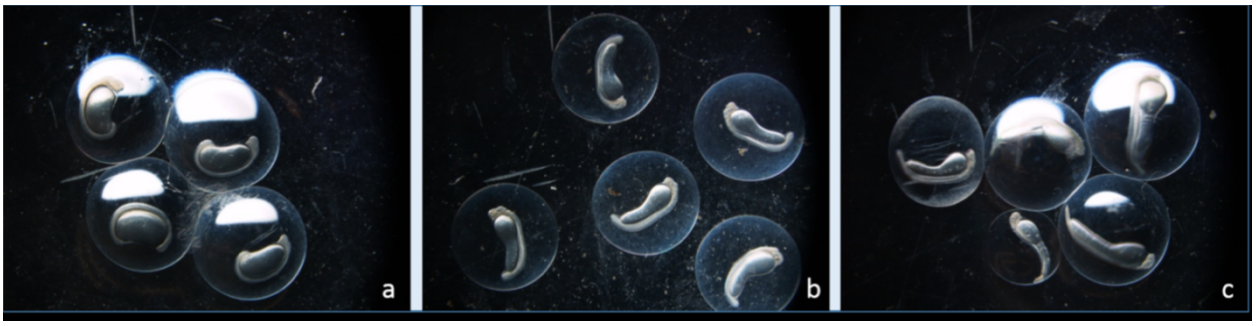

Fig. 4.1. Fertilized grass carp eggs seen in the microscope at different developmental stages. (a) 7 hours after fertilization, (b) 11 hours after fertilization, (c) 15 hours after fertilization.

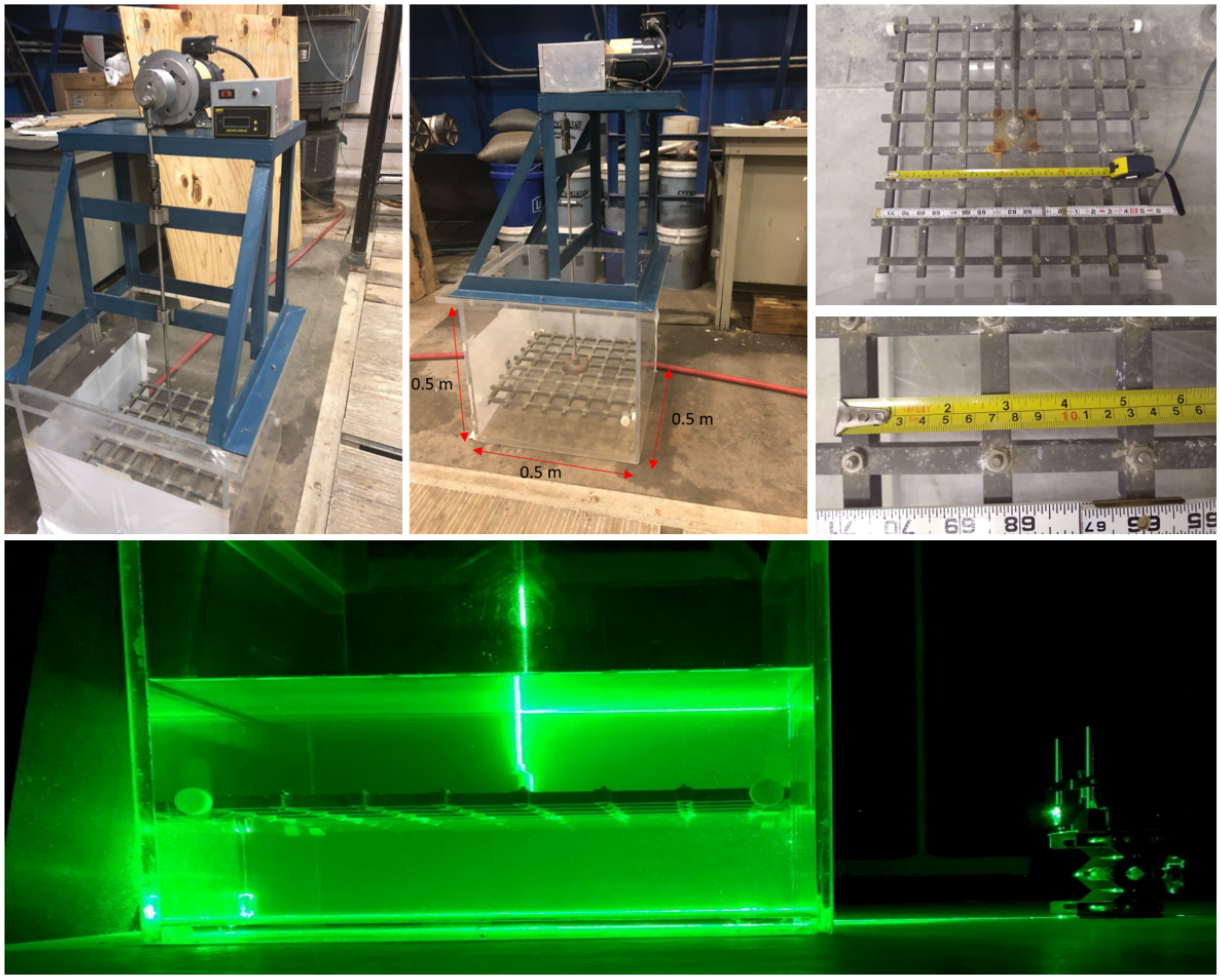

Fig. 4.2. Oscillating grid-stirred turbulence tank, its dimensions, and PIV system.

4.2.2. Turbulence quantification

Turbulence was characterized in the tank using a 2D Particle Image Velocimetry (PIV) system, with a 60fps 5MP monochromatic camera and a 5W Continuous-Wave 532nm Laser. A vertical laser sheet was generated perpendicular to the grid, entering from one side of the tank in the middle of its cross section, creating a vertical light sheet that illuminated neutrally-buoyant silver-coated hollow glass spheres with a mean diameter of 10 µm (Figure 4.2). Fields of turbulent kinetic energy ($k(x,z) = 0.5\left(2\overline{u'^2(x,z)} + \overline{w'^2(x,z)}\right)$) and Reynolds stresses ($\tau_{xz}(x,z) = \rho\left(\overline{u'(x,z) \cdot w'(x,z)}\right)$) were generated with the post-processing tool PIVlab in

MATLAB® (Thielicke & Stamhuis, 2014), where $u'(x,z) = u(x,z) - U(x,z)$ and $w'(x,z) = w(x,z) - W(x,z)$ are the turbulent fluctuations calculated from Reynolds decomposition.

Vertical flux of turbulent kinetic energy (Q_w) was found relevant to visualize the spread of *k* within the tank, thus we calculate it from our PIV data to better understand the turbulent mechanisms suspending and damaging the eggs. We calculate it as:

$$Q_w = \overline{q^2 w'} \tag{4.1}$$

where $q^2 = 2k$ (Lopez and Garcia, 1999).

4.3. Results

Fields of *k*, Q_w, and τ_{xz} obtained from PIV measurements in the 0.1-m gap are shown in Figures 4.3, 4.4, and 4.5 respectively. Time-averaged values of up to $k = 1.0$ m^2/s^2 and $\tau_{xz} = 30$ N/m^2, and maximum average magnitudes of $k_{max} = 2.70$ m^2/s^2 and $\tau_{max} = 37$ N/m^2 were registered slightly above mid-depth for the highest frequency of the stirred grid ($f = 400$ Hz). Eggs were observed in suspension within the 0.1-m gap as they were lifted by the turbulence fluctuations that spread everywhere as the fluxes (Q_w) indicate in Figure 4.4. Eggs that reached the grid passed within the grid openings, and did not impact the grid itself.

Figures 4.6a,b and 4.7a,b show percentages of intact membranes after the tests. Similar percentages were obtained for both pre-water-hardened and water-hardened eggs (near 70 to 80%) for the slower cases where k_{max} did not exceed 1.0 m^2/s^2 (or 15 N/m^2), suggesting that within this range the damage of few eggs was most likely due to handling. A drop in survival rates occured when k_{max} exceeded 1.0 m^2/s^2 (or 15 N/m^2) for both kinds of eggs (Figures 4.6a,b and 4.7a,b). At $k_{max} = 2.7$ m^2/s^2 and $\tau_{max} = 37$ N/m^2, all membranes of pre-water-hardened eggs were damaged under time exposures of 20 seconds or more, and 20% remained intact for exposure of 10 seconds (Figures 4.6a and 4.7a).

Sublethal and lethal effects observed after hatching ranged in severity from yolk sac deterioration, pericardial edema, and underdevelopment to spinal deformities and missing heads.

Those larvae showing any of these malformations were considered as "unlikely to recruit" (Figures 4.6c,d and 4.7c,d). The trend observed for recruitment was similar to the damaged membranes counts, although percentages were lower. Water-hardened eggs seemed to offer more protection to the larva inside, and about 30% of larvae successfully recruited even after exposure to 2.7 m^2/s^2 (or 37 N/m^2) for 10 and 20 seconds (Figures 4.6d and 4.7d).

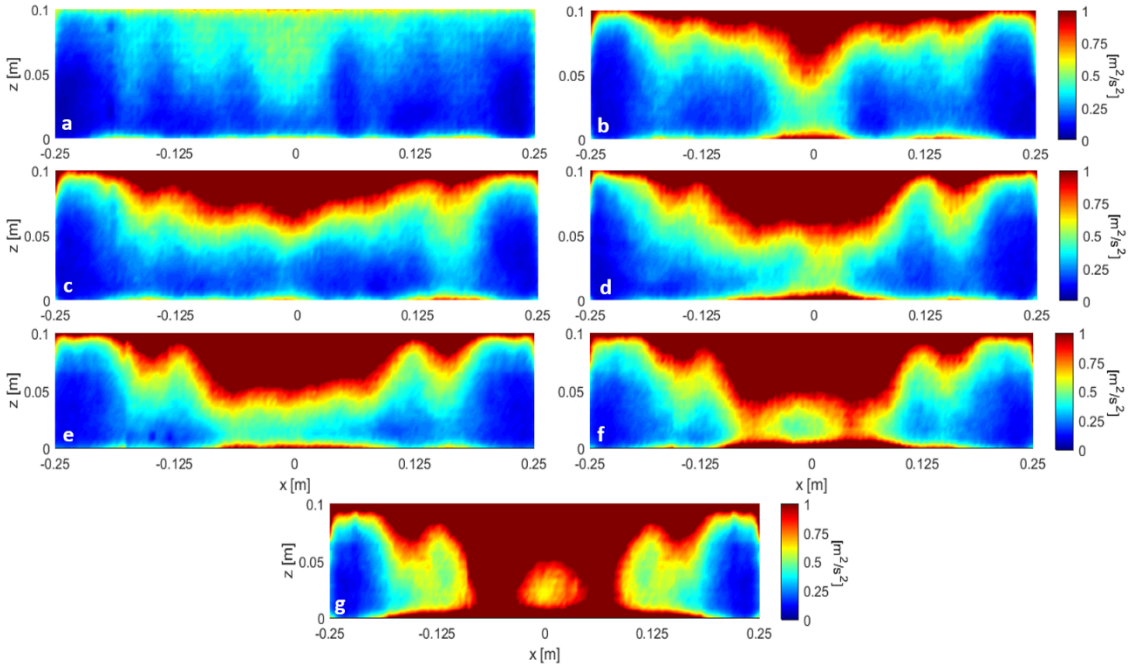

Fig. 4.3. Turbulent kinetic energy (k) fields for f = 100 Hz (a), f = 200 Hz (b), f = 240 Hz (c), f = 280 Hz (d), f = 320 Hz (e), f = 360 Hz (f), f = 400 Hz (g).

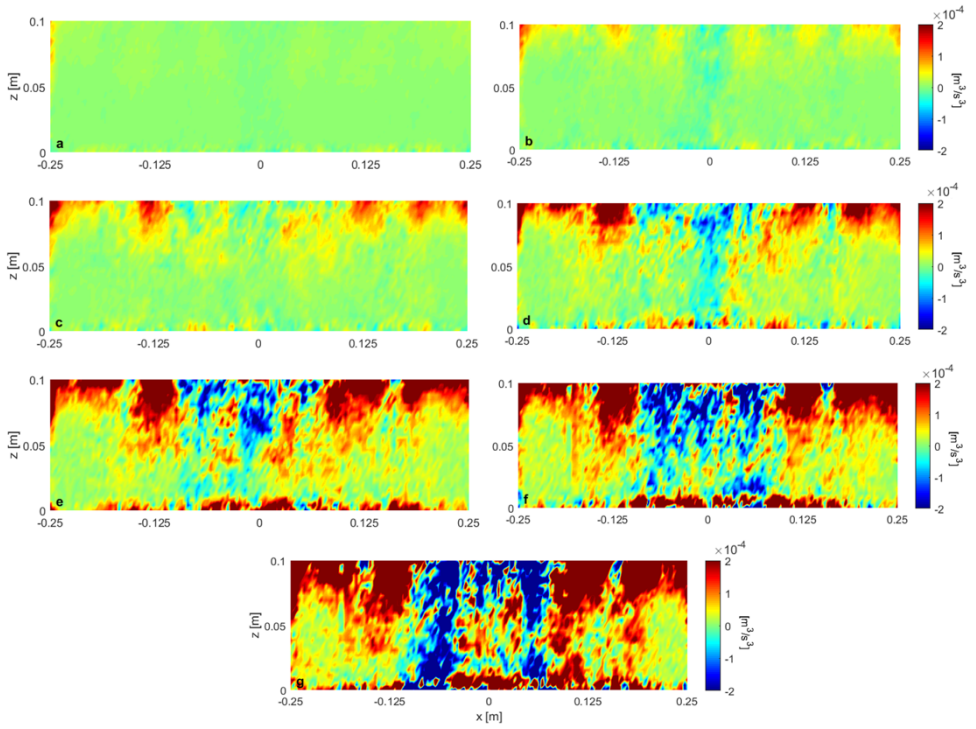

Fig. 4.4. Fluxes of turbulent kinetic energy (Q_w) for f = 100 Hz (a), f = 200 Hz (b), f = 240 Hz (c), f = 280 Hz (d), f = 320 Hz (e), f = 360 Hz (f), f = 400 Hz (g).

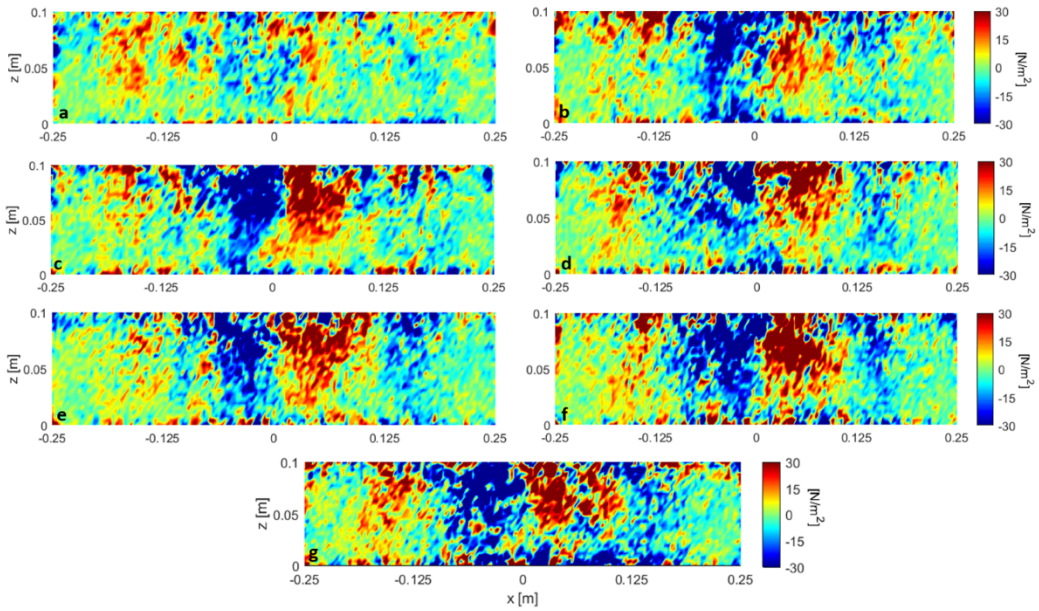

Fig. 4.5. Distribution of Reynolds stresses for f = 100 Hz (a), f = 200 Hz (b), f = 240 Hz (c), f = 280 Hz (d), f = 320 Hz (e), f = 360 Hz (f), f = 400 Hz (g).

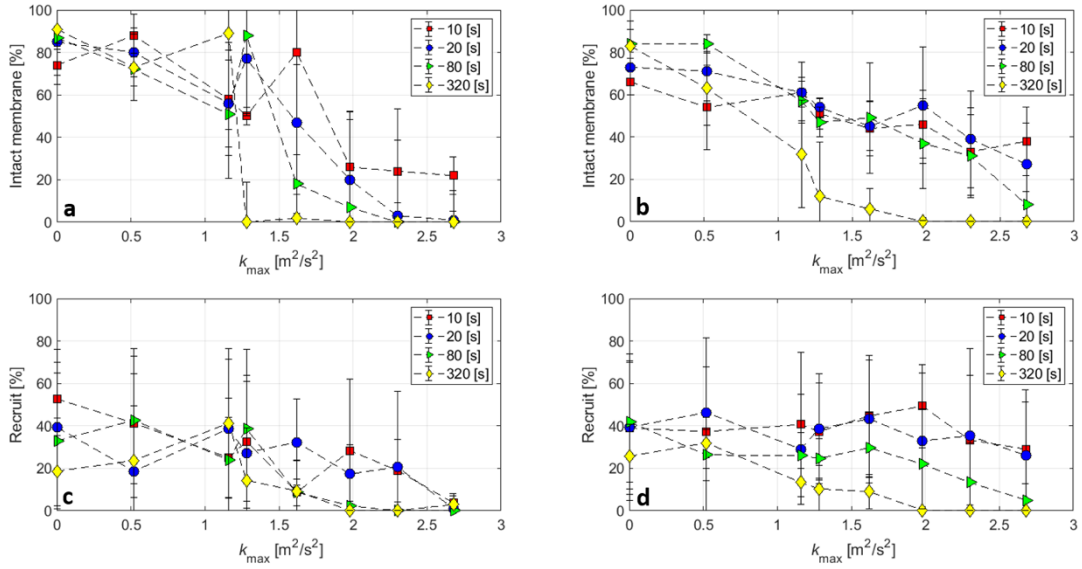

Fig. 4.6. Percentages of intact membranes for pre-water-hardened (a) and water-hardened eggs (b), and percentages of recruitment for pre-water-hardened (c) and water-hardened eggs (d) as a function of k and time exposure.

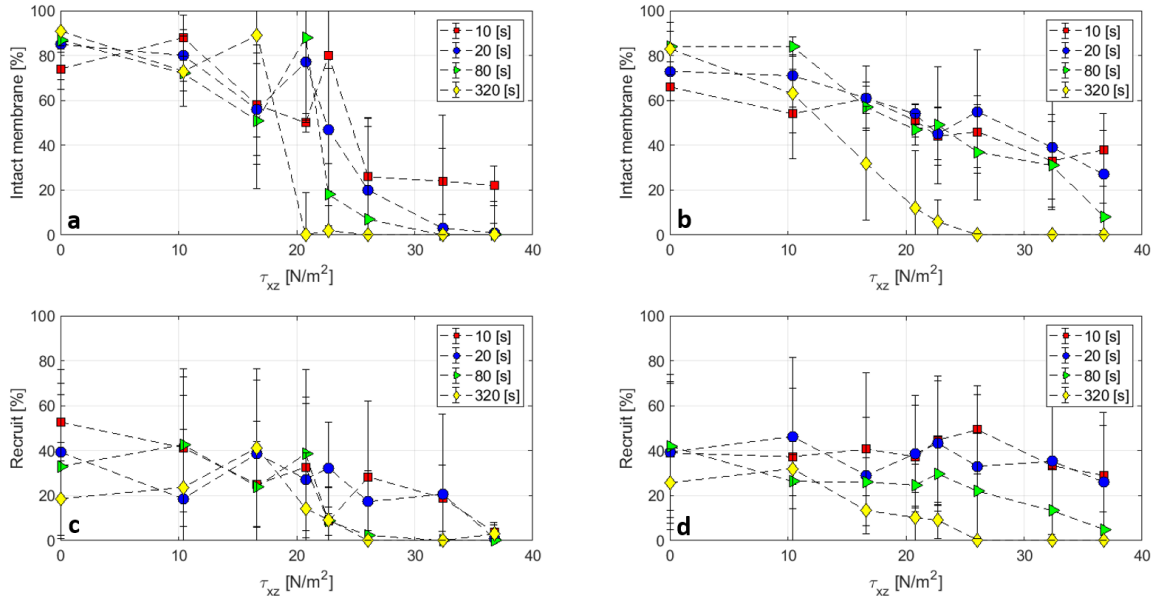

Fig. 4.7. Percentages of intact membranes for pre-water-hardened (a) and water-hardened eggs (b), and percentages of recruitment for pre-water-hardened (c) and water-hardened eggs (d) as a function of τ_{xz} and time exposure.

4.4. Discussion

Morgan et al. (1976) tested the damage of striped bass (*Morone saxatilis*) and white perch (*Morone americana*) eggs to shear stresses. They used an annular water tank to generate shear with the rotation of a plexiglass cylinder in the middle of the tank, and estimated damage in the 36-38% of eggs for 1 minute exposure, and 88-89% for 4 minutes exposure to shear stresses of 35 N/m^2. We tested the effect of shear and turbulence in a grid-stirred tank noticing an increase in egg membrane damage and morphologically abnormal embryos for magnitudes of turbulent kinetic energy greater than 1.0 m^2/s^2, and Reynolds stresses greater than 15 N/m^2 for exposures as short as 10 seconds. This time was sufficient to reduce the probability of recruitment to zero once k reached 2.7 m^2/s^2 ($\tau_{xz} > 35$ N/m^2) in the pre-water-hardened egg stage.

The membrane of water-hardened eggs showed more resistance to flow stresses, and although all membranes were damaged at $k_{max} = 2.7$ m^2/s^2 and $\tau_{max} = 37$ N/m^2 for 320 seconds, almost 40% remained intact after 10 seconds exposure, and more than 20% after 20 seconds (Figures 4.6b and 4.7b). The water-hardened stage offered also more protection to the larva inside as 30% of larvae successfully recruited even after exposure to 2.7 m^2/s^2 (or 37 N/m^2) for 10 and 20 seconds (Figures 4.6d and 4.7d). While many of the abnormalities observed after hatching are lethal, others have potential long-term sublethal effects that reduce the fitness and competitive ability of the larvae.

The values recreated in this study are consistent with tutrbulent features in the field. Magnitudes of shear and turbulence k_{max} reported in a stilling basin downstream of a dam spillway can reach 10 m^2/s^2 and maintain values above 2 m^2/s^2 for up to 100 m downstream of the spillway (Zhao and Wang, 2019). Odeh et al. (2002) listed previous reports that documented magnitudes of common shear stresses (in N/m^2) associated with average flows in natural streams (Table 4.1). Lancaster and Hildrew (1993) measured near-bed shear stresses in small streams (W = 1.38 to 3.15 m and D = 0.123 to 0.245 m, where W is mean channel width and D is mean channel depth) of 1 N/m^2 at moderate discharges (~0.006 m^3/s) and less than 7 N/m^2 at high discharges (~0.543 m^3/s), and Statzner and Müller (1989) reported 90 measurements of near-bed shear stress in 3 medium-sized streams (W = 2 to 6 m, with discharges of 0.4 to 1.42 m^3/s) with most estimates near 30 N/m^2. Large rivers, such as the Mississippi River, produce shear stresses

of 6 to 10 N/m^2 in flood stage (Costa 1987), though local shear stresses can be highly variable especially near in-stream structures (Jamieson et al., 2011).

Table 4.1. Estimates of shear stress in natural and altered aquatic systems (adopted from Odeh et al 2002)

Environment	Shear stress (N/m^2)	Reference
Water column in a trout stream, average flow	< 1.0	Fausch and White (1981)
Small streams, near bed	<1.0 – 7.0	Lancaster and Hildrew (1993)
Medium-sized streams, near bed	Most < 30, although some > 200	Statzner and Müller (1989)
Flash floods, small basins	61 – 2600	Costa (1987)
Floods, large rivers	6 – 10	Costa (1987)
Bulb turbine draft tube	500 – 5,421	McEwen and Scobie (1992)
Near ships' hulls and wakes	7.6 – 40.4	Morgan et al (1976)
Near barge propeller	≥ 5,000	Killgore et al (1987)

The thresholds of k and τ_{xz} found in our study can be used to identify areas in streams where most damage to the eggs is expected at various developmental stages, and to evaluate whether natural or anthropogenic features could cause mortality where survival of eggs is desirable. In-stream structures and control mechanisms, such as weirs or bubble curtains, could be designed to force grass carp eggs to pass through or be detained in high turbulence zones, potentially increasing mortality rates in streams during spawning seasons. Early-life stages of the bigheaded carps are largely similar to the grass carp, and these results are likely applicable to control or enhancement of those species as well. Furthermore, most North American fishes with drifting eggs and larvae spawn earlier in the year than grass carp or bigheaded carps (Galat et al. 2005), thus such control mechanisms might be deployed only at times which would minimize effects on native fish but maximize effects on invasive carps.

4.5. Conclusions

The proposed study investigated the susceptibility of pre-water-hardened and water-hardened eggs to be harmed by turbulence, and analyzed abnormalities after hatching. Many abnormalities were observed in embryos for exposures to increased turbulence, that can be easily found in the field, for periods as short as 10 seconds. These abnormalities can be lethal and others have potential long-term sublethal effects that reduce the fitness and competitive ability of the larvae. The membrane of water-hardened eggs offered more resistance to flow stresses and more protection to the larva inside compared to the pre-water-hardened egg stage.

These findings are a key factor in the design of in-stream structures in rivers to induce high turbulence, and thus potentially increase the damage of eggs before hatching in natural settings.

CHAPTER 5: TURBULENCE AS A BARRIER FOR INVASIVE FISH IN RIVERS: A LABORATORY STUDY ON GRASS CARP LARVAE

5.1. Introduction

The study of dispersion of invasive fish larvae in fluvial freshwater ecosystems is a challenging task, as the small size of larvae prevents a direct observation of this phenomenon in the field. Larvae do not behave simply as inert particles traveling with the flow. As larvae grow, they develop a major 'active' component to swim and resist the hydraulic forces in rivers (Pavlov et al 2008, Lechner et al 2014). This active swimming component is family-specific and stage-specific (Lechner et al 2014), as all larvae develop swimming capabilities to find safe nursery habitats with desirable water temperature and food availability, minimizing mortality and maximizing successful dispersal (Pavlov 1994, Keckeis et al 1997, Schiemer et al 2003).

Larvae go through several life stages where marked behavioral and anatomical changes determine their active swimming response (Chapman and George 2011, George and Chapman 2013, George et al 2015). Larvae transition from vertical to horizontal swimming as they develop the gas bladder emergence, which allows them to move laterally and hold position within the water column (George et al 2018). Larvae differ from adult fish in their interaction with the physical environment as they perceive their environment at their own relevant scales (Smith et al 2014). Several studies have reported how coherent turbulent structures may decrease fish swimming stability, especially eddies of similar size than the fish (e.g. Pavlov et al 2000, Cada and Odeh 2001, Metaxas 2001). Fish of larger size than the surrounding eddies are typically unaffected, whereas fish of similar size than eddies can be disturbed and destabilized (Metaxas 2001, Tritico and Cotel 2010).

If larvae are destabilized by the flow turbulence, they may lose their ability to maintain position and can be swept away by the river discharge, influencing also their dispersal (Reichard and Jurajda 2007, Schludermann et al 2012, Lechner et al 2018). Understanding the limitations of their swimming capabilities as a function of mean and turbulent flow parameters is thus critical to monitor, manage, and predict their spread at those early-life stages. In this study, we are particularly interested in characterizing the swimming response of grass carp larvae (*Ctenopharyngodon idella*) to contribute to better predictions of their transport in natural

streams, as they have become established in the central United States, where they are considered problematic invaders (Chick and Pegg 2001; Parker et al. 2016; Kočovský et al. 2018).

Prada et al. (2020) reported that grass carp larvae reacted and swam away from stem-scale eddies created by a submerged vegetation array with rigid elements of diameter size in the same order of magnitude as the size of larvae. Larvae showed in that case a preference to drift on top of the array where the vorticity generated by the elements was negligible, even if the mean flow velocity was higher than within the array. Likewise, other laboratory studies (e.g. George et al 2018, Prada et al 2018) have documented the swimming response of grass carp larvae to altered flow conditions and various turbulent scales. The estimation of threshold magnitudes of turbulence and turbulent spatial and temporal scales as triggers of larval response are thus of vital importance in controlling their spread and reproduction at early-life stages in North America.

The objective of this study is to observe the swimming response of grass carp larvae (in stage 38 based on stages described by Yi et al. 1988 and George and Chapman 2015) to altered flows recreated in a laboratory flume setup, and to quantify the physical processes driving such a response. Three different configurations were built in the flume: (1) a gravel bump, (2) a single cylinder, and (3) rigid-submerged vegetation, which created a broad range of flow conditions and turbulent scales, driven by changes of flow velocity and water depth. We report threshold values of turbulent kinetic energy and Reynolds stresses that triggered the response of larvae, based on the measured swimming speeds for each flow condition. The observed patterns will contribute to the enhancement of larvae sampling and collection in the field, as well as to the development of numerical tools for larvae transport in natural streams that consider their active swimming capabilities.

5.2. Materials and methods

5.2.1. Experimental setup

5.2.1.1. Race-track flume (RTF)

A series of laboratory experiments with live grass carp larvae (*Ctenopharyngodon idella*) was conducted at the Ven Te Chow Hydrosystems Laboratory (VTCHL) of the University of

Illinois at Urbana-Champaign. Authorization to use live eggs and larvae for research purposes was obtained from the Illinois Department of Natural Resources (Permit No. 18-050).

The VTCHL counts with a unique Odell-Kovasznay type flume (Odell & Kovasznay, 1971), which is a Race-Track Flume (RTF) where the flow is driven by a vertical-axis disk pump, designed to break down secondary flow structures as water moves in a continuous loop to reach fully developed flows. The disk pump is controlled by a frequency inverter, with a relationship between the inverter frequency (f) and the rotation speed (Ω) of the disk pump given by Ω [RPM] = 6.6 f [Hz]. The RTF has a constant width of 0.15 m and a straight test section of 2.0 m in length. A 0.1-m thick flat sediment bed was placed for the experimental series along the straight section. The sediment bed was composed of a mixture of walnut shells and sand (bulk sediment density ρ_p = 1250 kg/m^3, settling velocity $w_p = 1.89x10^{-2}$ m/s, and size {D16, D50, D84} = {0.41, 0.54, 0.66} mm) (Prada et al., 2018).

Swimming capabilities of grass carp larvae were measured at the test section, placing 3 different in-stream obstructions over the sediment bed. The in-stream obstructions were a gravel bump, a single cylinder, and arrays of rigid-submerged vegetation (Figure 5.1). Two different water depths were tested, H = 0.2 and 0.4 m measured over the sediment bed, for 4 disk pump frequencies of 10, 15, 20, and 25 Hz. The width-to-depth ratios in the straight section were 3/4 for H = 0.2 m and 3/8 for H = 0.4 m. The boundary layers created in this flume by the side walls are very thin, and do not affect the mean flow (Prada et al 2020).

The gravel bump placed in the middle of the test section had a height of 0.12-m and was composed of gravel (mean size of 350 mm) contained in a mesh bag (Figures 5.1a-b). The single cylinder embedded in the middle of the test section was a 2" (51 mm) PVC pipe that allowed for 49 mm of space between the cylinder and the walls of the flume (Figures 5.1c-d). The rigid-submerged vegetation array was extended along the test section (Figures 5.1e-f). The rigid vegetation followed a staggered configuration with average spacing between rods of 0.034 m, porosity of $6.3x10^{-3}$, and volumetric frontal area a = 1.27 [1/m], with acrylic rods of 6.4 mm in diameter and 100 mm in height (i.e. 100 mm protruding above the sand bed). The roughness density (ah) is 0.127 (intermediate regime), which ensures the onset of a two-layer flow and canopy-scale turbulence (e.g. Nepf 2012).

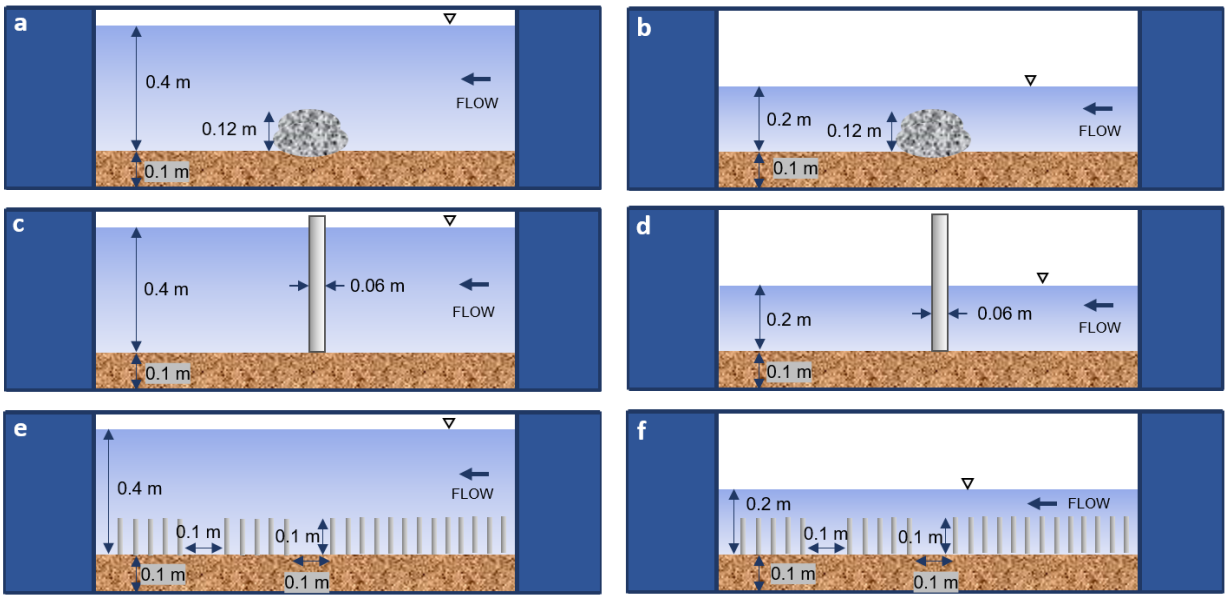

Figure 5.1. RTF straight test section for each flow scenario (not to scale). Gravel bump case for H = 0.4 m (a) and H = 0.2 m (b). Single cylinder case for H = 0.4 m (c) and H = 0.2 m (d). Rigid-submerged vegetation for H = 0.4 m (e) and H = 0.2 m (f).

Instantaneous velocity components in the x, y, and z directions are denoted by u, v, and w. The dominant mean-flow direction is in x, vertical is z, and lateral y. Flow was characterized using 2D Particle Image Velocimetry (PIV), illuminating neutrally-buoyant silver-coated hollow glass spheres of 10 μm in diameter with a laser sheet generated by a 5W Continuous-Wave 532nm laser. The laser sheet was generated at a fixed location from the top, parallel to the mean flow at the center of the in-stream obstruction. In the case of vegetation, a small gap of 0.1 m was set in the middle of the section to record the particle movement (Figures 5.1e-f). All PIV measurements were recorded at 60fps for 1 minute with a 5MP monochromatic camera after the tests with live-fish to avoid: a) dissolved microspheres affecting larval health, and b) altering larval behavior due to the laser light sheet.

The range of velocities tested went from 4 to 20 cm/s. Froude and Reynolds numbers considering the incoming free-stream velocity preceding the obstacle (U_c) and the corresponding characteristic length scale for each case (e.g. Rh = hydraulic radius, H = water depth, h = gravel bump height, D = cylinder diameter, d = rigid element diameter) indicate all flows are within subcritical, turbulent regimes (Table 5.1).

Table 5.1. Free-stream velocity U_c and non-dimensional parameters for the different scenarios.

Case		H = 0.2 m				H = 0.4 m			
	F [Hz]	10	15	20	25	10	15	20	25
	U_c [m/s]	0.044	0.064	0.084	0.104	0.08	0.11	0.15	0.19
All	Re_{Rh}	2,400	3,491	4,582	5,673	5,053	6,947	9,474	12,000
	Re_H	8,800	12,800	16,800	20,800	32,000	44,000	60,000	76,000
Gravel	Re_h	5,280	7,680	10,080	12,480	9,600	13,200	18,000	22,800
Cylinder	Re_D	2,244	3,264	4,284	5,304	4,080	5,610	7,650	9,690
Vegetation	Re_d	282	410	538	665	512	704	960	1,216
All	Fr	0.031	0.046	0.060	0.074	0.040	0.056	0.076	0.096

In the case of the rigid vegetation, the velocity decelerates within the canopy due to the canopy drag, and a mixing layer is formed (Chen et al. 2013). The initial velocity deceleration goes from the beginning of the canopy until a distance X_D downstream that scales with the canopy drag length scale (L_c) and the canopy drag coefficient (C_D) as $X_D = 1.5L_c(1 + 2.3C_D ah)$ (Chen et al. 2013). L_c is a function of the canopy density (a), and can be approximated as $L_c = 2/C_D a$ (Belcher et al. 2003). C_D is determined from the rigid element Reynolds number (Re_d) using an empirical relation presented by White (1991), $C_D = 1 + 10Re_d^{-2/3}$. We estimate from the Reynolds numbers Re_d = 282 – 1,216 (Table 5.1) a drag coefficient of C_D = 1.1. The canopy drag length scale would be L_c = 1.43 m, with an initial deceleration zone until X_D = 2.83 m.

The straight test section of the RTF is 2.0 m long (< X_D), and the PIV measurements for rigid vegetation were taken 1.3 m downstream from the leading edge of the canopy. Our results are thus within the initial adjustment region over the canopy, representative of finite vegetated patches in streams, rather than continuous fully developed vegetated flows. Flow at the top of the canopy, however, does generate the expected mixing layer given our canopy density, ah > 0.1, high enough to create an inflection point in the velocity profile and shift the maximum turbulence and Reynolds stress levels to the top of the canopy.

The gravel obstruction is representative of gravel mounds and is expected to generate a recirculation zone at the downstream end, with a shear layer developed between the low velocity

behind and high velocity above the obstruction, resulting in larger-than-larvae eddies oriented mainly on a vertical plane. The single cylinder is representative of piles. In contrast with the other two scenarios, this one is not expected to create a two-layer flow, but rather produce larger-than-larvae eddies in horizontal planes due to turbulent wake past the cylinder, with time- and length scales in function of its diameter and Re_d.

5.2.1.2. Live larvae

Adult grass carp were set for spawning by hormone injection at the U.S. Geological Survey Columbia Environmental Research Center (CERC) in Columbia MO. At CERC, spawned eggs were fertilized and then transported to the VTCHL in Urbana, IL. Prada et al (2020) documented the dispersion of the eggs and larvae over various developmental stages for the flume setups described in section 2.1.1. (Figures 5.1a,c,e) keeping a constant water depth of 0.4 m and a constant velocity for the duration of the tests.

In addition to the long-term (4-days) tests documented in Prada et al (2020), shorter experimental series were conducted with various velocities and water depths at the end of each test. Surviving larvae from the flume experiments and from the control hatching tanks as reported in Prada et al. (2020) were used for the tests presented in this manuscript. The total number of larvae used for the gravel bump, single cylinder, and vegetation array, were 2058, 2482, and 2482, respectively. The same surviving larvae from the single cylinder case was used for the rigid-submerged vegetation case.

Larvae for these tests were all at developmental stage 38 (according to Yi et al. 1988 and George and Chapman 2015), i.e., over 50 hours after egg hatching, with gas bladder already emerged, allowing larvae to swim horizontally and hold position within the water column. Larvae at this stage have a size of 6-7 mm and are often captured in off-channel low velocity habitats (George et al. 2017), which are often considered nursery areas for grass carp and, where development to older juvenile stages occurs.

Larvae swimming performance over the in-stream obstructions for each velocity and water depth was recorded in 5-min videos with a Nikon D5300 camera (1920 x 1080 video resolution) at 30 fps. The camera was placed 0.5 m in front of the RTF's test section. LED Edge Lit panels (Knema, LLC) were used to illuminate the test section from behind, creating a uniform illumination field. At the end of each test case, all larvae were euthanized using MS-222

(*tricaine methanesulfonate*) according to protocol, to prevent the escape of eggs or larvae from the facility. Remaining organic material was filtered and incinerated.

5.2.2. Data processing

5.2.2.1. Flow data

Series of images of the illuminated tracer particles in the flow were processed using the GUI-based open-source tool PIVlab in MATLAB® (Thielicke & Stamhuis, 2014). Post-processing yields instantaneous velocity fields $u(x,z)$ and $w(x,z)$ across the images field of view, where *x* is the horizontal coordinate increasing downstream from each obstruction and *z* is the vertical coordinate increasing upwards from the sediment bed.

Instantaneous velocity fields were time-averaged to obtain the mean velocities $U(x,z) = \overline{u(x,z)}$ and $W(x,z) = \overline{w(x,z)}$. Reynolds decomposition is used to calculate turbulent fluctuations as $u'(x,z) = u(x,z) - U(x,z)$ and $w'(x,z) = w(x,z) - W(x,z)$. Turbulent kinetic energy (*k*) and Reynolds stresses (τ_{xz}) were estimated as:

$$k(x,z) = 0.5\left(2\overline{u'^2(x,z)} + \overline{w'^2(x,z)}\right) \tag{5.1}$$

assuming $u' = v'$ (e.g. Tanino and Nepf 2007). And

$$\tau_{xz}(x,z) = \rho\left(\overline{u'(x,z) \cdot w'(x,z)}\right) \tag{5.2}$$

where ρ is the water density. Profiles of *k* and τ_{xz} for gravel bump and rigid vegetation cases were scaled using the characteristic velocity difference (U_s) for plane mixing layers (Pope 2000) given as:

$$U_s = U_h - U_l \tag{5.3}$$

where U_h and U_l are the mean uniform velocities of each layer ($U_h > U_l$). For single cylinder, U_s for a plane wake is given as:

$$U_s = U_c - \langle U(x,z) \rangle \tag{5.4}$$

where $\langle \quad \rangle$ represents spatial averaging over x within the field of view (Pope 2000).

Vertical flux of turbulent kinetic energy (Q_w) was found relevant to understand the spread of k from the mixing layers, thus we calculate it from our PIV data to assess whether is a useful metric to interpret larvae behavior. We calculate it as:

$$Q_w = \overline{q^2 w'} \tag{5.5}$$

where $q^2 = 2k$. Q_w is constant in the intermediate region of an open channel flow over a flat smooth bed (Lopez and Garcia, 1999), but it is expected to behave differently under flow scenarios like the ones tested in this series.

5.2.3. Larvae tracking

Videos of larvae swimming past the in-stream obstructions were processed with Particle Tracking Velocimetry (PTV) codes in MATLAB® (based on Brevis et al. 2011). For every flow condition in each flume setup, 1800 consecutive frames (i.e. 1 minute data) were extracted from the videos to track the position of individual larvae over time (Figure 5.2). The PTV routine produced binary images, which were processed using Gaussian particle detection routines to obtain the centroid of each larva (x, z coordinates). In stage 38, although larvae are still very small, pigmentation in the eyes and back allowed reliable detection of each individual larva, by setting threshold levels of pixel intensities that contrasted with the white background.

Algorithms of Cross-Correlation (CC) (Brevis et al. 2011, Uemura et al. 1989, Hassan et al. 1992) were implemented in the PTV codes to match identified larvae between consecutive frames. This algorithm tracks individual particles based on the highest cross-correlation coefficient within a square interrogation window with the size of the maximum expected displacement. The velocity associated with a matched particle is then estimated between pairs of consecutive frames, which we call in this study "larvae traveling speeds", u_t and w_t for each component in the x and z directions, respectively.

As we measured the distribution of flow velocities (U and W) at the same location with tracked larvae, we can estimate also larvae swimming speeds u_{sw} and w_{sw} as:

$$u_{sw} = U - u_t \tag{5.6}$$

$$w_{sw} = W - w_t \tag{5.7}$$

these swimming speeds can be defined as “burst swimming speeds” that represent instantaneous escape reactions without maintaining a constant mean swimming speed for several tail beats (Müller and van Leeuwen 2004, George et al 2018). Burst swimming speeds were defined as positive if the larva moves against the flow, and negative in the same direction of the flow.

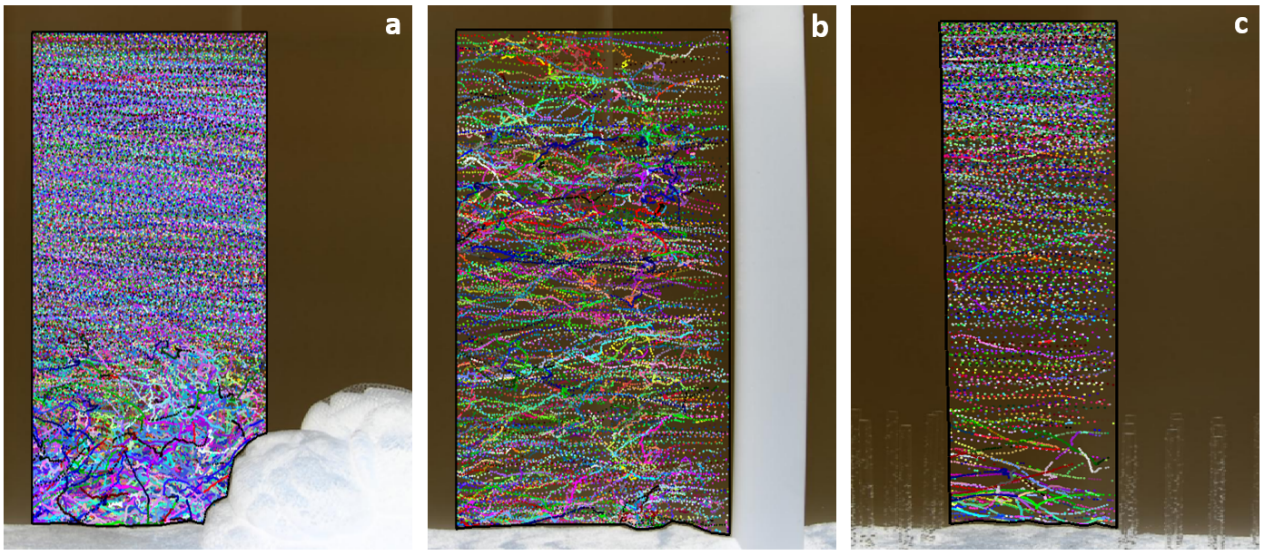

Figure 5.2. Trajectories of larvae detected using the PTV codes. a) case of gravel bump for H = 0.4 m. a) case of cylinder for H = 0.4 m. a) case of vegetation for H = 0.4 m (each colored line represents the trajectory of a single larva).

5.3. Results and discussion

5.3.1. Larvae preferential locations

Centroids of larvae captured with PTV codes were used to generate maps of their spatial distribution on the field of view of each obstruction. Figures 5.3a-c show some samples of these spatial distributions for each case with H = 0.2 m and a disk-pump frequency of F = 15 [Hz]. Each pixel in these plots has a size of 1 x 1 cm and the color indicates the percentage of centroids detected in each pixel compared to the total amount of centroids detected in the field of view during 1 minute. In Figures 5.3d-f, we show the flow velocity fields at the same locations of the spatial distributions also for H = 0.2 m and F = 15 [Hz].

In the cases of gravel bump and vegetation we observe a two-layer flow, high velocity on top of the obstacle, and low velocity within the obstructed region (Figures 5.3d and 5.3f). At the interface of the two layers, there is a mixing zone with increased levels of shear and turbulence.

This mixing zone was characterized by computing k and τ_{xz} using equations (5.1) and (5.2), respectively. Figures 5.4a,c,d,f and 5.5a,c,d,f show how k and τ_{xz} increase for all flow conditions compared to the other two layers. Further detail of the turbulence in all cases is presented as Supplementary Material, where we show scaled profiles of turbulent intensities u_{rms}/U_s (Figure 5.14) and w_{rms}/U_s (Figure 5.15).

Larvae tried to swim towards the low velocity zone in the case of the gravel bump (Figure 5.3a), as they are subjected to lower drag forces in there than in the high velocity zone above it. Within this wake region, larvae were able to freely swim in any direction. In high-velocity regions, however, larvae show a clear preference to swim against the current (Prada et al. 2020), in an effort to advance upstream. In our experiment setup, all larvae traveled downstream even for the slowest pump frequency (F = 10 [Hz]).

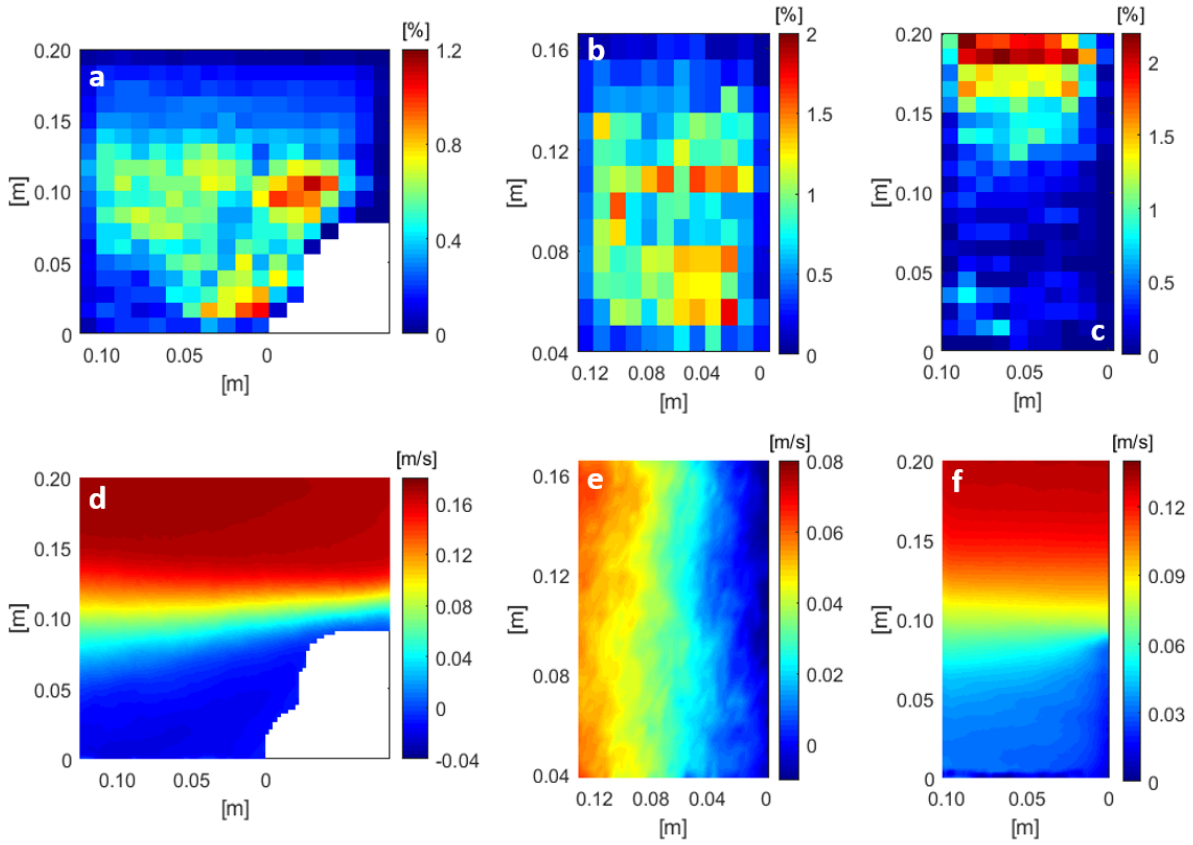

Figure 5.3. Samples of spatial larvae distributions and mean longitudinal velocity U (m/s) on the field of view of each obstruction for H = 0.2 m and F = 15 [Hz]. Spatial larvae distribution for (a) gravel bump, (b) single cylinder, and (c) rigid vegetation. Mean velocity U for (d) gravel bump, (e) single cylinder, and (f) rigid vegetation.

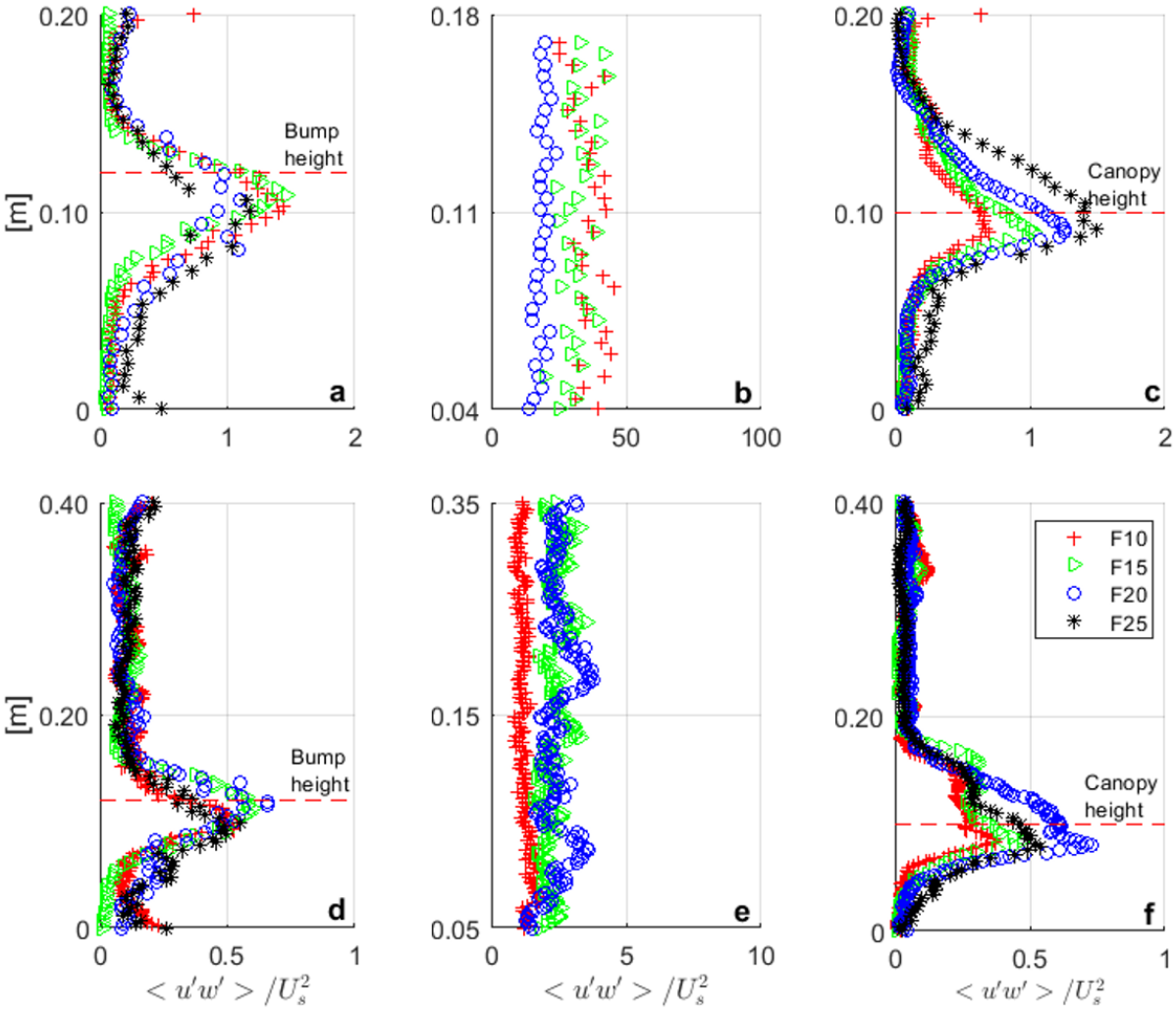

Figure 5.4. Non-dimensional Reynolds-stress profiles for all flow conditions in gravel bump at H = 0.2 m (a) and H = 0.4 m (d), single cylinder at H = 0.2 m (b) and H = 0.4 m (e) and rigid vegetation at H = 0.2 m (c) and H = 0.4 m (f).

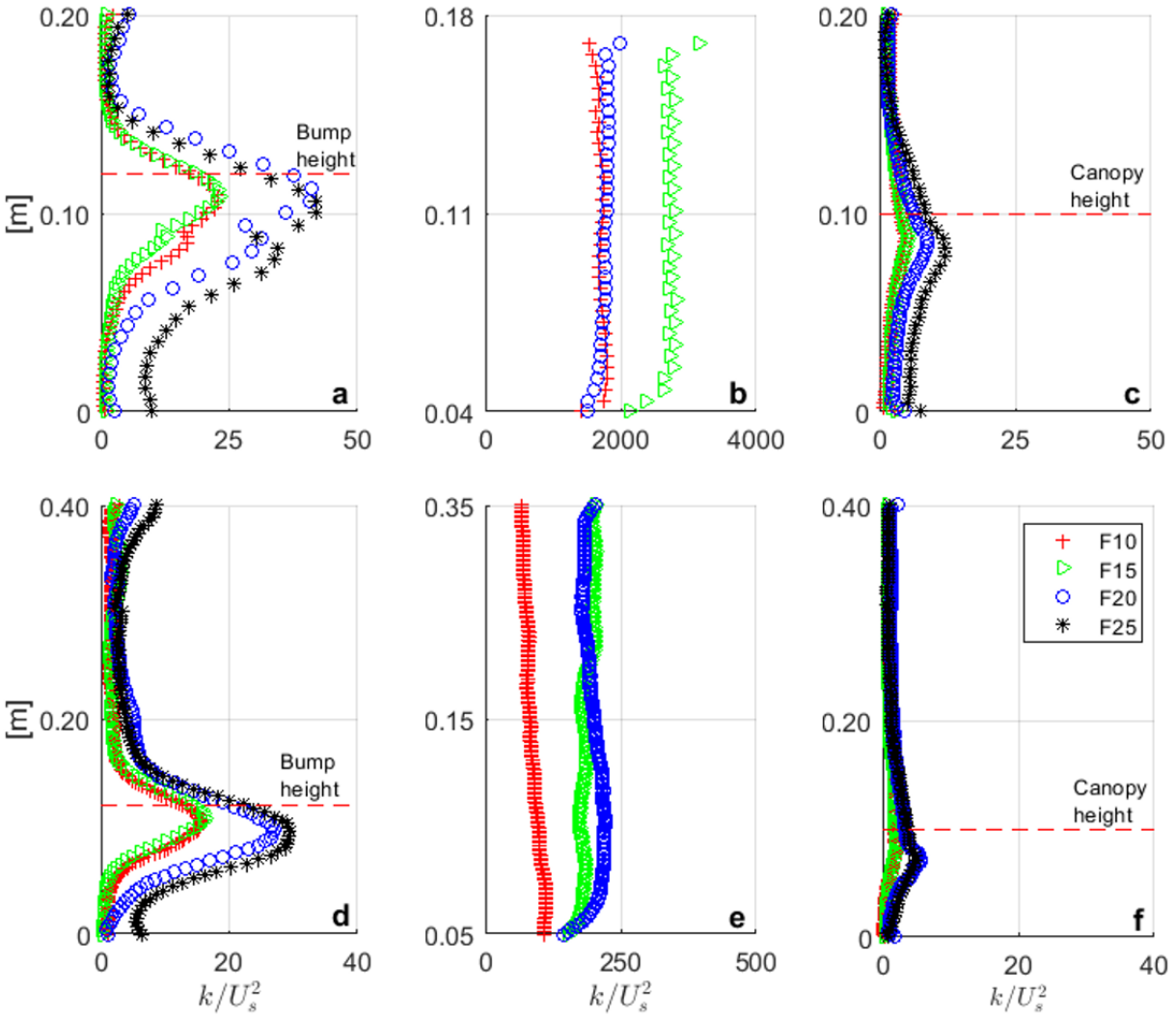

Figure 5.5. Non-dimensional turbulent kinetic energy profiles for all flow conditions in gravel bump at H = 0.2 m (a) and H = 0.4 m (d), single cylinder at H = 0.2 m (b) and H = 0.4 m (e) and rigid vegetation at H = 0.2 m (c) and H = 0.4 m (f).

The mean velocity fields for the gravel bump and the rigid vegetation (Figures 5.3d,f) look alike, but they result in a very different distribution of larvae (Figures 5.3a,c), showing that larvae do not respond solely to mean velocity. Even if rigid vegetation yields a region of low velocity, larvae preferred to swim above the canopy, facing higher speeds. Profiles of velocity and larvae distributions for the fastest case (F = 25 [Hz]) for both gravel bump and vegetation for both water depths (Figure 5.6) clearly show a different response, with larvae actively opting for low speed regions behind the gravel, but preferring higher speed regions above the canopy, consistent for both water depths investigated.

The turbulence metrics, k and τ_{xz}, reveal further insight on the larvae distribution across the water depth (Figure 5.7). Comparing gravel bump (Figure 5.7a,e) to rigid vegetation (Figure 5.7b,f) we see that magnitudes of k differ in about one order of magnitude between the gravel bump and vegetation cases for both water depths. However, the maximum stress, $\tau_{xz,}$ is about the same order of magnitude, and data show that larvae try to avoid areas with peak turbulent stresses (Figures 5.7c,d,g,h) for both gravel and vegetation. Larvae either swam below the mixing layer, or over it, even if it means facing higher drag forces in the high velocity zone (Figure 5.7d,h).

Data from the fastest flow condition (Figures 5.6 and 5.7) show a response driven mostly by k and τ_{xz} rather than mean velocity. In order to identify whether a threshold exist which triggers such a response in larval behavior, we calculate the turbulence properties for all four flow conditions for gravel (Figure 5.8) and rigid vegetation (Figure 5.9). For gravel bump, we see that for F = 10 and 15 [Hz] larvae did not avoid swimming within and across the mixing layer (Figures 5.8a-b), as turbulence levels were low enough to allow undisturbed passage between layers. However, for F = 20 [Hz] when peak turbulence levels reached $k = 1.0\ m^2/s^2$ and $\tau_{xz} = 20\ N/m^2$, there was a notable reduction in the percentage of larvae swimming in the mixing layer (Figure 5.8c,g). Such a decrease persists with higher flows (Figure 5.8d,h).

The profiles of vertical fluxes of turbulent kinetic energy (Q_w) in Figures 5.8i-l and 5.9i-l showed that this parameter was not constant for our cases, as it is in the intermediate region of flows over flat-smooth beds (Lopez and Garcia, 1999). Instead, fluxes increased over the mixing layers as expected. This finding did not reveal further insight of larvae behavior as the profiles follow a similar trend of those of k and τ_{xz}.

For rigid vegetation, even if the magnitudes of k were one order of magnitude smaller than for gravel bump, we can also notice how the larvae distribution splits into the two flow velocity zones once the peaks exceeded $k = 0.05$ m^2/s^2 or $\tau_{xz} = 10$ N/m^2 for F = 20 [Hz] (Figure 5.9c,g).

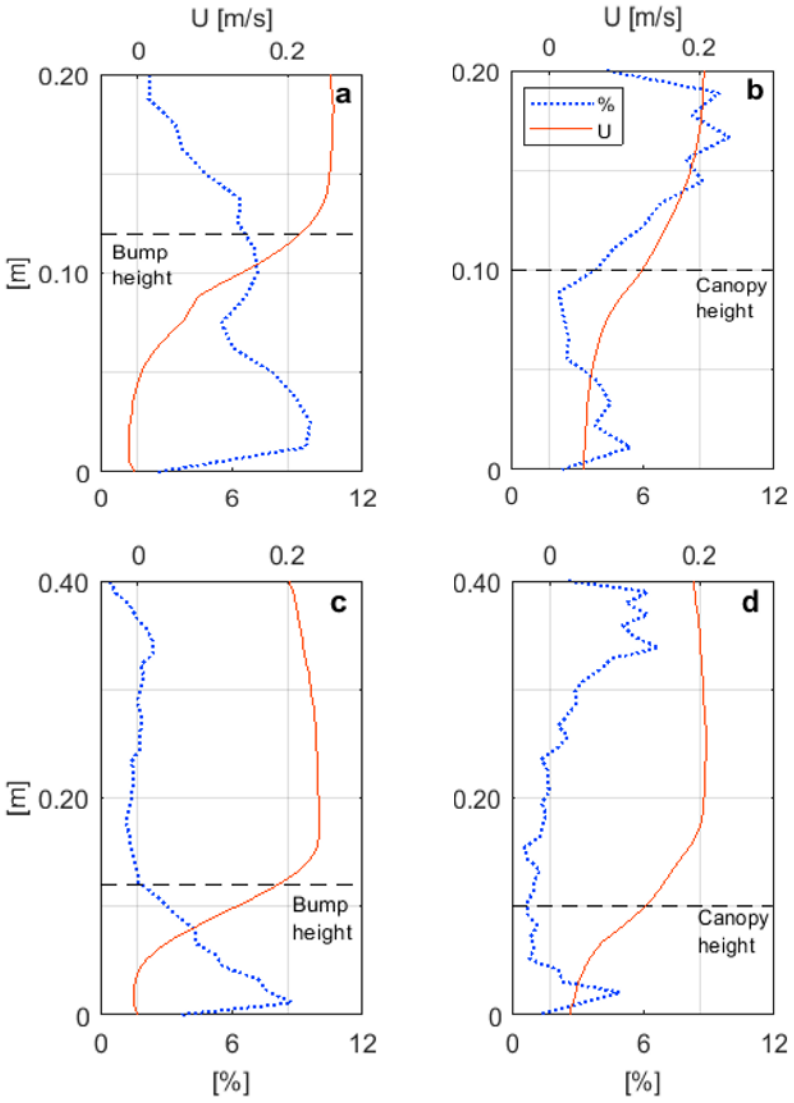

Figure 5.6. Profiles of larvae spatial distributions (dashed blue line) and their respective mean velocity profile U (solid red line) for gravel bump at H = 0.2 m (a) and H = 0.4 m (c), and rigid vegetation for H = 0.2 m (b) H = 0.4 m (d).

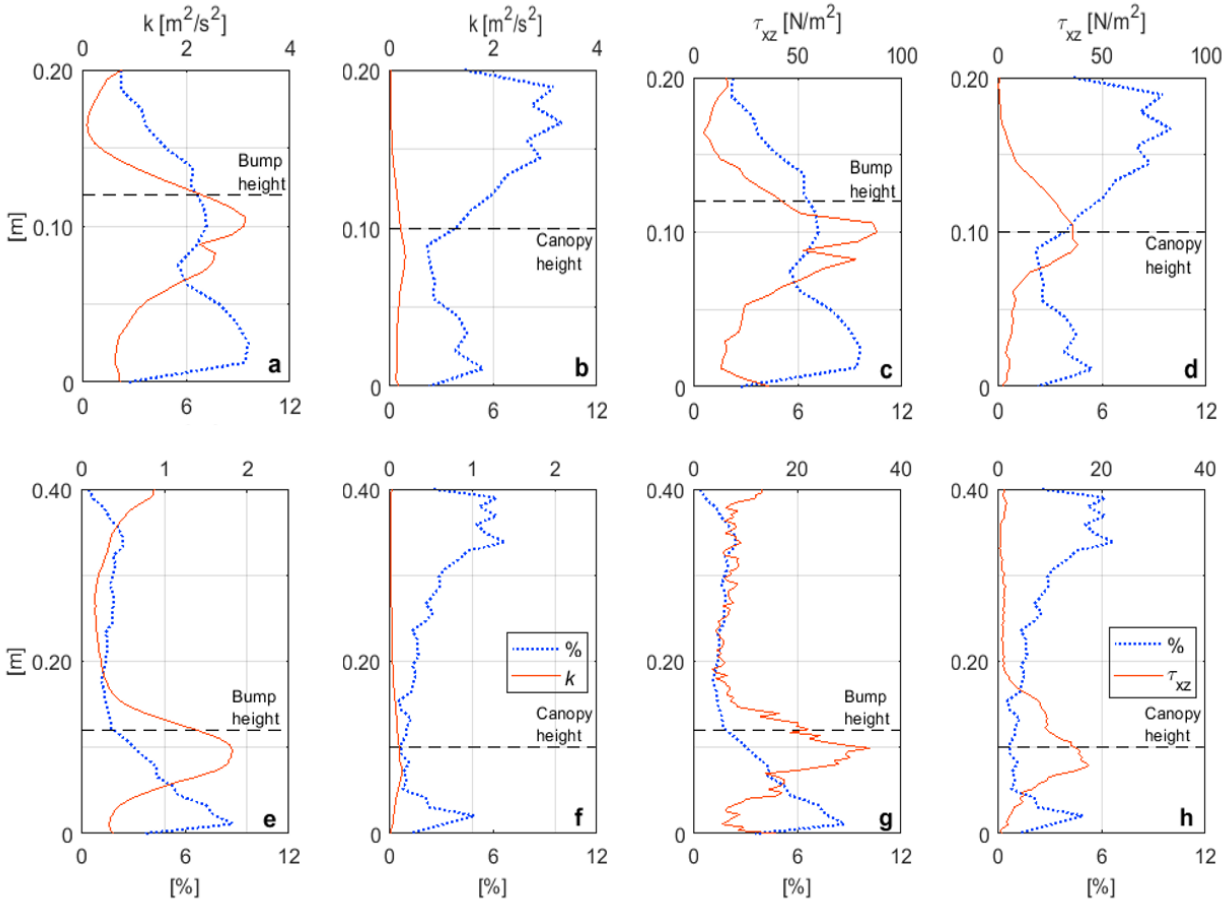

Figure 5.7. Profiles of larvae spatial distributions and profiles of turbulence properties (k and τ_{xz}) for gravel bump and vegetation cases at F = 25 [Hz]. a) k for gravel bump with H = 0.2 m. b) k for vegetation with H = 0.2 m. c) τ_{xz} for gravel bump with H = 0.2 m. d) τ_{xz} for vegetation with H = 0.2 m. e) k for gravel bump with H = 0.4 m. f) k for vegetation with H = 0.4 m. g) τ_{xz} for gravel bump with H = 0.4 m. h) τ_{xz} for vegetation with H = 0.4 m.

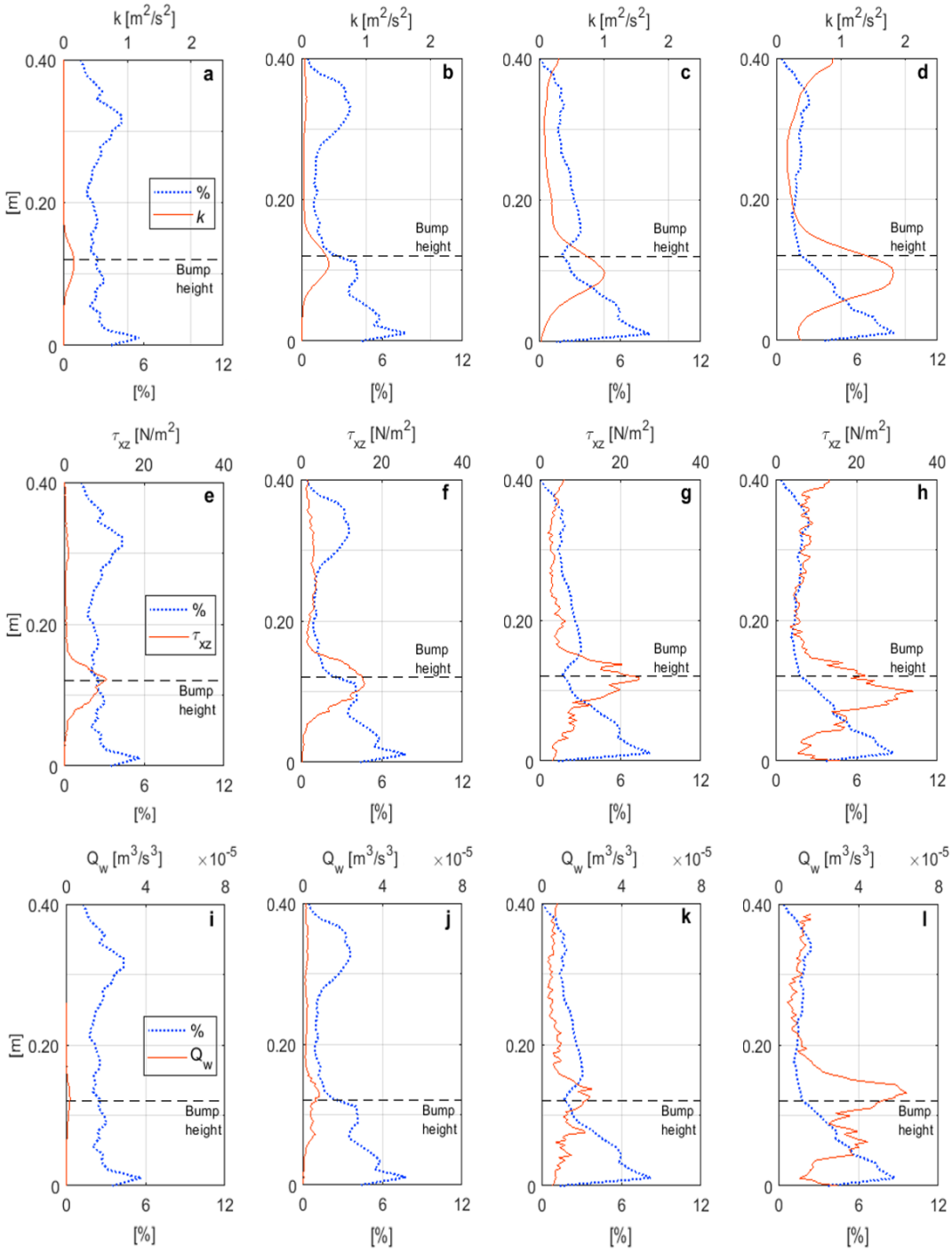

Figure 5.8. Profiles of larvae spatial distributions and profiles of turbulence properties (k, τ_{xz}, and Q_w) for gravel bump case with H = 0.4 m for all disk-pump frequencies. a) k at F = 10 [Hz]. b) k at F = 15 [Hz]. c) k at F = 20 [Hz]. d) k at F = 25 [Hz]. e) τ_{xz} at F = 10 [Hz]. f) τ_{xz} at F = 15 [Hz]. g) τ_{xz} at F = 20 [Hz]. h) τ_{xz} at F = 25 [Hz]. i) Q_w at F = 10 [Hz]. j) Q_w at F = 15 [Hz]. k) Q_w at F = 20 [Hz]. l) Q_w at F = 25 [Hz].

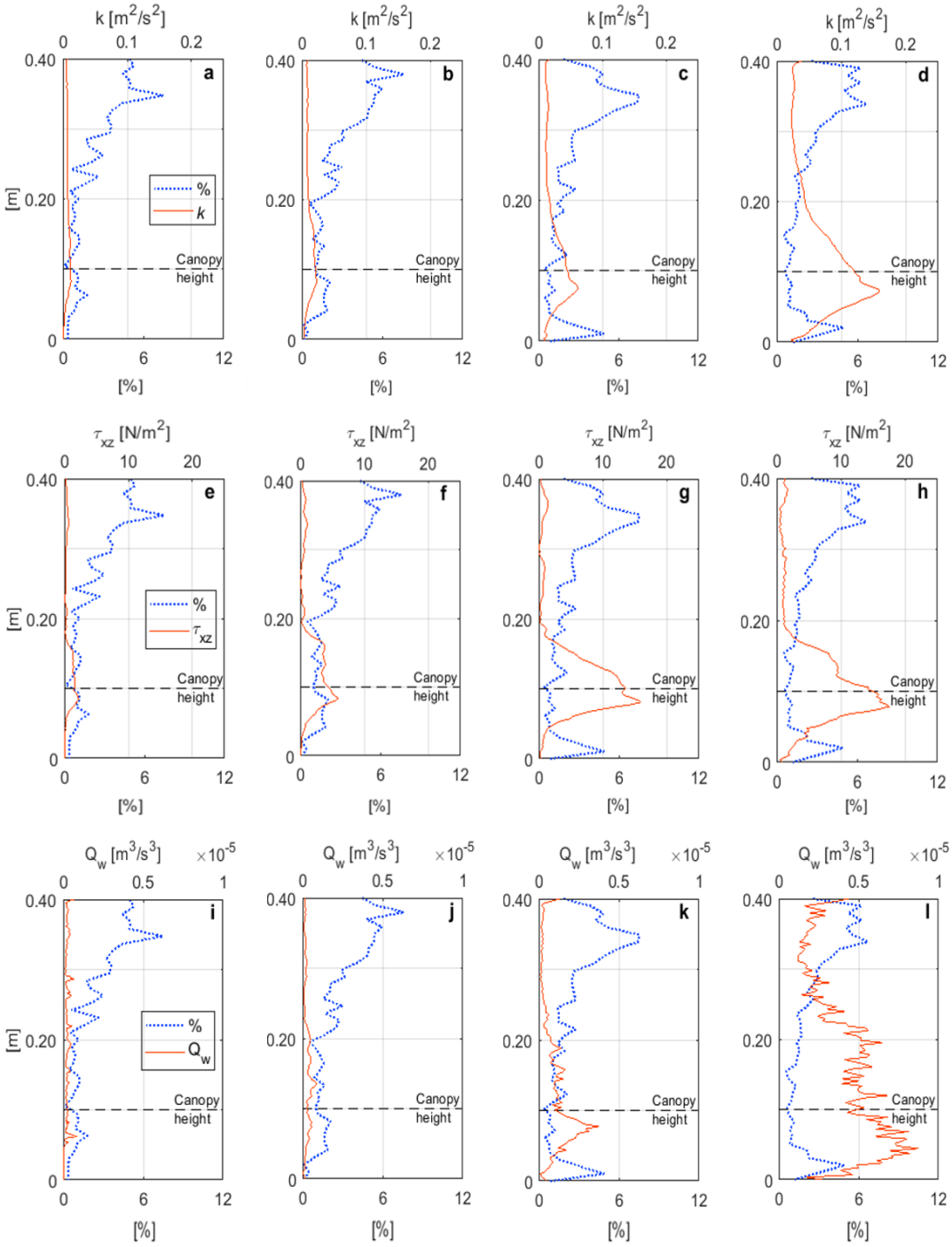

Figure 5.9. Profiles of larvae spatial distributions and profiles of turbulence properties (k, τ_{xz}, and Q_w) for vegetation case with H = 0.4 m for all disk-pump frequencies. a) k at F = 10 [Hz]. b) k at F = 15 [Hz]. c) k at F = 20 [Hz]. d) k at F = 25 [Hz]. e) τ_{xz} at F = 10 [Hz]. f) τ_{xz} at F = 15 [Hz]. g) τ_{xz} at F = 20 [Hz]. h) τ_{xz} at F = 25 [Hz]. i) Q_w at F = 10 [Hz]. j) Q_w at F = 15 [Hz]. k) Q_w at F = 20 [Hz]. l) Q_w at F = 25 [Hz].

5.3.2. Larvae swimming speeds

Looking at preferential locations of grass carp larvae (in stage 38) within a variety of flow conditions and turbulence levels, we found that they avoided swimming in localized regions of increased turbulence after a threshold is reached. To better understand their response, however, we need to quantify their swimming capabilities. Larvae tried to swim upstream, but were still pushed downstream by the flow in all cases. To quantify their swimming speed on all the flow conditions investigated, we used PTV and PIV data to estimate horizontal and vertical burst swimming speeds (Figure 5.10, from equations 5.5 and 5.6).

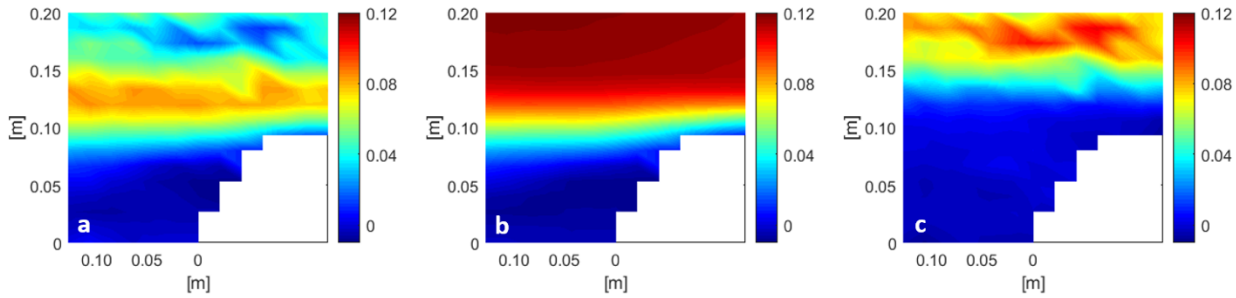

Figure 5.10. Larvae swimming speeds (a, from equation 5.5) are obtained by subtracting the travelling speeds (c, from PTV) from the time averaged velocities (b, from PIV), i.e. (a) = (b) – (c). Gravel bump at F = 10 Hz with H = 0.2 m shown.

The 2D maps of horizontal and vertical swimming speeds (as in Figure 5.10a) were spatially averaged over the longitudinal (x) direction to obtain vertical profiles as a function of the water depth (Figures 5.11, 5.12, and 5.13) for all 3 cases (gravel bump, cylinder, and vegetation), for both water depths and all disk-pump frequencies. For gravel bump case (Figure 5.11a,d) the horizontal swimming speeds increased within the mixing layer for all flow conditions up to reaching the same flow velocity (i.e., $u_{sw}/U \sim 1$). Even if within the mixing layer the flow velocity is not the highest across the water depth, the increased level of turbulence forced them to swim faster. For the cylinder (Figure 5.11b,e), most of the swimming speeds for both water depths were negative and some of them greater than the mean flow ($u_{sw}/U < -1$), i.e. they preferred to swim downstream with the direction of the flow to escape from the turbulent wake after the cylinder. For the rigid vegetation case (Figure 5.11c,f), rather than an increase of

swimming speed within the mixing layer as in the gravel bump, faster swimming speeds were measured on top of the canopy in response to higher velocities.

Vertical profiles of vertical swimming speeds (Figures 5.12 and 5.13) for all 3 cases, at both water depths and all disk-pump frequencies show that, for gravel bump, there is an apparent increment of the vertical swimming speeds within the mixing layer, and larvae are able to overcome the vertical flow velocities (w_{sw}/W > 1, Figure 5.12a,d) even up to 10 times faster, moving upwards above the layer and downwards below it (Figure 5.12a,d). However, when we scale the vertical swimming speeds with the vertical turbulent intensities (w'_{rms}) we observe that larvae can actually get in trouble trying to get out of the mixing layer (Figure 5.13a,d). A similar behavior can be observed for vegetation, with larvae having difficulty to overcome the vertical turbulent intensities (Figure 5.13c,f). For cylinder, there is no specific trend in the distributions of the vertical swimming speeds (Figure 5.12b,e), but larvae could move easily in any direction without getting trapped in any specific zone (Figure 5.13b,e).

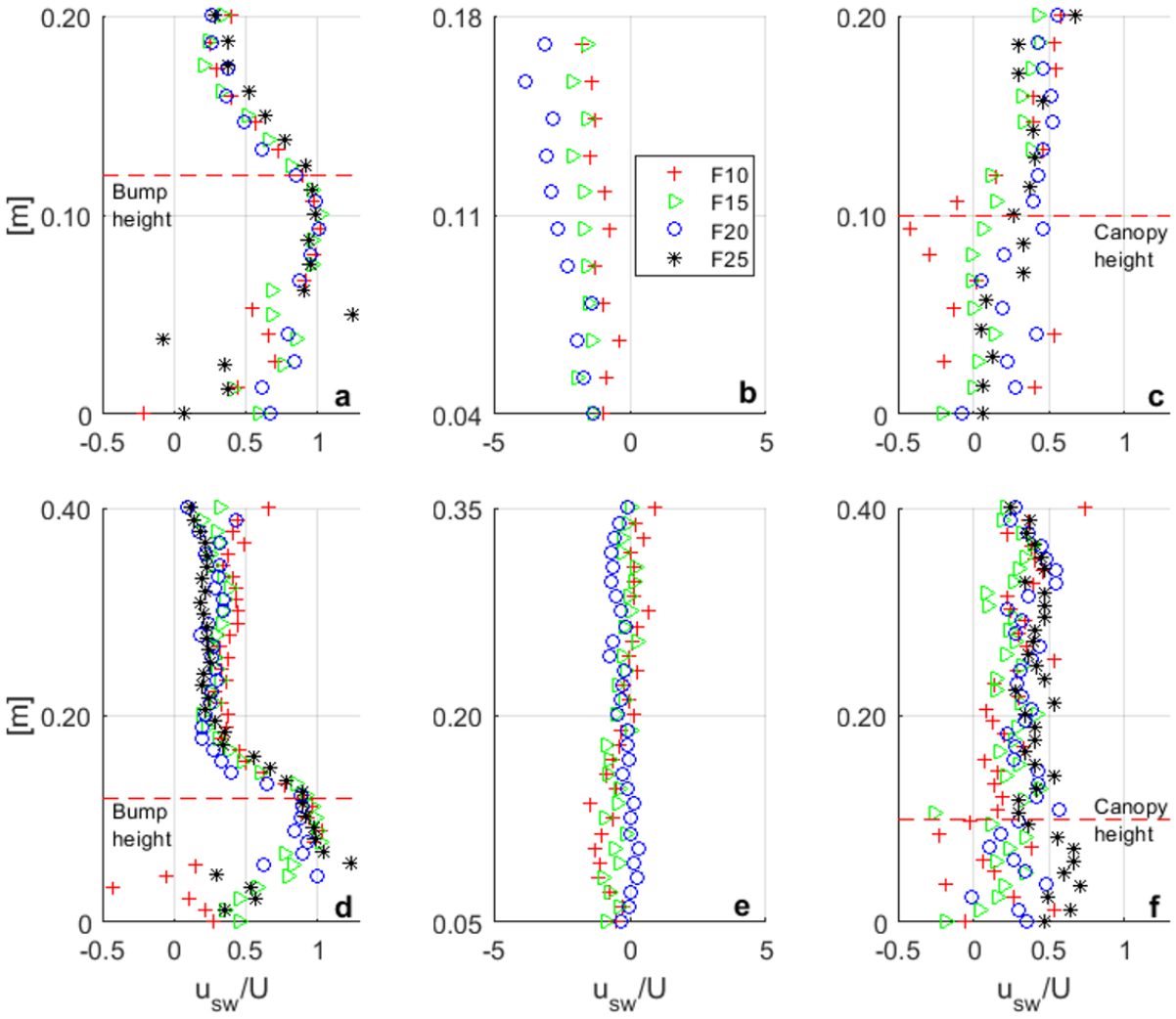

Figure 5.11. Scaled horizontal swimming speeds as a function of the water depth for gravel bump at H = 0.2 m (a) and H = 0.4 m (d), single cylinder at H = 0.2 m (b) and H = 0.4 m (e), and rigid vegetation at H = 0.2 m (c) and H = 0.4 m (f).

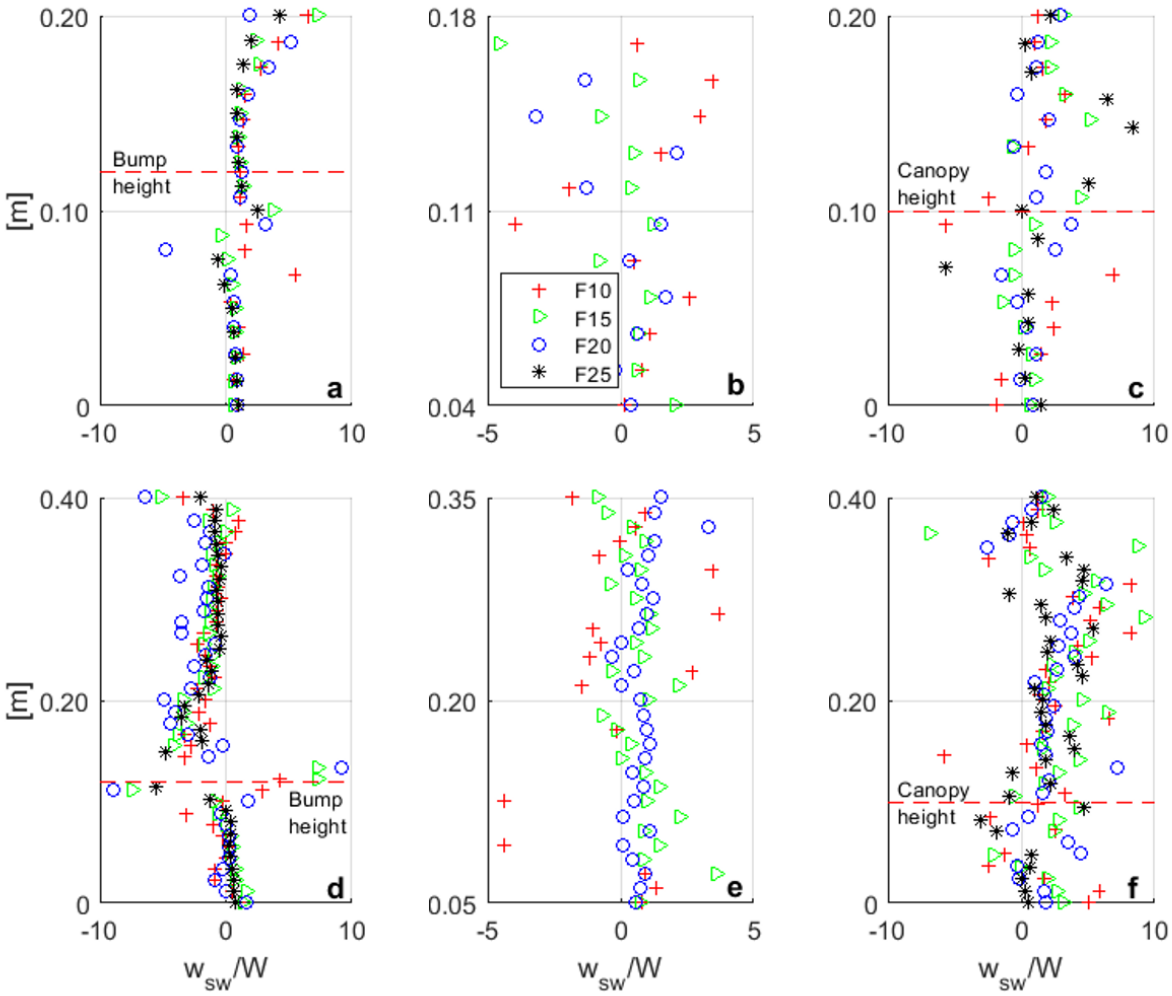

Figure 5.12. Scaled vertical swimming speeds and their swimming direction, with positive values meaning upward swimming and negative downward swimming. (a) Gravel bump at H = 0.2 m. (b) single cylinder at H = 0.2 m. (c) rigid vegetation at H = 0.2 m. (d) gravel bump at H = 0.4 m. (e) single cylinder at H = 0.4 m. (f) rigid vegetation at H = 0.4 m.

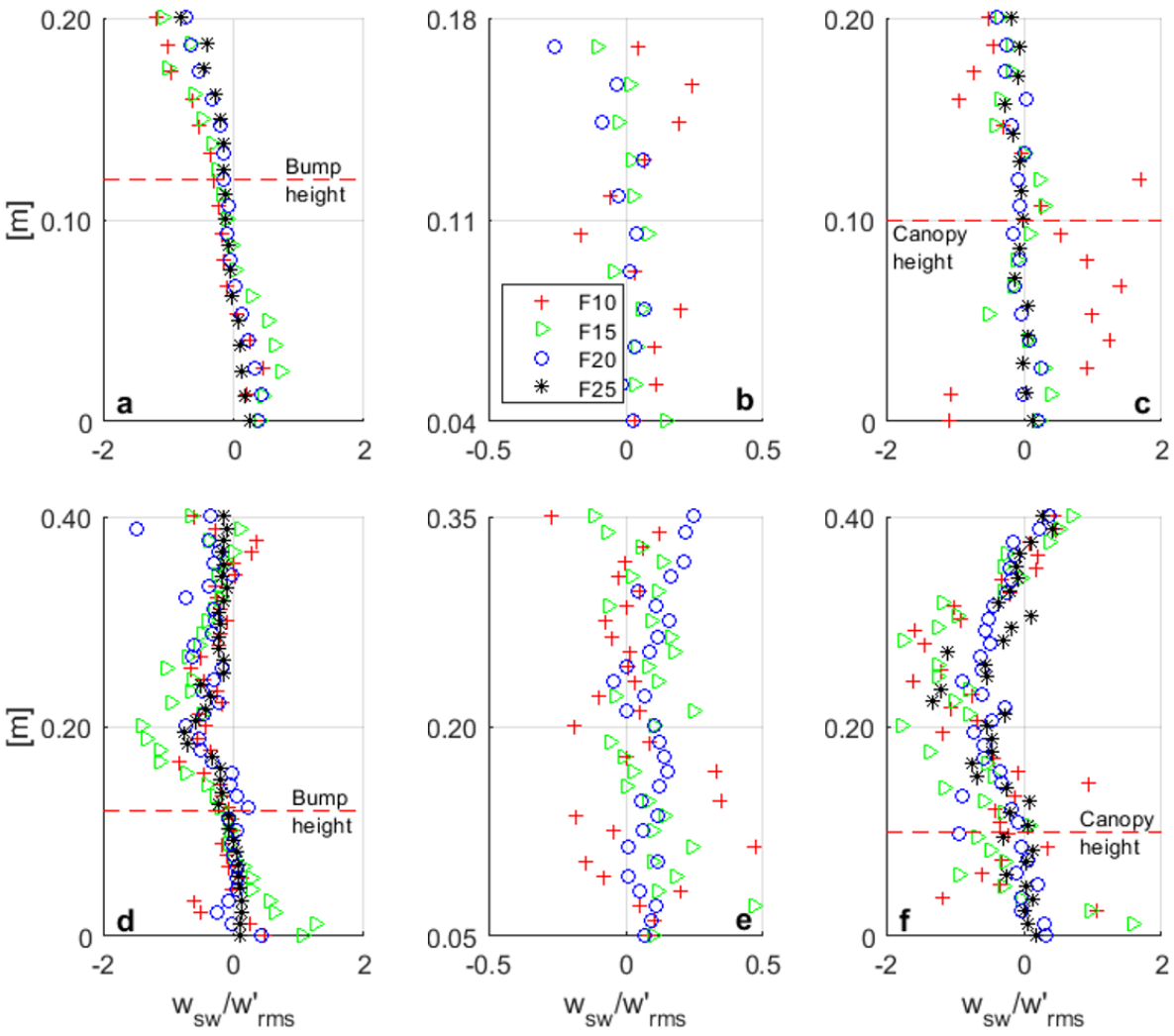

Figure 5.13. Scaled vertical swimming speeds and their swimming direction, with positive values meaning upward swimming and negative downward swimming. (a) Gravel bump at H = 0.2 m. (b) single cylinder at H = 0.2 m. (c) rigid vegetation at H = 0.2 m. (d) gravel bump at H = 0.4 m. (e) single cylinder at H = 0.4 m. (f) rigid vegetation at H = 0.4 m.

5.4. Conclusions

We compared three different configurations, representative of in-stream obstructions commonly found in natural streams, to subject grass carp larvae to a variety of hydrodynamic forces of different magnitudes and scales. In one the of flume setups, we had a cylinder in the middle of the experimental section that created a turbulent wake ($Re_D \sim 10^3$) for all of the incoming flow velocities. This obstacle generated distributed turbulence throughout the water depth provoking larvae to move away, i.e. downstream, to avoid regions of increased turbulence (consistent with data from Figures 5.7-5.9 for gravel bump and vegetation cases). Larvae seemingly avoid turbulence, in a possible effort to minimize energy expenditure (Müller et al. 2000). This is consistent with the other two cases (gravel and rigid vegetation Figures 5.11-5.13) where the higher turbulence within the mixing layer forces larvae to swim faster, resulting in higher expenditures of energy (Müller et al. 2000). In contrast to the gravel and vegetation, the cylinder did not create any low-flow low-turbulence zone attractive for larvae.

The gravel bump generated a recirculation zone with low levels of drag and turbulent forces, which larvae clearly preferred once the mean flow increased to levels that created an undesirable turbulence field for larvae in the mixing layer ($k > 1.0$ m^2/s^2 or $\tau_{xz} > 20$ N/m^2). A similar situation occurred for vegetation, where the mixing layer along the top of the canopy prevented larvae to swim there after turbulence exceeded 0.1 m^2/s^2 or 10 N/m^2 in this case. Despite the similarity of the mixing layer between the gravel bump and the vegetation, differences in the coherent turbulent structures may explain the differences in threshold magnitudes that induced larvae response. In rigid vegetation there is the presence of stem eddies in the y direction within the canopy that are of the same size as the larvae (6-7 mm), and also some entrainment of the canopy-scale eddies as $ah > 0.1$. The gravel bump provided full shelter from high drag and turbulent forces, where larvae remained without much flow disturbances. This correlation between flow characteristics and larvae behavior can be intentionally used in the field to design in-stream structures that attract or repel larvae for specific zones as desired. In the case of grass carp, larvae can be attracted to zones where they can be easily harvested, or repelled from zones with food availability.

Numerical models are also needed to forecast the spread of grass carp larvae in natural streams. By computing the swimming speeds we provided evidence that larvae do not simply

drift with the flow and behave as inert particles, but actually offer some resistance to the flow. They tried to swim upstream increasing their speeds up to the same horizontal flow velocity, and up to 10 times the vertical flow velocity, when they encounter zones of increased turbulence. Further research on a wider flume will allow us to predict lateral swimming capabilities as well, to have the full picture of larvae behavior.

5.5. Supplementary material

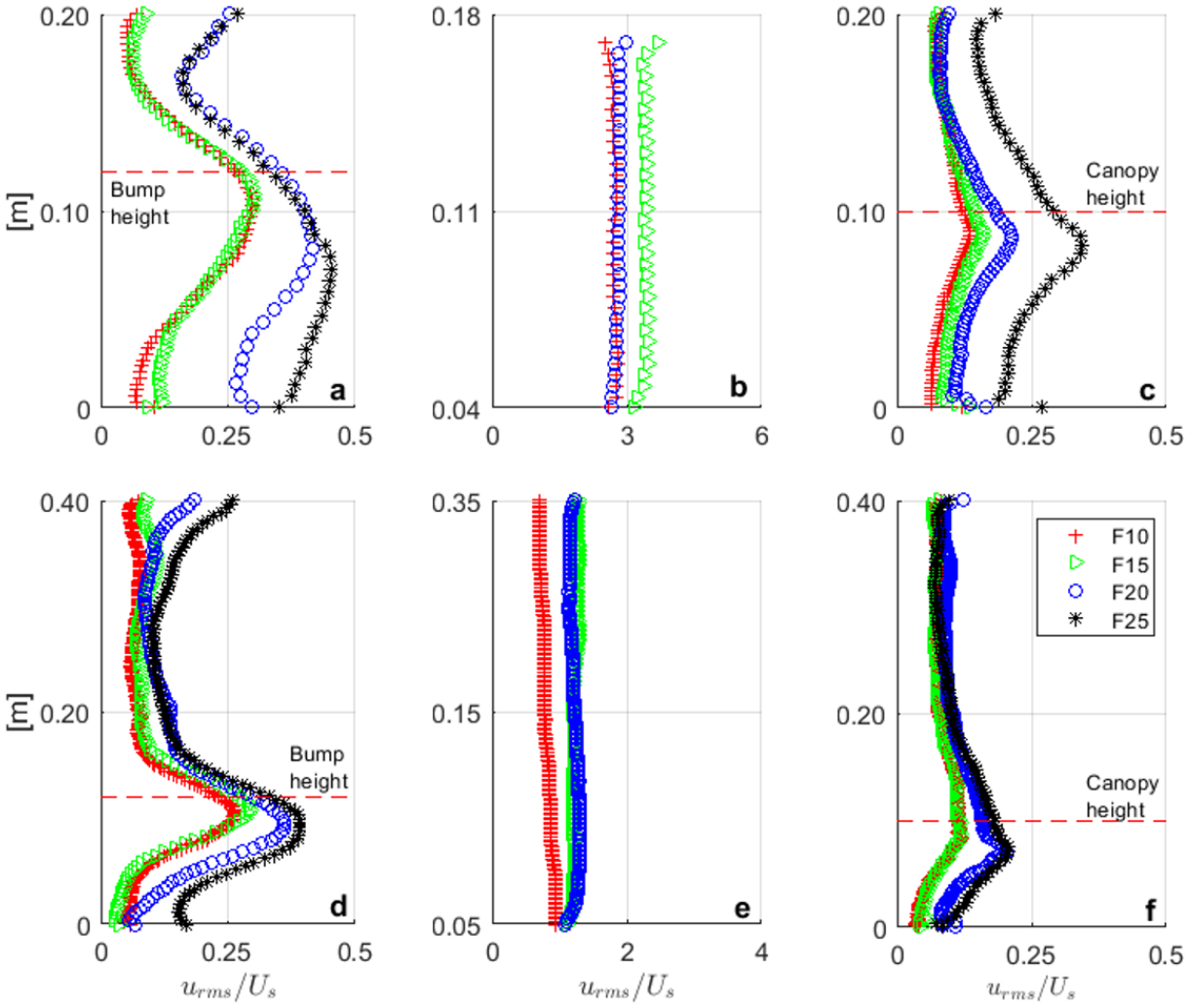

Figure 5.14. Scaled turbulent intensity (u_{rms}/U_s) profiles for all flow conditions in gravel bump at H = 0.2 m (a) and H = 0.4 m (d), single cylinder at H = 0.2 m (b) and H = 0.4 m (e) and rigid vegetation for H = 0.2 m (c) H = 0.4 m (f).

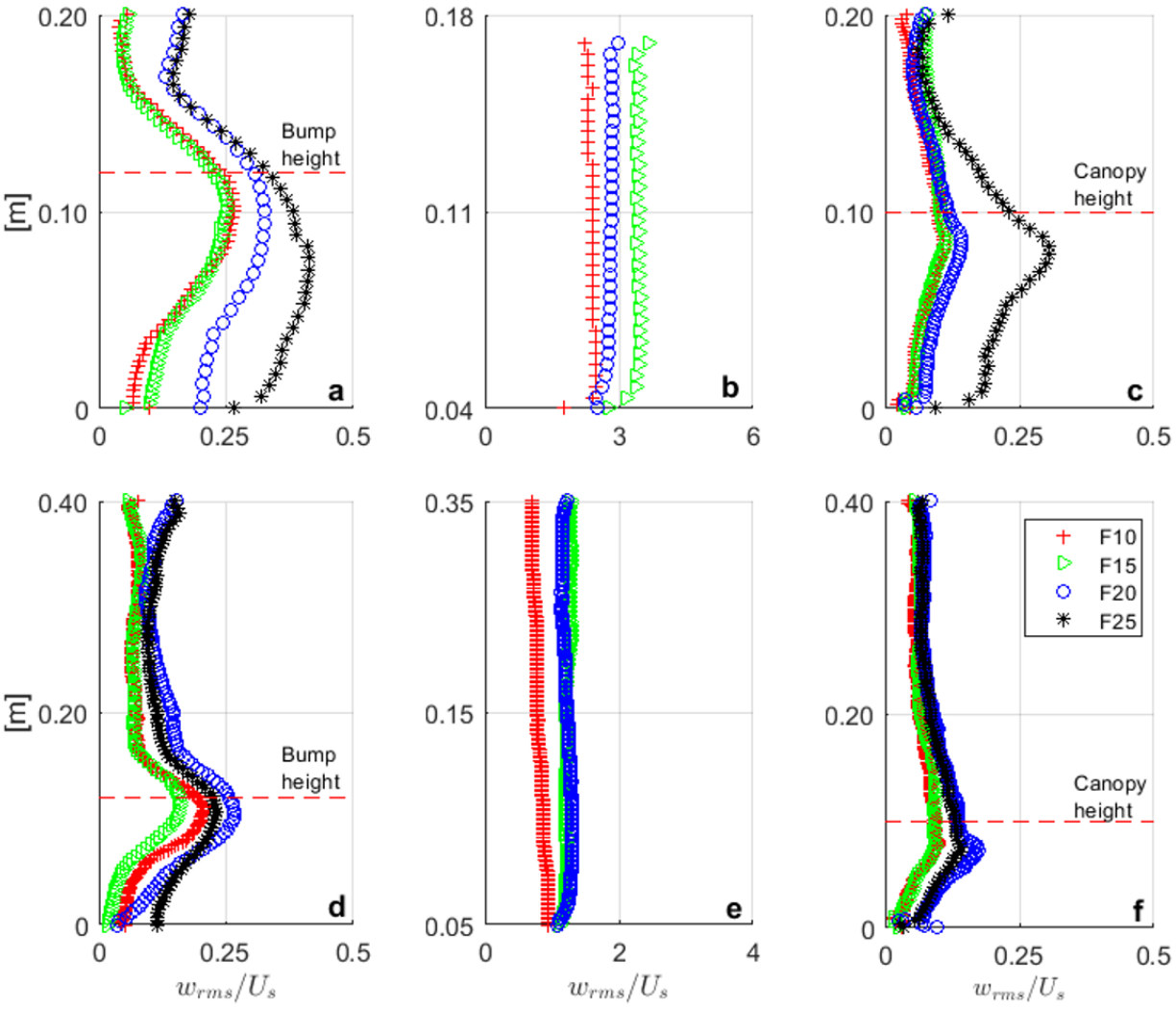

Figure 5.15. Scaled turbulent intensity (w_{rms}/U_s) profiles for all flow conditions in gravel bump at H = 0.2 m (a) and H = 0.4 m (d), single cylinder at H = 0.2 m (b) and H = 0.4 m (e) and rigid vegetation for H = 0.2 m (c) H = 0.4 m (f).

CHAPTER 6: CONCLUSIONS, IMPLICATIONS, AND SUGGESTED FUTURE WORK

6.1. Conclusions

Our laboratory studies with live eggs and larvae of *Ctenopharyngodon idella* have advanced our understanding of relevant ecohydraulic interactions with invasive species:

a) Grass carp eggs are heavy enough to sink to avoid predation at the surface, and light enough to stay in suspension with even low flows to avoid damage and burial, which provides them a survival and evolutive advantage.

b) The spread across the water depth changes as fish develop, so they can be found at different locations depending on their developmental stage. Eggs drifted mostly near the bottom and were carried by the flow towards recirculation zones.

c) A combination of higher shear and turbulence experienced by the eggs, along with abrasion sediment bed and fast moving suspended sediment particles increased the mortality as we observed in the flume, but relative contributions of each process are still unknown.

d) Flow stresses were able to damage egg membranes and affect the embryo inside. Many abnormalities were observed in embryos for exposures to increased turbulence for periods as short as 10 seconds. The membrane of water-hardened eggs offered more resistance to flow stresses and more protection to the larva inside compared to the pre-water-hardened egg stage.

e) Larvae after gas bladder emergence have the ability to remain suspended (swimming) at preferential depths and offer resistance to the flow, with swimming speeds proportional to the flow velocity. This ability allows them to escape from areas of higher turbulence levels.

f) Larvae showed difficulty swimming vertically, when they encountered zones of increased turbulence.

g) Larvae avoided the mixing layer over a gravel bump when turbulence exceeded $k > 1.0$ m^2/s^2 or $\tau_{xz} > 20$ N/m^2.

h) Our study with rigid cylinders allowed us to identify turbulence scales, as the stem-scale, which was close to the size of larvae and was not attractive for larvae. Each eddy would have the energy and momentum to transfer rotation over a submerged body of similar size.

i) Our data suggest the possibility to design in-stream structures to direct larvae into particular areas to reduce or enhance recruitment, as desired, based not only on magnitude of turbulence, but also on its representative length scales.

j) The study focused on grass carp, however results are likely applicable to other species of similar characteristics such as the bigheaded carps which are also undesirable invaders in North America, but at the same time are threatened by large dam construction in their native environment in China.

These findings will allow better monitoring, management, and capturing plans in rivers. However, there is still work needed to directly adapt our research in predictive models, and generalizations for other species will require proper studies.

6.2. Challenges

Our studies focused on longitudinal and vertical motion of eggs and larvae. In order to better identify larval response to larger horizontal gradients, experiments on a large scale or in the field should be conducted to understand the lateral swimming capabilities of larvae, which still remain unknown.

Some of the rising challenges in the control of invasive species in rivers are to predict their spread based on reliable parameters that can be easily-monitored, accurate, and low-cost in the field. Sampling of eDNA has been an effective technique for evaluation of aquatic species populations at large scales, and combined with physical understanding of larval advection and

dispersion, it could enhance the predictive power of existing models such as EFDC models coupled with the random walk particle tracking approximation. This kind of coupled models have been used for environmental applications such as the simulation of passive tracers (Zhu et al. 2017) and oil-particle aggregates (Zhu et al 2018), leading to refined predictions of particle transport as it allows the simulation of more realistic stream scenarios with in-stream structures, meanders, and lateral recirculation zones.

EFDC models could also be used to simulate the dispersion of eDNA itself, for monitoring of invasive or endangered freshwater fish species or mussels. Analytical solutions for determining the concentration and temporal variation of point-source releases can also be coupled with the hydrodynamic model. However, the challenge with eDNA is that the genetic material can be found in forms of blood, feces, tissues, urine, mucous, etc, i.e. a variety of particles of different sizes or substances of different properties that can range broadly in their transport behavior (Shogren et al. 2017). In addition to this, these particles and substances can react or degrade as they are transported, and can be temporarily retained or entirely removed by physical storage and retention in the streambed (Newbold et al. 2005, Arnon et al. 2010).
If the fundamental transport, mixing, reaction, and retention processes of eDNA in its different forms are uncovered, reliable numerical simulations can be performed, and its use will not be limited to qualitative detection for confirming presence-absence of a species somewhere in the fluvial network (Sansom and Sassoubre 2017). Instead, actual monitoring strategies can be implemented to identify where, when, and how many individuals exist in a fluvial system (Shogren et al. 2017).

The gaps in our understanding of the processes mentioned above can be addressed through laboratory experiments and field campaigns. Lateral motion can be investigated in wider laboratory flumes, with configurations such as: 1) unobstructed flow, 2) groyne-like structure to create dead zones, and 3) patch of synthetic emerged vegetation covering half the channel width. All scenarios should be run for multiple flow rates to estimate thresholds of turbulence that would trigger the response of larvae, to determine spatial distribution on a horizontal plane, and to identify trapping or preferential swimming areas around the investigated obstacles. PTV systems should be installed to track larvae trajectories across the width of the flume. This will allow us to quantify percentages of larvae using the lateral structures and determine the time of

residence on those low-turbulence and low-velocity zones depending on their lateral swimming capabilities after gas bladder emergence and the drag forces of the incoming free-stream flow velocity. Estimation of residence times of larvae on side-stream structures based on lateral swimming capabilities will ultimately influence the overall longitudinal dispersion.

Studies on eDNA should characterize the dilution and decay of genetic material in natural streams. This can be done on field where densities and diversity of native mussel communities can be characterized and identified. Sampling of eDNA should be accompanied with ADV measurements to quantify local mixing processes driving the dilution and decay of the genetic material. Extensive datasets are needed to determine best suitable models for mussel eDNA decay in their native environment to feed numerical models.

A more integrative study would incorporate dilution and physiological processes into ecological transport models. Two different effects of the mixing and turbulence processes in open-channel flows can be implemented into ecological transport models from the data collected in the field and in the laboratory. The first effect is the dilution and decay of eDNA, and the second is the lateral swimming response of larvae. As current transport models do not consider these effects, new subroutines can be developed to improve dispersion predictions on natural streams.

Data and models produced from these suggested studies can be employed by fellow scientists, engineers, managers, and entities such as US Army Corps of Engineers and the US Fish and Wildlife Service to not only to guide restoration and management efforts for endangered or invasive mussels and fish species, but to optimize monitoring strategies for any aquatic species. A specific application for monitoring invasive bigheaded carps trying to reach the Great Lakes Basin is needed in the Chicago Sanitary and Ship Canal (CSSC). The CSSC allows the traffic of commercial barges moving downstream through the electric dispersal barriers system. This traffic can facilitate the upstream passage of small fish through the barrier by reducing the voltage gradient of the barrier and causing localized upstream return currents (Davis et al. 2016, Davis et al. 2017, LeRoy et al. 2019). Numerical tools are needed to investigate the potential for entrainment, retention, and transport of early-life swimming fish within large gaps created at junction points between barges.

REFERENCES

Arnon S, Marx LP, Searcy KE, Packman AI (2010) Effects of overlying velocity, particle size, and biofilm growth on stream subsurface exchange of particles. Hydrol. Process. 24, 108e114.

Beamish FWH (1978) Swimming capacity. In: Hoar WS, Randall DJ, eds. Fish physiology. New York: Academic Press, 101-183.

Belcher S, Jerram N, Hunt J (2003) Adjustment of a turbulent boundary layer to a canopy of roughness elements. J. Fluid Mech. 488(1): 369–398. doi:10.1017/S0022112003005019.

Brevis W, Niño Y, Jirka GH (2011) Integrating cross-correlation and relaxation algorithms for particle tracking velocimetry. Exp Fluids 50(1): 135-147.

Cada GF, Odeh M (2001) Turbulence at Hydroelectric Power Plants and Its Potential Effects on Fish. BPA Report DOE/BP-26531-1. https://digital.library.unt.edu/ark:/67531/metadc715813/m2/1/high_res_d/781814.pdf. Accessed 3 Feb 2019.

Chapman DC (2006) Early development of four cyprinids native to the Yangtze River, China. U.S. Geological Survey, Data Series 239. https://pubs.usgs.gov/ds/2006/239/pdf/ds2006-239.pdf. Accessed 24 Sep 2018.

Chapman DC, Chen D, Hoover JJ, Du H, Phelps QE, Shen L, et al. (2016) Bigheaded carps of the Yangtze and Mississippi rivers: biology, status, and management. In: Chen Y, Chapman DC, Jackson JR, Chen D, Li Z, l KJ, et al., editors. Fishery resources, environment, and conservation in the Mississippi and Yangtze (Changjiang) river basins. Bethesda, MD: American Fisheries Society: 113–126.

Chapman DC, Davis JJ, Jenkins JA, Kocovsky PM, Miner JG, Farver J, et al. (2013) First evidence of grass carp recruitment in the Great Lakes Basin. J Great Lakes Res. 39: 547–554.

Chapman DC, George AE (2011) Developmental rate and behavior of early life stages of big head carp and silver carp. USGS Scientific Investigations Report 2011-5076.

Chen Z, Jiang C, Nepf H (2013) Flow adjustment at the leading edge of a submerged aquatic canopy. Water Resour Res. 49(9): 5537–5551. doi:10.1002/wrcr.20403.

Chick JH, Pegg MA (2001) Invasive carp in the Mississippi River Basin. Science 292(5525):2250–2251. doi:10.1126/science.292.5525.2250.

Chilton EW, Muoneke MI (1992) Biology and management of grass carp (*Ctenopharyngodon idella*, Cyprinidae) for vegetation control: a North American perspective. Rev. Fish Biol. Fisher. 2(4):283–320. https://doi.org/10.1007/BF00043520.

Conover G, Simmonds R, Whalen M (2007) Management and control plan for bighead, black, grass, and silver carp in the United States. Asian Carp Working Group, Aquatic Nuisance Species Task Force, Washington, DC. https://www.anstaskforce.gov/Documents/Carps_Management_Plan.pdf. Accessed 18 Oct 2018.

Costa JE (1987) Hydraulics and basin morphometry of the largest flash floods in the conterminous United States. J Hydrol 93:313–338. https://doi.org/10.1016/0022-1694(87)90102-8.

Coulter AA, Bailey EJ, Keller D, Goforth RR (2016) Invasive silver carp movement patterns in the predominantly free-flowing Wabash River (Indiana, USA). Biol. Invasions 18(2):471–485. https://doi.org/10.1007/s10530-015-1020-2.

Cudmore B, Jones LA, Mandrak NE, Dettmers JM, Chapman DC, Kolar CS, et al. (2017) Ecological risk assessment of grass carp (*Ctenopharyngodon idella*) for the Great Lakes basin. Fisheries and Oceans Canada, Canadian Science Advisory Secretariat. Report No.: Research Document 2016/118.

Cudmore B, Mandrak NE, Dettmers JM, Chapman DC, Kolar, CS (2012) Binational ecological risk assessment of bigheaded carps (Hypophthalmichthys spp.) for the Great Lakes Basin (No. 2011/114). DFO, Ottawa, ON. https://waves-vagues.dfo-mpo.gc.ca/Library/346685.pdf. Accessed 30 Nov 2018.

Davis JJ, Jackson PR, Engel FL, LeRoy JZ, Neeley RN, Finney ST, Murphy EA (2016) Entrainment, retention, and transport of freely swimming fish in junction gaps between commercial barges operating on the Illinois Waterway. J. Great Lakes Res. 42, 837–848. https://doi.org/10.1016/j.jglr.2016.05.005.

Davis JJ, LeRoy JZ, Shanks MR, Jackson PR, Engel FL, Murphy EA, Baxter CL, Trovillion JC, McInerney MK, Barkowski NA (2017) Effects of tow transit on the efficacy of the Chicago Sanitary and Ship Canal Electric Dispersal Barrier System. J. Great Lakes Res. 43, 1119–1131. https://doi.org/10.1016/j.jglr.2017.08.013.

Embke HS, Kocovsky PM, Garcia T, Mayer CM, Qian SS (2019) Modeling framework to estimate spawning and hatching locations of pelagically spawned eggs. Can. J. Fish. Aquat. Sci. 76(4):597–607, https://doi.org/10.1139/cjfas-2018-0047.

Embke HS, Kocovsky PM, Richter CA, Pritt JJ, Mayer CM, Qian SS (2016) First direct confirmation of grass carp spawning in a Great Lakes tributary. J Great Lakes Res. 42: 899–903.

Faillettaz R, Paris CB, Irisson JO (2018) Larval fish swimming behavior alters dispersal patterns from marine protected areas in the North-Western Mediterranean sea. Front. Mar. Sci. 5:97. doi: 10.3389/fmars.2018.00097.

Fausch KD, White RJ (1981) Competition between brook trout (*Salvelinus fontinalis*) and brown trout (*Salmo trutta*) positions in a Michigan stream. Can. J. Fish. Aquat. Sci. 38(10): 1220–1227. https://doi.org/10.1139/f81-164

Fedorenko AY, Fraiser FJ (1978) Review of grass carp biology. Fisheries and Marine Service, Tech. Rep. No. 786. http://www.dfo-mpo.gc.ca/Library/52357.pdf. Accessed 8 Feb 2019.

Ferguson RI, Church M (2004) A simple universal equation for grain settling velocity. J Sediment Res. 74(6): 933-937.

Galat DL, Berry CR, Gardner WM, Hendrickson JC, Mestl GE, Power G, Stone C, Winston MR (2005) Spatiotemporal Patterns and Changes in Missouri River Fishes. American Fisheries Society Symposium 45:249–91. https://pdfs.semanticscholar.org/56f2/1664e7a2ace39bc6cba3c9f16806fedd8439.pdf

Garcia MH (2007) Sediment transport and morphodynamics. In: Sedimentation Engineering: processes, measurements, modeling, and practice. Reston, VA: ASCE Manuals and Reports on Engineering Practice No. 110.

Garcia T, Jackson PR, Murphy EA, Valocchi AJ, Garcia MH (2013) Development of a Fluvial Egg Drift Simulator to evaluate the transport and dispersion of Asian carp eggs in rivers. Ecol modell. 263: 211–222.

Garcia T, Murphy EA, Jackson PR, Garcia MH (2015a) Application to the FluEgg model to predict transport of Asian Carp eggs in the Saint Joseph River (Great Lakes tributary). J Great Lakes Res. 41: 374–386.

Garcia T, Zamalloa CZ, Jackson PR, Murphy EA, Garcia MH (2015b) A Laboratory Investigation of the Suspension, Transport, and Settling of Silver Carp Eggs Using Synthetic Surrogates. PloS ONE. 10(12): e0145775. https://doi.org/10.1371/journal.pone.0145775 PMID: 26713855.

Garner AB (2008) High-density grass carp stocking effects on a reservoir invasive plant, water quality, and native fishes. Raleigh, NC: North Carolina State University.

George AE, Chapman DC (2013) Aspects of embryonic and larval development in Bighead Carp *Hypophthalmichthys nobilis* and Silver Carp *Hypophthalmichthys molitrix*. PLOS ONE 8(8):e73829.

George AE, Chapman DC (2015) Embryonic and larval development and early behavior in grass carp, *Ctenopharyngodon idella*: implications for recruitment in rivers. PLoS ONE 10(3): e0119023. doi:10.1371/journal.pone.0119023.

George AE, Chapman DC, Deters JE, Erwin SO, Hayer CA (2015) Effects of sediment burial on grass carp, *Ctenopharyngodon idella* (Valenciennes, 1844), eggs. J Appl Ichthyol. 31(6): 1120–1126.

George AE, Garcia T, Chapman DC (2017) Comparison of Size, Terminal Fall Velocity, and Density of Bighead Carp, Silver Carp, and Grass Carp Eggs for Use in Drift Modeling. Trans Am Fish Soc. 146(5): 834–843. https://doi.org/10.1080/00028487.2017.1310136.

George AE, Garcia T, Stahlschmidt BH, Chapman DC (2018) Ontogenic changes in swimming speed of silver carp, bighead carp, and grass carp larvae: implications for larval dispersal. PeerJ 6:e5869; DOI 10.7717/peerj.5869.

George AE, Stahlschmidt BH, Carlson CL, Prada AF, Tinoco RO, Chapman DC. Development of sensory systems in larval grass carp evaluated by behavior: implications for dispersal and settlement. *In review* – Journal of Fish Biology.

Gertzen EL, Midwood JD, Wieman N, Koops MA (2017) Ecological consequences of grass carp, *Ctenopharyngodon idella*, in the Great Lakes basin: vegetation, fishes and birds. DFO Canadian Science Advisory Secretariat. Report No.: Research Document 2016/117.

Ghisalberti M, Nepf HM (2004) The limited growth of vegetated shear layers. Water Resour Res. 40, W07502, 1–12. doi:10.1029/2003WR002776.

Hassan YA, Blanchat TK, Seeley CH (1992) PIV flow visualization using particle tracking techniques. Meas Sci Technol 3:633–642. https://doi.org/10.1088/0957-0233/3/7/001.

Hearn CJ (2008) The dynamics of coastal models. Cambridge University Press.

Heer T, Wells MG, Jackson PR, Mandrak NE. Modelling Grass Carp egg transport using a 3-D hydrodynamic river model: The role of egg retention in dead zones on spawning success. *In review* – Ecological Modelling.

Hogan JD, Mora C. (2005) Experimental analysis of the contribution of swimming and drifting to the displacement of reef fish larvae. Mar Biol. 147: 1213-1220.

Houde ED. (1997) Patterns and trends in larval-stage growth and mortality of teleost fish. J Fish Biol. 51(Supplement A): 52-83.

Houde ED (2002) Mortality. In: Fuiman LA, Werner RG (eds) Fishery science. The unique contributions of early life stages. Blackwell, UK. pp 64–87.

Jamieson EC, Rennie CD, Jacobson RB, Townsend RD (2011) 3-D flow and scour near a submerged wing dike: ADCP measurements on the Missouri River. Water Resour. Res., 47, W07544, doi:10.1029/2010WR010043.

Jennings DP (1988) Bighead carp (*Hypophthalmichthys nobilis*) a biological synopsis. U.S. Fish and Wildlife Service, Biol. Rep. 88(29). https://apps.dtic.mil/dtic/tr/fulltext/u2/a322554.pdf. Accessed 15 Jul 2018.

Jones LA, Drake AR, Mandrak NE, Jerde CL, Wittmann ME, Lodge DM, et al. (2017) Modeling survival and establishment of grass carp, *Ctenopharyngodon idella*, in the Great Lakes basin. Fisheries and Oceans Canada, Canadian Science Advisory Secretariat. Report No.: Research Document 2016/101.

Keckeis H, Winkler G, Flore L, Reckendorfer W, Schiemer F (1997) Spatial and seasonal characteristics of O+ fish nursery habitats of nase, Chondrostoma nasus in the River Danube, Austria. Folia Zoologica 46:133–150.

Killgore KJ, Miller AC, Conley KC (1987) Effects of turbulence on yolk-sac larvae of paddlefish. T. Am. Fish. Soc. 116(4):670-673. https://doi.org/10.1577/1548-8659(1987)116<670:EOTOYL>2.0.CO;2.

Kirkagac M, Demi N (2003) The effects of grass carp on aquatic plants, plankton and benthos in ponds. J Aquat Plant Manage. 42: 32-39.

Kočovský PM, Chapman DC, Qian S (2018) "Asian carp" is sociatelly and scientifically problematic. Let's replace it. Fisheries 43(7): 311–316.

Korwin-Kossakowski M (2008) The influence of temperature during the embryonic period on larval growth and development in carp, *Cyprinus carpio L*., and grass carp, *Ctenopharyngodon idella* (Val.): theoretical and practical aspects. Archives of Polish fisheries, 16(3), pp.231-314, doi: 10.2478/s10086-008-0020-6

Kozarek JL, Hondzo M, Kjelland ME, Piercy CD, Swannack TM (2018) Effects of turbulence exposure on zebra mussel (*Dreissena polymorpha*) larval survival. Aquat. Sci. 80:12. https://doi.org/10.1007/s00027-017-0563-y.

Laird CA, Page LM (1996) Non-native fishes inhabiting the streams and lakes of Illinois. Illinois Natural History Survey Bulletin 35(1). http://www.archive.org/details/nonnativefishesi351lair. Accessed 20 Jan 2019.

Lamer JT, Ruebush BC, Arbieva ZH, McClelland MA, Epifanio JM, Sass GG (2015) Diagnostic SNPs reveal widespread introgressive hybridization between introduced big head and silver carp in the Mississippi River Basin. Mol. Ecol. 24(15):3931–3943. doi:10.1111/mec.13285.

Lancaster J, Hildrew AG (1993) Characterizing in-stream flow refugia. Can. J. Fish. Aquat. Sci. 50(8): 1663-1675. https://doi.org/10.1139/f93-187.

Lechner A, Keckeis H, Schludermann E, Humphries P, McCasker N, Tritthart M (2014) Hydraulic forces impact larval fish drift in the free flowing section of a large European river. Ecohydrol 7(2):648-658. https://doi.org/10.1002/eco.1386.

Lechner A, Keckeis H, Glas M, Tritthart M, Habersack H, Andorfer L, Humphries P (2018) The influence of discharge, current speed, and development on the downstream dispersal of larval nase (Chondrostoma nasus) in the River Danube. Can. J. Fish. Aquat. Sci. 75(2):247-259, https://doi.org/10.1139/cjfas-2016-0340.

Lembi CA, Ritenour BG, Iverson EM, Forss EC (1978) The effects of vegetation removal by grass carp on water chemistry and phytoplankton in Indian ponds. T. Am. Fish. Soc. 107(1):161–171. https://doi.org/10.1577/1548-8659(1978)107<161:TEOVRB>2.0.CO;2.

LeRoy JZ, Davis JJ, Shanks MR, Jackson PR, Murphy EA, Baxter CL, Trovillion JC, McInerney MK (2019) Efficacy of increasing discharge to reduce tow-mediated fish passage across an electric dispersal barrier system in a confined channel. J. Great Lakes Res. 45, 1320–1331. https://doi.org/10.1016/j.jglr.2019.08.007.

Leslie AJ Jr, Nall LE, Van Dyke JM (1983) Effects of vegetation control by grass carp on selected water-quality variables in four Florida lakes. T. Am. Fish. Soc. 112(6):777–787. https://doi.org/10.1577/1548-8659(1983)112<777:EOVCBG>2.0.CO;2.

Liu M, Lin J, Peng Q, Yu L, Chen D, Liu S, Duan X (2018) Relationship between the distribution of broodstock and vorticity of spawning grounds of four major Chinese carps in the middle reaches of the Yangtze River during ecological operation of the Three Gorges Dam. Water 10(10): 1487. https://doi.org/10.3390/w10101487.

Long CE, Wiberg PL, Novell ARM (1993) Evaluation of Von Kármán's constant from integral flow parameters. J Hydraul Eng. 119: 1182-1190.

Lopez F, Garcia MH (1999) Wall similarity in turbulent open-channel flow. J Eng Mech 125(7): 789-796. https://doi.org/10.1061/(ASCE)0733-9399(1999)125:7(789).

McEwen D, Scobie G (1992) Estimation of the hydraulic conditions relating to fish passage through turbines. NPC001. National Engineering Laboratory, East Kilbride, Glasgow. 155 p.

Metaxas A (2001) Behaviour in flow: perspectives on the distribution and dispersion of meroplanktonic larvae in the water column. Can. J. Fish. Aquat. Sci. 58: 86–98. doi: 10.1139/cjfas-58-1-86.

Mitzner L (1978) Evaluation of biological control of nuisance aquatic vegetation by grass carp. T. Am. Fish. Soc. 107(1):135–145. https://doi.org/10.1577/1548-8659(1978)107<135:EOBCON>2.0.CO;2.

Morgan RP, Ulanowicz RE, Rasin VJ, Noe LA, Gray GB (1976) Effects of shear on eggs and larvae of striped bass, *Morone saxatilis*, and white perch, *M. americana*. T. Am. Fish. Soc. 105(1):149-154. https://doi.org/10.1577/1548-8659(1976)105<149:EOSOEA>2.0.CO;2

Müller UK (2008) Swimming and muscle. In: Finn RN, Kapoor BG, eds. Fish larval physiology: enfield. New Hampshire: Science Publishers Inc., 523-549.

Müller UK, Stamhuis EJ, Videler JJ (2000) Hydrodynamics of unsteady fish swimming and the effects of body size: comparing the flow fields of fish larvae and adults. J. Exp. Biol. 203(2):193–206. http://jeb.biologists.org/content/203/2/193.

Müller UK, van den Boogaart JGM, van Leeuwen JL (2007) Flow patterns of larval fish: undulatory swimming in the intermediate flow regime. J. Exp. Biol. 211(2):196–205. https://doi.org/10.1242/jeb.005629.

Müller UK, van Leeuwen JL (2004) Swimming of larval zebrafish: ontogeny of body waves and implications for locomotory development. J. Exp. Biol. 207, 853-868. doi: 10.1242/jeb.00821.

Murphy EA, Jackson PR (2013) Hydraulic and water-quality data collection for the investigation of Great Lakes Tributaries for Asian carp spawning and egg-transport suitability. U.S. Geological Survey Scientific Investigations Report 2013-5106.

Nepf H (2012) Hydrodynamics of vegetated channels. J. Hydraulic Res. 50(3): 262–279. https://doi.org/10.1080/00221686.2012.696559.

Newbold JD, Thomas SA, Minshall GW, Cushing CE, Georgian T (2005) Deposition, benthic residence, and resuspension of fine organic particles in a mountain stream. Limnol. Oceanogr. 50, 1571e1580.

Noatch MR, Suski CD (2012) Non-physical barriers to deter fish movements. Environ Rev. 20(1): 71–82.

Odeh M, Noreika, JF, Haro A, Maynard A, Castro-Santos T, Cada GF (2002) Evaluation of the effects of turbulence on the behavior of migratory fish. U.S. Geological Survey, BPA Report DOE/BP-00000022-1.

Odell G, Kovasznay L (1971) A new type of water channel with density stratification. J Fluid. Mech. 50(3):535–543. https://doi.org/10.1017/S002211207100274X.

Parker AD, Glover DC, Finney ST, Rogers PB, Stewart JG, Simmonds Jr RL (2016) Fish distribution, abundance, and behavioral interactions within a large electric dispersal barrier designed to prevent Asian carp movement. Can. J. Fish. Aquat. Sci. 73:1060–1071. dx.doi.org/10.1139/cjfas-2015-0309.

Pavlov DS (1994) The downstream migration of young fishes in rivers: mechanisms and distribution. Folia Zoologica 43(3):193-208.

Pavlov DS, Lupandin, AI, Skorobogatov MA (2000) The effects of flow turbulence on the behavior and distribution of fish. J. Ichthy. 40(2):232–261.

Pavlov DS, Mikheev VN, Lupandin AI, Skorobogatov MA (2008) Ecological and behavioural influences on juvenile fish migrations in regulated rivers: a review of experimental and field studies. Hydrobiologia 609:125–138. https://doi.org/10.1007/s10750-008-9396-y

Piper RG, McElwain IB, Orme LE, McCraren JP, Fowler LG, Leonard JR (1982) Fish hatchery management. U.S. Fish and Wildlife Service. Washington, DC.

Prada AF, George AE, Stahlschmidt BH, Chapman DC, Tinoco RO (2018) Survival and drifting patterns of grass carp eggs and larvae in response to interactions with flow and sediment in a laboratory flume. PLoS ONE 13(12): e0208326. https://doi.org/10.1371/journal.pone.0208326

Prada AF, George AE, Stahlschmidt BH, Jackson PR, Chapman DC, Tinoco RO (2020) Patterns of drifting and swimming pathways of grass carp eggs and larvae under turbulent flows at various developmental stages. Aquat. Sci. 82:16. https://doi.org/10.1007/s00027-019-0689-1

Pope SB (2000) Turbulent Flows. Cambridge Univ. Press, Cambridge, UK.

Rehmann CR, Stoeckel JA, Schneider DW (2003) Effect of turbulence on the mortality of zebra mussel veligers. Can. J. Zool. 81(6):1063–1069. https://doi.org/10.1139/z03-090.

Reichard M, Jurajda P (2007) Seasonal dynamics and age structure of drifting cyprinid fishes: an interspecific comparison. Ecol Freshw Fish 16:482-492. doi: 10.1111/j.1600-0633.2007.00229.x.

Sansom BJ, Sassoubre LM (2017) Environmental DNA (eDNA) Shedding and Decay Rates to Model Freshwater Mussel eDNA Transport in a River: Environmental Science & Technology, v. 51, no. 24, p. 14244-14253, 10.1021/acs.est.7b05199.

Schiemer F, Keckeis H, Kamler E (2003) The early life history stages of riverine fish: ecophysiological and environmental bottlenecks. Comparative Biochemistry and Physiology. Comp Biochem Physiol A Mol Integr Physiol 133(3):439-49. doi: 10.1016/S1095-6433(02)00246-5.

Schlichting H (1979) Boundary Layer Theory. 7th ed. New York: McGraw-Hill.

Schludermann E, Tritthart M, Humphries P, Keckeis H (2012) Dispersal and retention of larval fish in a potential nursery habitat of a large temperate river: an experimental study. Can. J. Fish. Aquat. Sci. 69(8):1302-1315, https://doi.org/10.1139/f2012-061.

Schrank SJ, Guy CS (2002) Age, growth, and gonadal characteristics of adult big head carp, *Hypophthalmichthys nobilis*, in the lower Missouri River. Environ. Biol. Fishes. 64(4):443–450. https://doi.org/10.1023/A:1016144529734.

Sentchev A, Korotenko K (2004) Stratification and tidal current effects on larval transport in the Eastern English Channel: observations and 3D modeling. Environ Fluid Mech 4(3): 305-331. https://doi.org/10.1023/B:EFMC.0000024246.39646.1d.

Shireman JV, Smith CR (1983) Synopsis of biological data on the grass carp, *Ctenopharyngodon idella* (Cuvier and Valenciennes, 1844). FAO Fisheries Synopsis No. 135. http://www.fao.org/3/a-ap938e.pdf. Accessed 21 Nov 2018.

Shogren AJ, Tank JL, Andruszkiewicz E, Olds B, Mahon AR, Jerde CL, Bolster D (2017) Controls on eDNA movement in streams: Transport, Retention, and Resuspension. Sci Rep 7: 5065. DOI:10.1038/s41598-017-05223-1.

Soria J (1996) An investigation of the near wake of a circular cylinder using a video-based digital cross-correlation particle image velocimetry technique. Exp. Therm. Fluid Sci. 12(2):221–233. https://doi.org/10.1016/0894-1777(95)00086-0.

Smith DL, Goodwin RA, Nestler JM (2014) Relating Turbulence and Fish Habitat: A New Approach for Management and Research. Rev. Fish. Sci. Aquac. 22(2):123–130. https://doi.org/10.1080/10641262.2013.803516.

Soulsby RL, Dyer KR. The form of the near-bed velocity profile in a tidally accelerating flow. J Geophys Res. 1981; 86(NC9): 8067-8074.

Stainbrook KM, Dettmers JM, Trudeau TN (2007) Predicting suitable Asian carp habitat in the Illinois waterway using geographic information systems. INHS Tech. Rep. (07) http://hdl.handle.net/2142/18155. Accessed 23 Jan 2019.

Stapleton KR, Huntley DA. Seabed stress determinations using the inertial dissipation method and the turbulent kinetic energy method. Earth Surf Process Landforms. 1995; 20(9): 807-815.

Statzner B, Müller R (1989) Standard hemispheres as indicators of flow characteristics in lotic benthos research. Freshwater Biol. 21(3):445–459. https://doi.org/10.1111/j.1365-2427.1989.tb01377.x.

TaninoY, Nepf HM (2007) Experimental investigation of lateral dispersion in aquatic canopies. In Proc. 32nd Congress of IAHR (ed. G. Di Silvio & S. Lanzoni).

Thielicke W, Stamhuis EJ (2014) PIVlab – Towards User-friendly, Affordable and Accurate Digital Particle Image Velocimetry in MATLAB. J. Open Res. Softw. 2(1), p.e30. doi: http://doi.org/10.5334/jors.bl.

Thompson CEL, Amos CL, Jones TER, Chaplin J (2003) The manifestation of fluid-transmitted bed shear stress in a smooth annular flume-a comparison of methods. J Coast Res. 19(4): 1094-1103.

Tritico HM, Cotel AJ (2010) The effects of turbulent eddies on the stability and critical swimming speed of creekchub (Semotilus atromaculatus). J Exp Biol 213: 2284-2293. doi: 10.1242/jeb.041806.

Uemura T, Yamamoto F, OhmiK(1989)Ahigh-speed algorithm of image analysis for real time measurement of a two-dimensional velocity distribution. Flow visualization, ASME FED-85, pp 129–134.

Van Rijn LC. (1984) Sediment transport, Part II: Suspended load transport. J Hydraul Eng. 110(11): 1613-1641.

White FM. (1991) Viscous Fluid Flow, McGraw-Hill, New York.

Wieringa JG, Herbst SJ, Mahon AR (2017) The productive viability of grass carp (Ctenopharyngodon idella) in the western basin of Lake Erie. J Great Lakes Res. 43: 405–409.

Wittmann ME, Annis GM, Kramer AM, Mason L, Riseng C, Rutherford ES, et al. (2017) Refining species distribution model outputs using landscape-scale habitat data: forecasting grass carp and Hydrilla establishment in the Great Lakes region. J Great Lakes Res. 43: 298–307.

Yi B, Liang Z, Yu Z, Lin R, He M (1988) A comparative study on the early development of grass carp, black carp, silver carp, and big head of the Yangtze River. In: Gezhouba water control project and four famous fishes in the Yangtze River, China. Wuhan, China: Hubei Science and Technology Press.

Zens B, Glas M, Tritthart M, Habersack H, Keckeis H (2018) Movement patterns and rheoreaction of larvae of a fluvial specialist (nase, Chondrostoma nasus): the role of active versus passive components of behaviour in dispersal. Can J Fish Aquat Sci. 75: 193-200.

Zhou Z, Wang J (2019) Numerical Modeling of 3D Flow Field among a Compound Stilling Basin. Mathematical Problems in Engineering, Article ID 5934274, https://doi.org/10.1155/2019/5934274

Zhu Z, Motta D, Jackson PR, Garcia MH (2017) Numerical modeling of simultaneous tracer release and piscicide treatment for invasive species control in the Chicago Sanitary and Ship Canal, Chicago. Illinois. Environ Fluid Mech 17(2):211–229. https://doi.org/10.1007/s10652-016-9464-1.

Zhu Z, Waterman D, Garcia MH (2018) Modeling the transport of oil–particle aggregates resulting from an oil spill in a freshwater environment. Environ. Fluid Mech. 18(4): 1–10. https://doi.org/10.1007/s10652-018-9581-0.